# The Creep Behaviour Of Oriented And Isotropic Polyethylene

**Mark James Bonner**

**Submitted in accordance with the requirements for the degree of Doctor of Philosophy**

**The University Of Leeds**

**Department of Physics**

**September 1995**

The candidate confirms that the work submitted is his own and that appropriate credit has been given where reference has been made to the work of others.

## Abstract

The long term plastic deformation, (creep), behaviour in tension of both oriented and isotropic polyethylene has been studied using a variety of relatively simple experimental techniques, primarily dead loading creep tests.

In an attempt to gain an understanding of the mechanisms controlling creep two different viscoelastic models have been applied to the data. The first of these was a two process model, involving two activated Eyring processes in parallel. The second was a Fotheringham and Cherry type model, with a co-operative jump based on a single activated process.

In the oriented state the two process model has been successful in describing the behaviour of the material. The Fotheringham and Cherry type model was not successful in describing the behaviour of this material. A complete expression of the two process model has been shown to fully describe the behaviour of one grade at one draw ratio, and an approximation of the model for the other draw ratios and grades has indicated that creep of oriented polyethylene is controlled by a c-shear mechanism.

Because of time constraints it was only possible to analyse the behaviour of one grade of the isotropic material with the Fotheringham and Cherry model. Whilst this was successful the activated parameters obtained from it seem very low and would seem to indicate a chain rotation mechanism. Whilst it appears that the two process model should also describe this data, it has not been possible to produce a conclusive fit. It is considered that this is due to limitations in the computing software used for fitting. Hence an approximation of the model was used to produce approximate activation parameters.

In addition to the investigation into the rate controlling mechanism of creep the data obtained for the oriented state has been shown to be consistent with the existence of a unique relationship between three important mechanical properties, (strain, strain rate and stress). This relationship holds provided that the initial morphology of the material is equivalent prior to orientation taking place. It has also been shown that the creep data obtained for the isotropic state are consistent with the existence of double yield points in polyethylene.

Finally the creep data have been used in a computer model of craze deformation in order to investigate the rate controlling mechanism of slow crack growth. This has shown that craze failure, and hence crack lifetime is controlled by tensile creep to failure of fibrils at the base of the craze.

**Acknowledgements**

This project was supervised by Professor I.M. Ward and Dr. R.A. Duckett, whom I would like to thank for their invaluable help and guidance throughout its duration. I would also like to thank Dr P. O'Connell for his support and guidance, and Dr. N. Brooks and Mr D. Appleyard for their advice on practical matters.

This project was a SERC CASE award sponsored by BP Chemicals Ltd., Grangemouth and I would like to thank them for their financial assistance. I wish also to thank my industrial supervisors, Dr G. Capaccio, Mr A. Channell and Mr L. Rose for their contributions to the project.

I would also like to thank my family for putting up with me during this work, my friends and fellow students within the department for stimulating discussions and the odd laugh and Ms. A. Franklin and Ms. F. Worthy for keeping me sane and supplying the coffee.

## Contents

## Contents

## Contents

## List Of Tables

# List Of Tables

## List Of Figures

## List Of Figures

## List Of Figures

## List Of Figures

## List Of Figures

## List Of Figures

# Chapter 1

# Introduction

## 1·1 Introduction

A polymer is a series of long molecular "chains" held together by some kind of intermolecular force, (usually van der Waals force). Each of the long chains is composed of a repeating series of smaller units, normally based on some form of carbon to carbon bonding. These repeating units are known as monomers. The monomers in the main section of the chain, (the part which forms the main length of the chain), compose the backbone of the polymer. Attached to this backbone can be either branches or side groups. These branches and side groups can be mini polymers, also composed of monomers, (but not necessarily the same monomer as in the backbone), like the backbone but smaller in length, or single chemical units, ranging from simple $CH_3$ units to highly complex chemical structures.

Polymers are not new. Natural polymers have been used by man for many years. Natural polymers include wood, cotton, wool and rubber. However since World War II the use of man made or synthetic polymers has increased greatly. These synthetic polymers are sometimes cheaper than the natural polymers, and can be better suited to the tasks they are used for, (although some people would dispute this; for example wool is still a popular choice for clothing purposes, even though there are many synthetic fabrics available). This is because chemists can now produce such a wide range of polymers that it is often possible to obtain a polymer which meets a specific set of target properties.

Although there are many physical characteristics of a polymer the three most important are chain length, intermolecular forces and branching.

Chain Length

The effect of chain length on the physical properties of the polymer is complicated by factors such as the type of bonding between chains and the presence and type of side groups or branches. The melting point of a polymer is influenced by the thickness of the crystals within it. A large number of polymers form crystals by folding their chains back on themselves in a regular fashion, so that the chains all lie aligned parallel to each other, with the folds forming the top and bottom edges of the crystal. In general longer fold distances occur at higher crystallisation temperatures, and longer chains crystallise at higher temperatures. The same relationship holds for the tensile strength of the chain, although in general there is very little increase in strength for extra monomer units added after the first 500 in the chain. Any real polymer has an entire spectrum of chain lengths, and so generally the average chain length is used.

Intermolecular Forces The greater the force between the chains the higher the strength of the polymer and its melting point. Some polymers, such as Bakelite, have rigid chemical bonds between the chains and are very strong and degrade rather than melt. This type of polymer is a thermoset, (a polymer which melts is thermoplastic).

Branching The more branches a polymer has on the backbone the less well it can pack together. The presence of branches limits the distance between folds along the chain when forming crystals, since the only type of branch that can be contained by the crystal is a methyl branch; all other branch types must be outside the crystal. Hence the crystal thickness is limited to the distance between branches and the melting point is reduced. The presence of branching may increase some physical properties however, since they provide some extra barrier to the movement of a chain through a crystal under stress.

The length of a polymer chain can be related to its molecular weight. However, as stated earlier there are many different chain lengths within a typical commercial polymer, and therefore a spread of molecular weights. For a polymer there are many methods of calculating average molecular weights and two of the most important are given below. These are the number average molecular weight, ($\overline{M_N}$), and the weight average molecular weight, ($\overline{M_W}$). The ratio of these quantities is called the polydispersity, and gives a measure of the spread of chain lengths within the polymer. These parameters are carefully controlled during the production of the polymer to ensure the correct properties are produced.

$$\overline{M_N} = \frac{\Sigma_i N_i M_i}{\Sigma_i N_i} \qquad (1\cdot1)$$

$$\overline{M_w} = \frac{\Sigma_i N_i M_i^2}{\Sigma_i N_i M_i} \qquad (1\cdot2)$$

Where $M_i$ is the molecular mass of a chain and $N_i$ is the number of moles of chains of that mass.

The synthetic polymers can be split into two categories, bulk and specialist. Bulk polymers are produced in huge quantities, (millions of tons per year), and utilised

for a wide variety of everyday items. Some examples are polyethylene, used for carrier bags and bottles, polypropylene, used for ropes, crates and bottles, Nylon, used for textiles and PVC, used for fabric coatings and electrical insulation on cables. Specialist polymers are produced in smaller quantities for specific tasks. An example is Kevlar, which is used in high tensile strength applications, such as replacing steel hawsers for lifting heavy objects, or where the ability to absorb a large amount of kinetic energy before breaking is required, such as in bullet proof vests.

**1·2 Polyethylene**

The work carried out in this investigation was sponsored by BP Chemicals, Grangemouth, under a CASE studentship. It was initially intended as part of a much wider investigation into slow crack growth in polyethylene.

Polyethylene is the most common of the so called bulk polymers. Technically an addition polymer, its basic structure is shown below.

$$\left(-CH_2-CH_2-\right)_n$$

It was discovered by ICI in 1933, and the original production process involved heating ethene, (with traces of oxygen), up to 200°C at a pressure of 1,200 atmospheres. This produced a polyethylene with many branched chains and a melting point in the region of 105°C, which is known as Low Density Polyethylene, (LDPE).

Production methods involving catalysts were first developed by Ziegler in the 1950s. These processes use lower temperatures and pressures, and are capable of producing much more ordered structures with few branches. Polyethylene with few branches is more rigid than low density polyethylene, and has a higher melting point. These rigid polyethylenes are known as High Density Polyethylene, (HDPE). The article by Sherwood in reference 1 provides a more complete history of the discovery and development of polyethylene.

Polyethylene does not have a specific set of characteristics, and many of its basic properties vary widely. The molecular weight for example extends to very large values, with Ultra High Molecular Weight Polyethylene having $\overline{M}_w$ of up to 3,000,000. In addition to the varying molecular weight, the amount of side chain branching also varies extensively, from linear systems with virtually no side chain branches, to systems with several tens of branches per thousand carbon atoms in the backbone. The composition of the side chains themselves can vary, from the simplest $CH_3$ units to units that are complex chemical molecules in their own right.

Each of the possible combinations of molecular weight and side chain branching that is produced, by companies such as BP Chemicals, is termed a grade. These grades are standard and the polymer of each grade will be nominally constant in terms of its processing characteristics throughout its production life, though quite wide variation in properties can often be found between different batches of the same grade.

Because of the wide range of properties of polyethylene it is used in many different ways. For example low density polyethylene is used for making films and sheets for manufacture into bags and wrappings. It is also used to produce moulded articles, such as washing up bowls and some types of bottles. High density polyethylene is used where more rigidity is required, such as containers for bleach, and milk bottle crates. Using specialised processing routes it is possible to introduce large amounts of orientation into polyethylene fibres. This product is known as Ultra High Modulus Polyethylene, (UHMPE), and provides high tensile strength and good energy absorbent properties with relative chemical stability and at a lower cost than specialist polymers such as Kevlar.

However one of the most important uses of polyethylene, (both financially and in everyday life), is its use in pipes. These pipes are used to provide extra protection and insulation for electrical cables when laid underground, and also to provide transmission routes for water and gas from the mains supply to individual consumers. In all three cases the pipes are laid underground and are expected to withstand the extremes of conditions that exist in the British climate, as well as some disturbance caused by being driven over and occasionally dug up by mistake. In the last two applications, (gas and water transmission), the substances carried by the pipes are under pressure, and over an extended period of time this pressure can provide the driving force for the initiation of a crack which will ultimately lead to the failure of the pipe. Obviously from a commercial point of view it is desirable to use materials in which few cracks are initiated in order to increase service lifetimes and reduce the need for expensive replacement work.

Since 1991 it has been apparent[2] that there are many similarities between the creep and fatigue modes of failure in polyethylene. It has been shown recently by researchers at BP Chemicals Ltd.[3,4], and by research within this department[5,6], that the performance of polyethylene under conditions of slow crack growth is related to its performance under conditions of creep, and indeed that it is the fibrils within the craze present in a crack which provides the major rate controlling mechanism in slow crack growth.

The work described in this thesis is a study of the creep performance of three grades of polyethylene, including one grade commercially used to make pipes, (00240). The creep properties have been studied in both the oriented state, (discussed in chapter

3), and in the isotropic state, (discussed in chapter 4). The creep data have been used by other workers in an attempt to determine the major rate controlling process of slow crack growth, (a variant of the published work is discussed in appendix 1).

Creep can be defined as the long term deformation of a material under nominally constant stress. The time span involved can be as short as a few minutes, or it can extend over many years.

As well as its importance to slow crack growth, creep resistance is an important property that needs to be investigated for material liable to be used with a constant component of stress acting upon it. Whilst nearly all materials creep, polymers are much less creep resistant than traditional construction materials, such as metal. Thus in order that polymers can be made more creep resistant a thorough knowledge of their creep behaviour and the underlying mechanisms that control creep must be acquired.

A great deal of work has been carried out in the past on creep and plastic deformation of highly drawn polyethylene. There is a long history of this kind of work being performed in this department, most notably by Wilding and Ward[7,8], and more recently by Rasburn, Klein and Ward[9], (all on relatively highly drawn material). Outside this department it has been carried out by people such as Karpov, Bitskii, Strel'tses and Yel'yashevich[10] on material oriented to draw ratio 15. Findley[11] has even performed creep tests on polyethylene lasting 26 years.

The investigations of Wilding et al., concentrated on strains in the region of draw ratio 20, because of the importance of creep in high modulus polyethylene fibre applications. The work on oriented material to be presented here has been conducted on material that has been drawn at room temperature, over a range of strains, with a maximum strain achieved of approximately draw ratio 15, because of the relevance to failure of fibrils in crazes in polyethylene.

Creep experiments were also performed on fully isotropic material. Previous work within this department on isotropic material, such as that by Truss, Clarke, Duckett and Ward[12], has concentrated on constant strain rate yield behaviour. Outside this department isotropic creep has been studied by people such as Dixonstubbs[13]. It is intended to show that creep and yield behaviour complement each other. The work of Brooks[14], and Brooks, Duckett and Ward[15] on the yield of isotropic polyethylene has shown the existence of two yield points. The investigation to be reported in chapter 4 on the creep of isotropic polyethylene supports this finding.

Two models have been used in this investigation to attempt to describe the behaviour of the materials. The first of these was the two process model of Wilding and Ward[8], which involves stress activated Eyring viscosity. This has been applied successfully to the oriented material, both in this work and that of others, (Wilding and

Ward[8] and Rasburn et al.[9]), but as will be shown here, it is less successful in describing the behaviour of the isotropic material in this investigation.

The second model is the co-operative jump model of Fotheringham and Cherry[16]. This has been used in the past by Fotheringham and Cherry[16], Brooks[14] and Brooks, Duckett and Ward[15] to model successfully the yield behaviour of isotropic polyethylene. In this work it is again used successfully to model the isotropic material, but it is unable to give satisfactory results when applied to the oriented material.

**1·3 Activated Rate Theory**

The basis for any investigation into an activated process is an attempt to gain an understanding of the physical mechanism at the molecular level which controls the rate dependence of the deformation.

There are several definitions of creep. It can be used to refer to the entire viscoelastic deformation response of a material under load, or to the plastic component of the material response.

The initial response of a viscoelastic material is an elastic component which is recoverable. However as time under load increases the elastic response is swamped by a viscous flow, the plastic response which is largely irrecoverable. For a more thorough introduction to viscoelastic behaviour see "The Mechanical Properties of Solid Polymers" by Ward[17].

Most models, and certainly those used in this work, view plastic deformation as a time dependent kinetic process in which some, (as yet), unspecified entities of the polymer move over potential energy barriers which hinder their progress. These entities can make both forward and backward jumps over the barrier; that is, they can jump in such a way as to increase the strain level of the material or to decrease it. In an unstressed condition forward and backward jumps are equally likely, and thus an equilibrium condition exists where equal numbers of forward and backward jumps are made and hence the overall strain level of the material is unchanged.

When a stress is applied the energy barrier is biased so that it requires less energy for a jump over the barrier to occur in the direction of the applied stress, and more energy for a jump against the direction of the stress. Hence the probability of a forward jump is increased, and the probability of a backward jump decreased. Thus more jumps in the direction of the applied stress occur, and these have the cumulative effect of changing the strain level of the material. This situation is shown schematically in figure 1·1.

Figure 1·1

Schematic representation of the potential energy barrier in creep.

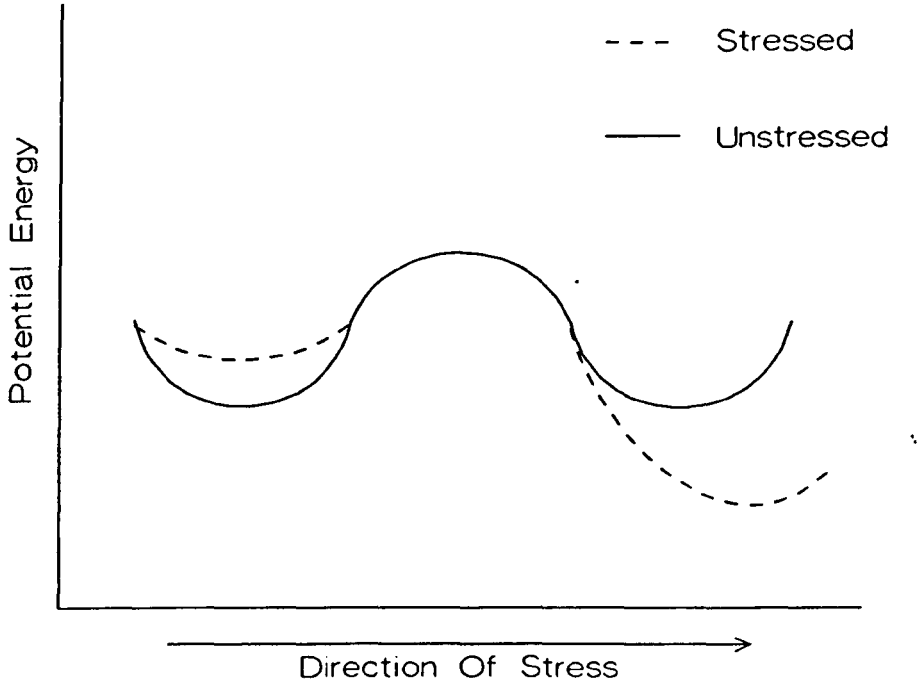

There are several possible candidates for the deformation mechanisms in the polymer during straining. These include extension of the intercrystalline amorphous polymer, interlamellar slip, intermolecular slip and interfibrillar slip, all of which have, according to Cowking[18], been detected in polyethylene.

The first theories of plastic deformation to contain both rate and temperature dependence were formulated in the 1920s and a great deal of work has been carried out on metals since then. The application of a rate theory to polymers is a more complex procedure than that required for metals, since polymers often exhibit strain hardening effects and a high dependence of the strain rate on the applied stress and strain.

The model to be described here is based on two activated Eyring type processes in parallel. It was devised for situations where there was no change in the strain rate during creep tests, i.e. it is an equilibrium model. The best way to present creep data in order to view whether an equilibrium situation has been achieved is to plot the data after the manner of Sherby and Dorn[19]. A Sherby Dorn plot has log (strain rate) plotted against strain, and a schematic Sherby Dorn plot for a constant nominal stress is shown in figure 1·2.

All the Sherby Dorn plots produced in this investigation exhibited the same basic form, that is all displayed the two distinct strain rate regions shown in figure 1·2.

Region 1 was characterised by a rapid decrease in strain rate with increasing strain. Region 2 was characterised by a slowly decreasing strain rate with increasing strain, although for some materials the gradient in region 2 approaches zero implying a tendency to an equilibrium creep rate. The reasons for the shape of these Sherby Dorn plots will be discussed in chapters 3 and 4.

Figure 1·2

Schematic representation of the Sherby Dorn plot as used in creep experiments.

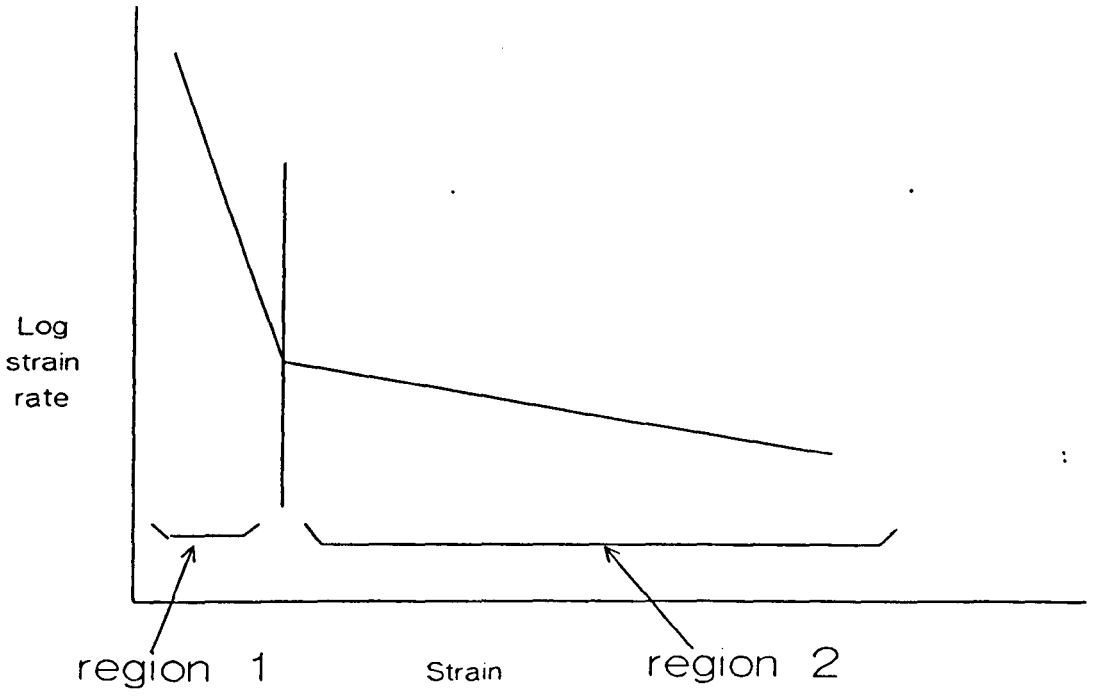

### 1·3·1 Eyring Approach

The activated Eyring[20] rate process is described mathematically by

$$\dot{\varepsilon} = \dot{\varepsilon}_0 \exp\left(\frac{-\Delta U}{kT}\right)\sinh\left(\frac{\sigma V}{kT}\right) \qquad (1\cdot3)$$

where

$\dot{\varepsilon}$ is the rate of the activated process.

$\dot{\varepsilon}_0$ is a "pre exponential" factor.

$\Delta U$ is the activation energy of the process.

$k$ is the Boltzmann constant.

$T$ is the temperature in Kelvin.

$\sigma$ is the applied stress.

$V$ is the activation volume of the process.

The process can therefore be described by the three parameters $\dot{\varepsilon}_0$, $\Delta U$ and $V$ for a given stress and temperature.

### 1·3 2 Activation Volume

It is difficult to assign a physical significance to the activation volume $V$, although metallurgists have suggested it may be thought of as being related to the degree of localisation of the activated event. The product $\sigma V$ represents the work done by the applied stress during the activated process.

If sufficiently high stresses are considered, (i.e. $\sigma V > 3kT$), then the sinh term approximates to an exponential and equation 1·3 may be rearranged into

$$\log_{10}\dot{\varepsilon} \cong \log_{10}\left(\frac{\dot{\varepsilon}_0}{2}\right) - \frac{\Delta U}{2\cdot 3kT} + \frac{\sigma V}{2\cdot 3kT} \qquad (1\cdot4)$$

Hence a plot of $\log_{10}(\dot{\varepsilon})$ against applied stress at a constant temperature should be a straight line of gradient $\dfrac{V}{2\cdot 3kT}$

### 1·3·3 Activation Energy

$\Delta U$, the activation energy, can also be derived from equation 1·4, since

$$\log_{10}(\dot{\varepsilon}) = \log_{10}\left(\frac{\dot{\varepsilon}_0}{2}\right) - \frac{1}{2\cdot 3kT}\{\Delta U - \sigma V\} \qquad (1\cdot5)$$

Thus a plot of $\log_{10}(\dot{\varepsilon})$ against $1/T$ at constant stress and strain should yield a straight line of gradient $\left\{-\left(\frac{\Delta U - \sigma V}{2\cdot 3k}\right)\right\}$ for a single activated process.

### 1·3·4 Other Approaches

Because of the association of this department with Wilding and Ward their approach has been used in this work. It should however be pointed out that other approaches to activated rate theory exist.

For example the work of Escaig and Lefebvre[21], and the early work of Coates[22] use partial derivatives, which make it implicitly clear that variables such as activation volume should be determined at constant temperature and strain. That is they define quantities such as activation volume in terms of partial derivatives, so that, (using terminology consistent with this work),

$$V = kT\left(\frac{\partial \ln \dot{\varepsilon}}{\partial \sigma}\right)_{T,P,\varepsilon} \qquad (1\cdot6)$$

This makes it expressly clear that the activation volume should be derived at constant strain, temperature and pressure.

### 1·3·5 Two Process Approach

It will become apparent later that a single process with invariant activation parameters cannot be used to describe the behaviour of the material fully, although at sufficiently high stress levels it is possible to determine approximate values of the activation parameters by assuming that the material is behaving as though there was only one activated process present, that is that we have a single process present with effective activation parameters determined by the activation parameters of the two separate processes. A variable activation parameter approach, (where there is a single process whose parameters change with both stress and strain), will also be shown to be

unlikely, since it will be shown that although there is a smooth and relatively simple dependence of the activation volume on strain, there would need to be a much more complex dependence upon stress.

With this in mind the two process approach will be examined. In this approach the situation can be thought of as 2 elements in parallel, as shown in figure 1·3.

Dashpot 2 controls the behaviour of the material at high stress levels, and is associated with a relatively low activation volume. Dashpot 1 is associated with an activation volume which is several times larger than the activation volume for dashpot 2, and controls the low stress response of the material.

At low stresses the viscosity of dashpot 1 is much larger than that of dashpot 2. Thus at low stress levels dashpot 1 can be regarded as having infinite viscosity, and the model reduces to the standard linear solid.

When high stresses are applied the dashpot with the smaller activation volume, dashpot 2, takes most of the stress and thus the overall behaviour of the material will tend towards the behaviour of the element containing this dashpot.

During the initial stage of creep both springs extend, until a pseudo equilibrium is reached. This can be thought of as the polymer network taking up tension. After the springs have reached their equilibrium extension the dashpots yield and permanent flow takes place.

The response of both individual elements to an applied strain rate is shown in figure 1·4, as is the combined stress, which is simply the sum of the stresses on each individual arm of the model, (i.e. $\sigma_T = \sigma_1 + \sigma_2$).

Each element can be modelled using an Eyring type expression, (equation 1·3). The large activation volume of dashpot 1 means that $\sigma_1 V_1$ is much larger than kT and thus the sinh term in equation 1·3 will approximate to an exponential. However $\sigma_2 V_2$ is of the order of kT and hence the sinh term must be retained.

Rearranging the equations in terms of stress we obtain

$$\sigma = \frac{2\cdot 3kT}{V_1}\left(\log_{10}(\dot{\varepsilon}) - \log_{10}\left(\frac{[\dot{\varepsilon}'_0]_1}{2}\right)\right) + \frac{kT}{V_2}\sinh^{-1}\left(\frac{\dot{\varepsilon}}{[\dot{\varepsilon}'_0]_2}\right) \qquad (1\cdot 7)$$

Figure 1·3

Schematic representation of the mechanical interpretation of the Eyring two process model.

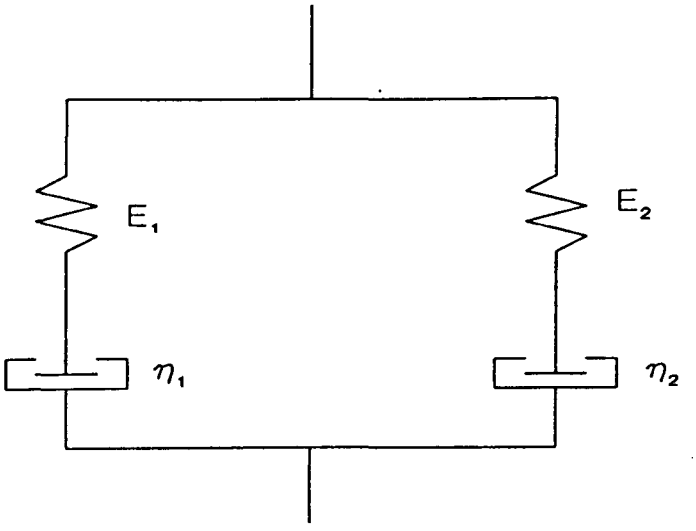

Figure 1-4

Schematic representation of the response of both halves of the two process model.

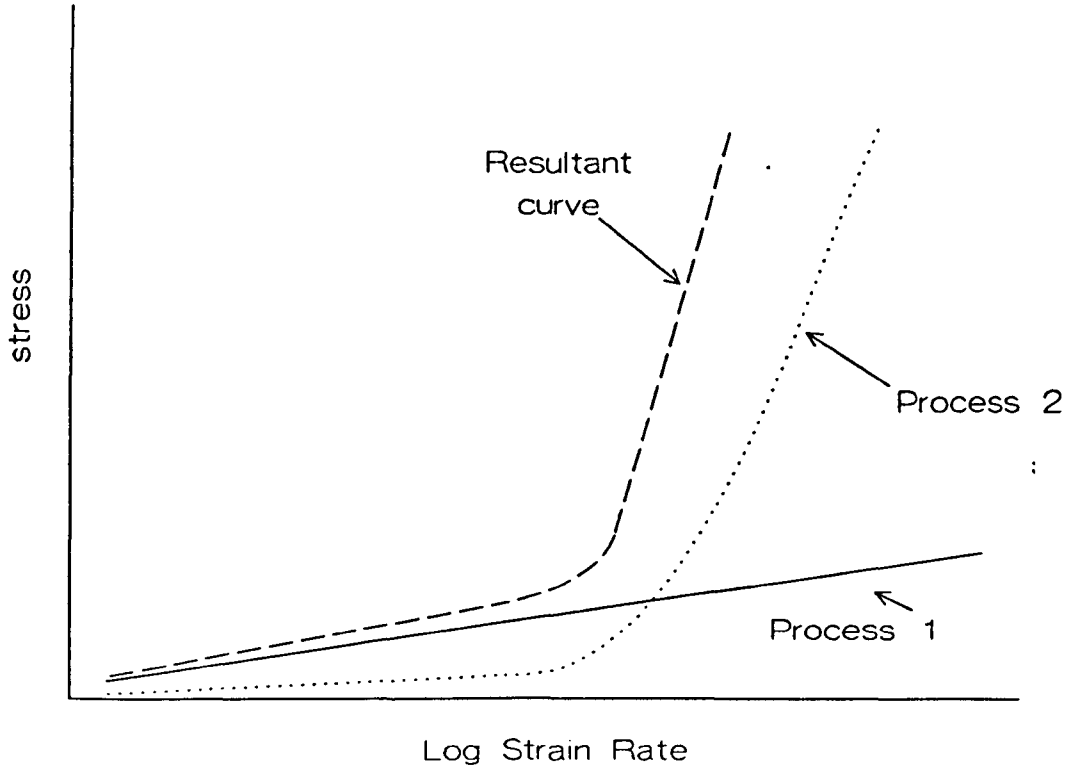

where

$$[\dot{\varepsilon}_0']_n = \dot{\varepsilon}_{0n} \exp\left(\frac{-\Delta U_n}{kT}\right) \qquad (1\cdot8)$$

with n denoting that the parameters belong to process 1 or 2.

This two activated process approach has been used for both the oriented and isotropic states of polyethylene. It should be pointed out however, that although the same model has been used, the activation parameters change dramatically between the isotropic and oriented states.

In the oriented state the spring $E_1$ has generally been shown to have a lower modulus[8] than the spring $E_2$, but for the isotropic material this work found that the modulus of the two springs was, (at least initially), nearly identical.

For both the isotropic and oriented states at low stress levels any deformation will be recoverable because neither dashpot 1 nor dashpot 2 flow and deform permanently. This is because the high viscosity of dashpot 1 prevents it from flowing initially, and spring $E_1$ can drive the weaker dashpot 2 back to zero strain. Once dashpot 1 starts to flow then deformation will be irrecoverable, because its high viscosity makes it practically impossible for it to be driven back by spring $E_2$.

As mentioned earlier it is possible to determine effective parameters by assuming only one process is present. An example is the activation volume, $V_{effective}$. Differentiating equation 1·7 with respect to $\log_{10} \dot{\varepsilon}$ we obtain for high stresses

$$\frac{d\sigma}{d\log\dot{\varepsilon}} = 2\cdot3kT\left(\frac{1}{V_1}+\frac{1}{V_2}\right) \qquad (1\cdot9)$$

so with the definition of activation volume from equation 1·6 we obtain

$$\frac{1}{V_{effective}} = \frac{1}{V_1}+\frac{1}{V_2} \qquad (1\cdot10)$$

**1·4 Fotheringham And Cherry Approach**

Whilst sharing many of the features of the two Eyring process model described previously, the Fotheringham Cherry model is sufficiently different to warrant its full description, and an explanation of the reasons why it was decided to use it to attempt to fit the data.

### 1·4·1 The Yield Work Of Brooks et al.

The Fotheringham and Cherry[16] model was used because of the similarities of some factors of the creep work with the work of Brooks, Duckett and Ward[15] on double yield points in polyethylene. The latter performed work on two of the grades of polyethylene also used in this work, (6007 and 00240). They also went on to use the Fotheringham and Cherry model successfully on 00240. One of the most striking features to emerge in the work was the existence of two yield points in polyethylene, which were found by residual strain experiments.

In these experiments cylindrical samples were compressed in an Instron tensile testing machine at a fixed temperature and strain rate, to a range of applied strain values. They were then left unconstrained for a period of three days, after which the residual strain, (the strain still held by the material), was measured.

The residual strain was then plotted against the applied strain, and a schematic representation of the resulting graph is shown in figure 1·5. For a single yield point this graph would have zero gradient before the yield point, (total elastic recovery), and unit gradient after the yield point, (no recovery). The actual graph shows a third region between these two, a region of partial recovery.

Creep experiments on initially isotropic samples conducted in this investigation appeared also to show these two yield points, as will be described in chapter 4. The first yield point of Brooks et al. coincided with the strain at which the Sherby Dorn plots of the same material made the transition from region 1 to region 2. The second yield point of Brooks et al., (which was shown to be associated with the formation of a sharp neck in a tensile sample), appeared at strains close to those at which creep samples formed a sharp neck.

### 1·4·2 Transient Stress Dip Tests

These were conducted on the quenched and slow cooled morphologies of all three grades using the experimental method of Fotheringham and Cherry[16] which will be described in chapter 2.

In order to gain useful data from these experiments it is necessary to slightly modify the mechanical interpretation of the two process model discussed previously, figure 1·3. In this modification dashpot 1 is assumed to have a much larger viscosity than dashpot 2. It is also assumed that dashpot 1 does not yield. Hence the model collapses to the standard linear solid. Recovery in the model is driven by the first spring $E_1$.

Figure 1·5

Schematic representation of the residual strain experiments of Brooks et al..

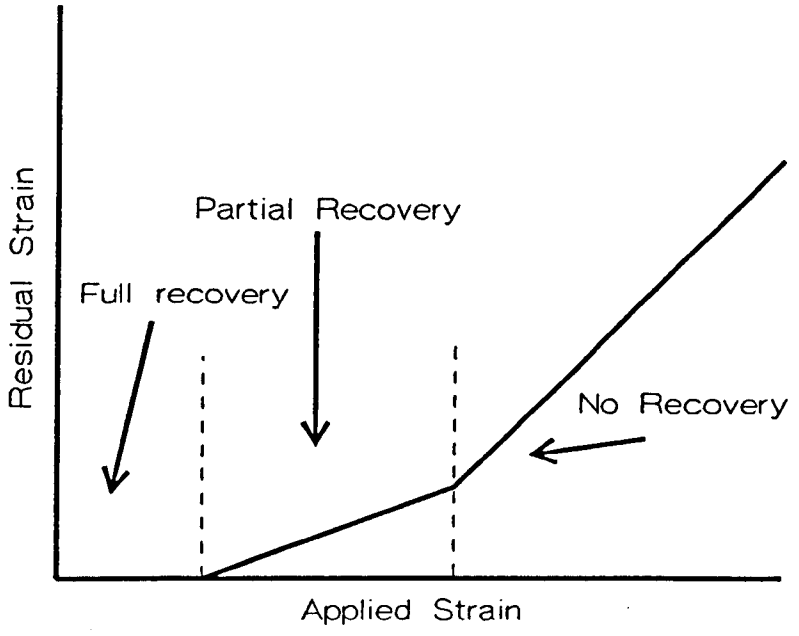

As will be described these tests involve a rapid unloading from one stress, ($\sigma_a$, the applied stress), to another lower stress, ($\sigma_t$, the test stress). The effective stress acting on dashpot 2 is given by

$$\sigma_e = \sigma_t - \sigma_r \qquad (1\cdot11)$$

where $\sigma_r$ is the primary value of interest and is the recovery stress. This is the stress in the spring $E_1$, which drives the recovery process.

It is possible for the test stress to be above, below or equal to the recovery stress.

When the test stress is above the recovery stress the effective stress on dashpot 2 is positive and hence the dashpot will flow with a positive strain rate leading to a relaxation of the test stress with time.

When the test stress is below the recovery stress the effective stress on dashpot 2 is negative. This relaxes to zero as the dashpot flows, and the test stress will increase with time.

When the test stress is equal to the recovery stress the effective stress on dashpot 2 is zero and hence there is no flow in the dashpot. Consequently the stress will remain constant with time.

The appearance of these three conditions on the load time output of the Instron tensile testing machine are shown in figure 1·6.

Thus by searching for the value of the test stress, $\sigma_t$, at which the stress remains constant it is possible to determine the stress in the spring $E_1$, which is $\sigma_r$.

### 1·4·3 Fotheringham And Cherry Approach To Modelling

Having separated the two stress components by the transient dip method the strain rate dependence of each component can be studied. It will be shown that the conventional Eyring formulation does not work well and so it was decided to use the Fotheringham and Cherry co-operative jump approach to see if it provided a better explanation.

This approach was used by Fotheringham and Cherry[16] on a linear polyethylene, and by Brooks[14] and Brooks et al.[15] on the 00240 grade of polyethylene. It involves fitting the strain rate to the effective stress determined by transient stress dip tests.

Fotheringham and Cherry considered the thermally activated transition of a deformation entity across an energy barrier of height Q under the influence of an "effective" or "internal" shear stress, ($\sigma_e$).

Figure 1·6

Schematic representation of the chart recorder output of an Instron during a transient stress dip test, showing the responses for different $\sigma_t$ and $\sigma_r$ conditions.

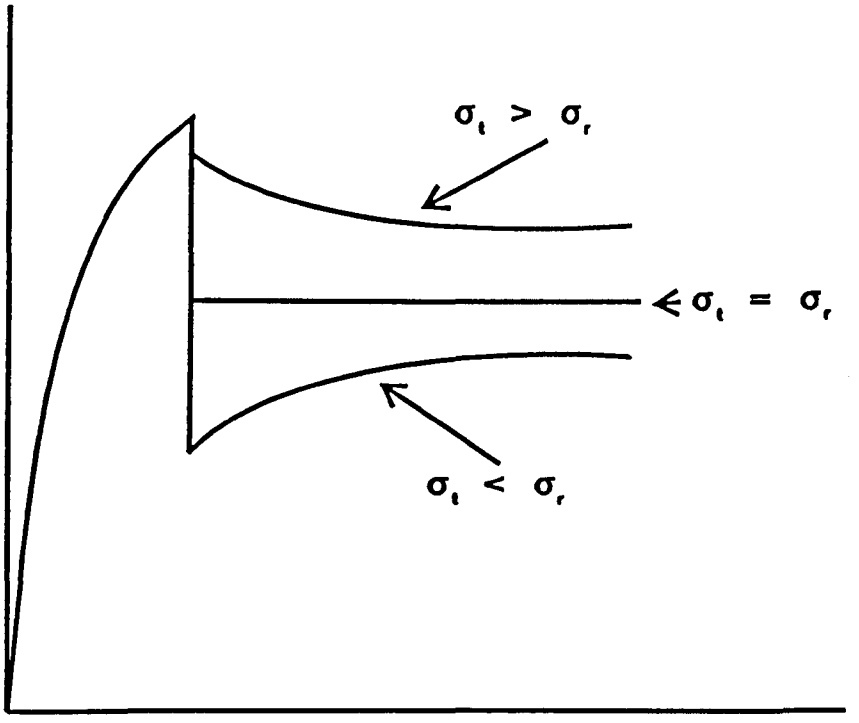

Under the defined recovery stress conditions, (recovery stress equal to applied stress, giving zero strain rate), the energy states on either side of the barrier are equivalent, and hence the probability of the entity being either side of the barrier will be equal.

Under the action of an extra stress, $\sigma_e$, the energy barrier is biased, (see figure 1·1), and the resulting increase in transitions caused by this biasing can be determined using the Eyring model.

$$R = R_0 \exp\left(\frac{-Q}{kT}\right)\sinh\left(\frac{V^*\sigma_e}{2kT}\right) \qquad (1\cdot12)$$

where $V^*$ is the activation volume , Q the activation energy and $R_0$ is a function of temperature which includes the translation partition function and the transmission coefficient.

Thus the overall probability per unit time of a single deformation entity making the transition in the direction of the biasing stress is

$$P_1 = P_0 \exp\left(\frac{-Q}{kT}\right)\sinh\left(\frac{V^*\sigma_e}{2kT}\right) \qquad (1\cdot13)$$

It is proposed that this is a co-operative jump of an average of n deformation entities which make the transition at any one time. The probability of n entities jumping per unit time is

$$P_n = P_0 \exp\left(\frac{-nQ}{kT}\right)\sinh^n\left(\frac{V^*\sigma_e}{2kT}\right) \qquad (1\cdot14)$$

If the macroscopic strain resulting from each co-operative jump is $\varepsilon_0$, then the strain rate is given by

$$\dot{\varepsilon} = K_0 \exp\left(\frac{-nQ}{kT}\right)\sinh^n\left[\frac{V^*\sigma_e}{2kT}\right] \qquad (1\cdot15)$$

where $K_0$ is a constant dependent upon $P_0$, $\varepsilon_0$ and n.

For a single temperature equation 1·15 can be simplified to

$$\dot{\varepsilon} = K_T \sinh^n\left(\frac{V^*\sigma_e}{2kT}\right) \tag{1·16}$$

where

$$K_T = K_0 \exp\left(\frac{-nQ}{kT}\right) \tag{1·17}$$

### 1·4·4 Fitting

Equation 1·16 can be rearranged to give

$$\sigma_e = \frac{2kT}{V^*}\sinh^{-1}\left(\frac{\dot{\varepsilon}}{K_T}\right)^{1/n} \tag{1·18}$$

This is then fitted to a master curve of $\frac{\sigma_e}{T}$ against ln $(\dot{\varepsilon})$ data at a single temperature by a least squares fitting routine.

The master curve is produced by shifting the various data sets produced by performing experiments at different temperatures to a single reference temperature. The data sets are shifted parallel to the strain rate axis, so that all the data sets lie on a single curve. This shifting is done by eye.

### 1·4·5 Activation Energy

At high stresses equation 1·15 can be approximated to

$$\dot{\varepsilon} = K_0 \exp\left(\frac{-nQ}{kT}\right)\exp\left(\frac{nV^*\sigma_e}{2kT}\right) \tag{1·19}$$

or

$$\dot{\varepsilon} = K_0 \exp\left\{\frac{n}{kT}\left(\left[\frac{V^*\sigma_e}{2}\right] - Q\right)\right\} \tag{1·20}$$

so

$$\ln \dot{\varepsilon} = \ln K_0 + \frac{n}{kT}\left\{\left(\frac{V^*\sigma_e}{2}\right) - Q\right\} \tag{1·21}$$

where ln $K_0$ is a constant.

When the curves are shifted to provide the master curve we get a shift factor, a, defined as

$$a = \ln \dot{\varepsilon}_{T_1} - \ln \dot{\varepsilon}_{T_2} \tag{1·22}$$

where $T_2$ is the higher temperature and $T_1$ is the lower temperature.

Thus

$$a = \frac{nV^*\sigma_{e_1}}{2kT_1} - \frac{nQ}{kT_1} - \frac{nV^*\sigma_{e_2}}{2kT_2} + \frac{nQ}{kT_2} \tag{1·23}$$

But since the shift is parallel to the strain rate axis

$$\frac{\sigma_{e_1}}{T_1} = \frac{\sigma_{e_2}}{T_2} \tag{1·24}$$

and thus

$$a = \frac{nQ}{k}\left(\frac{1}{T_2} - \frac{1}{T_1}\right) \tag{1·25}$$

Since the $T_1$ is the temperature to which everything is shifted, it is constant. Thus a plot of a against $1/T$, should have a linear gradient of $\frac{nQ}{k}$. Hence a value for nQ can be derived.

## 1·5 References and Bibliography

Chemistry in Context, 2nd Edition, Hill, G.C. and Holman, J.S., Nelson, 1987

1. Sherwood, M., Chemistry in Industry, No. 6, (1983), 237
2. Reynolds, P.T., and Lawrence, C.C., J. Mat. Science, **26**, (1991), 6197
3. Rose, L.J., Channell, A.D., Frye, C.J. and Capaccio, G., J. App. Polymer Sci., **54**, (1994), 2119
4. Cawood, M.J., private communication, 1991
5. O'Connell, P., private communication, 1993
6. O'Connell, P, Bonner, M.J., Duckett, R.A. and Ward, I.M., Polymer, **36**, (1995), 2355
7. Wilding, M.A. and Ward, I.M., J. Polym. Sci., Polymer Physics Edition, **22**, (1984), 561
8. Wilding, M.A. and Ward, I.M., J. Mat. Sci., **19**, (1984), 629
9. Rasburn, J., Klein, P.G., and Ward, I.M., J Polym. Sci., Polymer Physics Edition, **32**, (1994), 1329
10. Karpov, Y.A., Bitskii, A.E., Strel'tses, B.V. and Yel'yashevich, G.K., Polymer Science USSR, **33**, (1991), 1236, (translated into English from the original in Vysokomolekulyarnye Soedineniya Seriya A, **33**, (1991), 1334)
11. Findley, W.N., Polymer Engineering and Science, **27**, (1987), 582
12. Truss, R.W., Clarke, P.L., Duckett, R.A. and Ward, I.M., J Polym. Sci., Polymer Physics Edition, **22**, (1984), 191
13. Dixonstubbs, P.J., J. Mat. Sci., **16**, (1981), 389
14. Brooks, N.W., PhD Thesis, University of Leeds, 1993
15. Brooks, N.W., Duckett, R.A. and Ward, I.M., Polymer, **33**, (1992), 1872
16. Fotheringham, D.G. and Cherry, R.W., J. Mat. Sci., **13**, (1978), 951
17. Mechanical Properties of Solid Polymers, 2nd Edition, Ward I.M., Wiley, 1983
18. Cowking, A., J. Mat. Sci., **10**, (1975), 1751
19. Sherby, O.D. and Dorn, J.E., J. Mech. Phys. Solids., **19**, (1956), 165
20. Eyring, H.J., J. Chem. Phys., **4**, (1936), 283
21. Lefbvre, J.M. and Escaig, B., J. Mat. Sci., **20**, (1985), 438
22. Coates, P.D., Phd Thesis, University of Leeds, 1976

# Chapter 2

# Experimental Techniques

## 2·1 Introduction

This chapter will introduce the three grades of polyethylene used in this investigation, giving their physical characteristics prior to the production of isotropic sheets. It will also define the terms strain rate, strain and natural draw ratio as they were used in this work.

The production of isotropic sheets and test samples will be described and the crystallinity, yield stress and natural draw ratio of these isotropic sheets will be presented. The method used to produce oriented samples will be described, as will some of the physical characteristics of the material in the oriented state.

Whilst the experimental methods used were relatively simple, they and the equipment used to gather the data which will be presented in the following chapters will also be described.

## 2·2 Materials

Three grades of polyethylene have been studied. They are HD 6007 EA, a linear high density material, HD 5502 XA and 00240, both lightly branched copolymers, with comonomers of n-hexene and n-ethene, which produce butyl branches off the polyethylene backbone. All materials were supplied by BP Chemicals Ltd, Grangemouth.

Their physical data are presented in Table 2·1 below.

| Grade | $\overline{M_W}$ | $\overline{M_N}$ | Branch Content (per 1000 carbons) | Density (Quenched) |
|---|---|---|---|---|
| 6007 | 131,000 | 19,100 | less than 0.1 | 947.1 $kgm^{-3}$ |
| 5502 | 156,000 | 17,000 | 1 to 2 | 943.1 $kgm^{-3}$ |
| 00240 | 206,000 | 12,900 | 6.2 | 932.6 $kgm^{-3}$ |

**Table 2·1**

Table showing the physical properties of the three grades of polyethylene studied.

The density data for HD 6007 EA and HD 5502 XA were supplied by Dr P. O'Connell, all other data were supplied by BP.

## 2·3 Definitions

Strain Rate

Unless explicitly stated otherwise in the text, any strain rate quoted will be a true strain rate calculated using the following equation.

$$\dot{\varepsilon} = \frac{1}{l}\frac{dl}{dt} \qquad (2\cdot1)$$

Where $l$ is the current length of the specimen and $\frac{dl}{dt}$ is the rate of change of the length with time.

Strain

The strain quoted will either be percentage strain or draw ratio. Percentage strain is used for the isotropic material, with fully isotropic material having zero strain. It is usually calculated directly from the increase in the length of the isotropic sample, using the following formula.

$$\varepsilon = \left(\frac{l}{l_0} - 1\right) \times 100 \qquad (2\cdot2)$$

Where $l$ is the current length and $l_0$ is the original length.

Draw ratio is used for the oriented material, and is always referenced to the fully isotropic material, which has a draw ratio of 1. It is calculated by using the following equation

$$\lambda = \frac{l}{l_0} \qquad (2\cdot3)$$

Where $l$ is the current length of the sample and $l_0$ is the length of the isotropic sample.

The definition of percentage strain is not strictly consistent with the definition of true strain rate given in equation 2·1, (a strictly consistent definition would be

$\varepsilon = \int \frac{dl}{l} = \ln \frac{l}{l_0} = \ln \lambda$), but since the percentage strain is only used for the isotropic material any differences are minor.

Natural Draw Ratio

This is the strain present in the material immediately it has passed through the neck, before any further plastic deformation has taken place. It was determined by one of two methods.

(1) An isotropic dumbbell sample was prepared and ink dots were placed a known distance apart down the gauge length. The sample was then drawn until the neck had travelled through all the gauge length and was moving into the shoulders of the dumbbell, at which point the stress was removed. The separation of the ink dots was measured after a period of twenty-four hours at zero stress and the draw ratio calculated from the average of all the draw ratios obtained for each pair of ink dots. The twenty-four hour waiting period allowed the specimen to relax so that the dimensions did not change significantly whilst the separation of the ink dots was being determined.

(2) An isotropic dumbbell sample was prepared and marked as above. However instead of letting the neck move right through the material the drawing was stopped once a single pair of dots had the neck passed through them, and the natural draw ratio was determined from these, after the twenty-four hour relaxation period had passed. This method was generally used for the slow cooled morphologies which were more difficult to draw.

These two methods produced results which were equivalent within the associated error limits.

## 2·4 Sample Preparation, Isotropic Sheets

Capaccio[1] et al. established that varying the initial thermal treatment of a linear polyethylene during processing produced drastic changes in the initial morphology. They demonstrated that a large change occurred in the crystalline content of the isotropic polymer if the compression moulded sheets produced were slow cooled to 110°C before quenching to 20°C in a water bath, rather than quenching straight from 160°C.

Consequently in order to produce two different morphologies for testing the quench cooling and slow cooling treatments described below were chosen.

Two differing morphologies were required since the work of Coates[2] had shown that a unique relationship existed between true stress, true strain rate and draw ratio for

a range of materials, and this work intended to investigate whether these relationships were independent of the initial morphology. That is it was intended to investigate whether the act of drawing the material to its natural draw ratio would destroy any dependence of the behaviour of the material on its initial morphology.

The polymers were supplied in the form of pellets by BP Chemicals Ltd, Grangemouth.

In order to prepare isotropic sheets of the material, a quantity of the pellets were placed between clean brass plates. Initially brass spacers 0·1 mm thick were placed at the extreme edges of the plates, but these spacers damaged easily, and it was found that high quality sheets could be produced without them. These brass plates were then placed between the platens of a hot press pre heated to 160°C. Placing cold brass plates onto the hot platens reduced the temperature of the platens. The temperature was allowed to stabilise back to 160°C before contact pressure was applied to the press.

This contact pressure was held for five minutes before being increased steadily to a value of 20 tons on a four inch diameter ram. This pressure was held for five minutes before the brass plates were cooled at one of two rates:

Quench cooling.

In quench cooling the brass plates were removed from the platens of the hot press and placed immediately into a bath of water at room temperature.

Slow cooling.

In slow cooling the brass plates were left in the hot press. The platens of the hot press were cooled at a controlled rate of 2°C per minute by a mist of water in compressed air which was injected into them. This cooling continued until the temperature of the platens had dropped to 70°C, when the brass plates were removed and opened, and the polyethylene sheet allowed to cool to room temperature naturally in air.

The resulting sheets were between 0·15 and 0·30 mm in thickness, and approximately 30 cm in diameter, and were marked with a permanent OHP marker pen before being stored, out of direct sunlight, in air in a temperature controlled, (20±2°C), laboratory.

**2·5 Characterisation**

The percentage crystallinity of the material was determined by differential scanning calorimetry, and is shown in Table 2·2 below. These percentage crystallinity results were derived assuming that a 100% crystalline sample would have a melting peak area[3] of 288 $Jg^{-1}$. It is evident that a much more crystalline isotropic sample was produced by the slow cooling method.

The values of lamella thickness are also shown in Table 2·2, and were obtained by rearranging the Thomson equation, (equation 2·4).

$$T = T_0\left\{1-\left(\frac{2\sigma L}{H_m}\right)\right\} \qquad (2\cdot4)$$

to give

$$L = \frac{T_0 K_0}{T_0 - T} \qquad (2\cdot5)$$

where

$$K_0 = \frac{2\sigma}{H_m} \qquad (2\cdot6)$$

where $\sigma$ is the surface energy of the basal face, $(70\times10^{-3}\ Jm^{-2})^3$, $H_m$ is the enthalpy of melting per unit volume, $(288\times10^{6}\ Jm^{-3})^3$, $T_0$ is the equilibrium melting temperature of an infinite crystal, $(414{\cdot}5\ K)^3$, and L is the lamella thickness. The lamellar thickness values were derived with T being assigned the value of the temperature at which the maximum of the melting peak occurred.

The yield stress, measured at the conventional yield point of zero gradient on the load time output of the Instron, of 16 mm gauge length samples drawn at 5 mm $min^{-1}$, and natural draw ratio, (drawn at the standard draw rates), rank with the percentage crystallinity and lammella thickness as shown in Table 2·2.

| Grade | Yield Stress (MPa) | Natural Draw Ratio | Percentage Crystallinity | Lamella Thickness (Å) |
|---|---|---|---|---|
| 6007S | 30·7 ±·1 | 10·5 ± 0·5 | 77·2 ± 1·5 | 360 ± 7 |
| 5502S | 28·3 ±·2 | 9·1 ± 0·5 | 68·4 ± 1·4 | 249 ± 5 |
| 6007Q | 21·3 ±·3 | 8·4 ± 0·5 | 64·3 ± 1·3 | 204 ± 4 |
| 5502Q | 19·5 ±·4 | 6·8 ± 0·3 | 60·1 ± 1·2 | 172 ± 4 |
| 00240S | 17·1 ±·3 | 6·4 ± 0·3 | 54·6 ± 1·1 | 151 ± 3 |
| 00240Q | 14·9 ±·2 | 5·2 ± 0·3 | 49·2 ± 1·0 | 122 ± 2 |

**Table 2·2**

Table showing yield stress, natural draw ratio percentage crystallinity and lamellar thickness for the three grades of polyethylene studied.

Dumbbell shaped cutters were used to cut samples from the isotropic sheets. These cutters had a width of 2 mm and the straight parallel sided sections were either 16 mm or 81 mm in length.

For isotropic creep tests the 81 mm gauge length samples were generally used.

For drawing of the isotropic sheet the 16 mm gauge length samples were used unless the required strain rate was too low to run the Instron at a reasonable speed, in which case the 81 mm gauge length samples were used instead.

## 2·6 Sample Preparation, Oriented Specimens

Oriented material was prepared by cold drawing the dumbbell shaped specimens on an Instron tensile testing machine. In order to keep conditions as uniform as possible two standard nominal strain rates were chosen for drawing, and these are shown in Table 2·3 below.

| Material | Nominal Strain Rate ($sec^{-1}$) |
|---|---|
| Quenched | 0·005 |
| Slow Cooled | 0·0002 |

**Table 2·3**

Table showing the standard nominal strain rates used to draw the material.

These nominal strain rates were developed initially for the quenched materials, when the materials were drawn with a range of differing nominal strain rates. The linear draw ratio, (calculated from the change in separation of ink dots placed down the length of the isotropic sample), was compared to the area draw ratio, (calculated from the change in cross sectional area). The highest nominal strain rate which gave equivalent values of these two draw ratios was chosen as the standard draw rate.

Higher drawing rates produced differing draw ratios when calculated by these two methods, with the linear draw ratio being higher than the area draw ratio. This indicates that voids were formed within the material at these higher draw rates.

The draw rates for the slow cooled materials were arrived at by lowering the draw rates for the quenched materials until approximately 50% of the specimens produced usable lengths of oriented material. It would have been preferable to draw at lower rates, but this would have made the production of samples for further testing unreasonably slow.

The drawn samples were attached to a piece of card by one end, (either by the shoulder area or an undrawn piece of material), and left in an unconstrained state in a temperature controlled, (20±2°C), laboratory. The drawn samples were left for a period

of 24 hours before use. This allowed some ageing to occur, (a full investigation into ageing effects was beyond the scope of this work), but ensured that a common amount of ageing occurred so that all results were comparable. Any samples that were not used after this 24 hour period were discarded.

The percentage crystallinity of the drawn samples was measured using differential scanning calorimetry in the same manner as for the isotropic samples, and the same value of 288 $Jg^{-1}$ was assumed for the area of the melting peak of a 100% crystalline sample. The percentage crystallinities of the drawn specimens compared to the isotropic sheets is shown in Table 2·4 below.

| | Quenched | | Slow Cooled |
|---|---|---|---|
| | Isotropic | Oriented | Isotropic |
| 6007 | 64·3 | 69·1 | 77·2 |
| 5502 | 60·1 | 63·3 | 68·4 |
| 00240 | 49·2 | 50·9 | 54·6 |

**Table 2·4**

Table showing the percentage crystalline content for each grade of polyethylene in both the isotropic and oriented states.

It is apparent that in all cases drawing slightly increases the percentage crystallinity of the material.

## 2·7 Creep

Creep experiments on both oriented and isotropic material were performed on dead loading creep rigs designed and built within the Polymer research group of the Physics Department at the University of Leeds.

The rigs are housed in a temperature controlled laboratory at 20±2°C.

Of the four creep rigs used three were built specifically for this investigation, and were of an improved design. This design is shown schematically in figure 2·1, and incorporated a long throw linear voltage displacement transducer, (with ± 25 mm of travel in the linear region), in a movable carrier. The carrier was able to drop in four steps of around 20 mm each. Each carrier was individually calibrated by using a cathetometer to measure the displacement of the top of the transducer as the carrier was dropped.

Figure 2·1

Schematic representation of the long throw creep rigs.

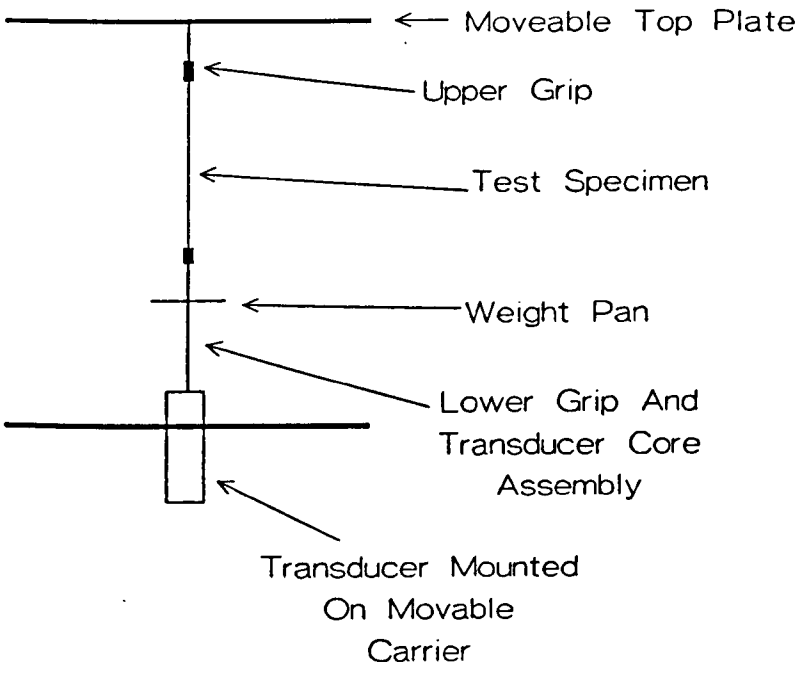

The fourth creep rig was of an older design, with a transducer of only 15 mm of travel available in the linear region, and without the movable carrier. However this rig was equipped with an environmental chamber which was capable of maintaining temperatures in excess of room temperature, in the temperature range from 20°C to 70°C, with a variation of less than ±0·5°C at 20°C and less than ±1°C at 70°C. It was also capable of exceeding 100°C, but the range above 60°C was not used.

Both designs of creep rig shared common features.

The top plate, to which the upper grip assembly of the rig was attached, was capable of moving linearly in the vertical axis by approximately 150 mm. This allowed the position of the upper grip to be adjusted so that the maximum amount of transducer travel could be obtained for a wide range of specimen gauge lengths. During a test this movable plate was held securely in place by lock screws which tightened against the guides upon which the plate moved.

The weight pan was designed so that it was not permanently fixed to the lower grip assembly. A support for the weight pan consisting of an arm capable of vertical movement on a rack system was present on each rig. This support meant that the mass needed to produce the required stress level in the sample could be placed on the weight pan before the weight pan was lowered onto the lower grip assembly and ensured that all the stress was applied at the same time. It was also possible to set the support so that it stopped the applied mass before it hit the transducer in the event of the sample failing. This prevented damage to the transducers.

The long throw transducers were calibrated on the creep rigs every few months by following the travel of the lower grip assembly with a cathetometer as the transducer core was moved and recording the output voltage of the transducer. This allowed the change in output voltage with displacement to be calculated for the control programme of the computer.

The short throw transducer was calibrated on the creep rig every time a test was performed, by means of a vernier scale calibrated in 0·02 mm divisions and a subroutine in the control programme which automatically collected the voltage output from the transducer and calculated the voltage change with displacement once the distance the transducer had been moved had been entered. The linearity of this transducer was checked every few months by using the same method as used to calibrate the other three transducers.

Specimens for the creep tests were cut from the parallel sided sections of the dumbbells for isotropic tests, and from the section with the most uniform draw ratio, (derived from the change in separation of ink dots placed a known distance apart on the isotropic dumbbell prior to drawing), for oriented material.

Gauge lengths were typically 60 to 70 mm for isotropic experiments and 70 to 100 mm for oriented materials. These gauge lengths meant that the sample underwent deformation in plane stress conditions, apart from very close to the grips, where the conditions changed to plane strain due to the constraining effects of the grips.

Initial tests were conducted with ink lines drawn across the width of the specimen in order to check that deformation was occurring homogeneously across the sample.

The computer which monitored the creep rigs ran a control program which initialised the timing of the test and data recording when it sensed a 0·2% change in the nominal strain of the specimen. This automatic start to recording ensured a very good zero point and was very easy to use. Once data capture had begun the program automatically recorded data either after the specimen had changed nominal strain by ±0·2%, or at exponentially increasing time periods, (whichever occurred first). The program was able to monitor up to four creep rigs running simultaneously, allowing maximum use to be made of the available equipment.

The loads used were generally less than 1250g, with the maximum load used being in the region of 1500g. The creep rigs were built to withstand loads of 5000g, so machine deflection was negligible, (equivalent to less than 0·2% strain with the gauge lengths commonly used in this work), and has been ignored.

The samples were not conditioned, so that some settling of the sample into the grips was inevitable. In order to measure the magnitude of this settling a highly oriented specimen of 6007 was taken and placed into the grips of the creep rig. An ink dot was placed at each end of the sample close to the grips and the distance from the ink dots to the grips was measured by using a travelling microscope.

The sample was then loaded in the rig with a 1250g load applied for 60 seconds. The load was then removed and the sample allowed to recover for 1200 seconds. The separation of the grips and ink dots were then remeasured using the travelling microscope.

The total change in separation of the grips and ink dots was 0·3 mm. This compared to a predicted maximum of 0·03 mm from creep alone. Thus the slippage in the grips is of the order of 0·27 mm.

A highly oriented sample was used since the creep tests conducted before this check was performed indicated that a highly oriented sample would undergo the minimum amount of deformation due to creep, so that any change in the separation of the grips and the ink dots would be due to slippage in the grips rather than creep of the sample in the region between the grips and the ink dots.

In straight creep experiments this amount of slippage can be neglected, since it is of the order of the error in measuring the initial gauge length, and much more creep takes place.

The creep rigs could effectively cover a strain rate range between $10^{-9}$ $sec^{-1}$ and $10^{-3}$ $sec^{-1}$.

At low strain rates, below $10^{-9}$ $sec^{-1}$, the time interval between individual readings became too long, (in some cases several weeks would have elapsed before another reading was taken), to justify the continued use of the creep rig on the test.

At high strain rates, above $10^{-3}$ $sec^{-1}$, the limitations of the internal clock in the monitoring computer became apparent. At these higher strain rates the time taken for the specimen to extend by 0·2% was less than one second. Due to inefficiencies in the monitoring program, caused mainly by the computer language utilised to run it, nearly a complete second was required to scan all the channels, recognise that a reading should be taken and then write all the data to disk. Thus the computer attempted to take a reading whilst it was still processing data from the previous reading, which resulted in inaccurate time and strain readings being recorded.

The control programme gathered time and strain data which was stored as an ASCII data file and imported into a spreadsheet, (Aseasyas versions 4 and 5), in order to perform the data analysis. In order that the duration of the experiments may be grasped sample strain versus time plots for 00240 and 6007 are shown in figure 2·2. These are for oriented samples at "medium" stress levels. Higher stress levels had lower durations, lower stress levels could take considerably longer. It is noticeable in the case of 00240 that the graph is approaching the horizontal, and so the period between readings was increasing in such a way that it became unfeasible to continue the test, (since each 0·2% increase in strain required a significantly longer time period to occur than the one before it).

Figure 2-2

Strain versus time plots for typical creep tests on oriented 6007 and 00240.

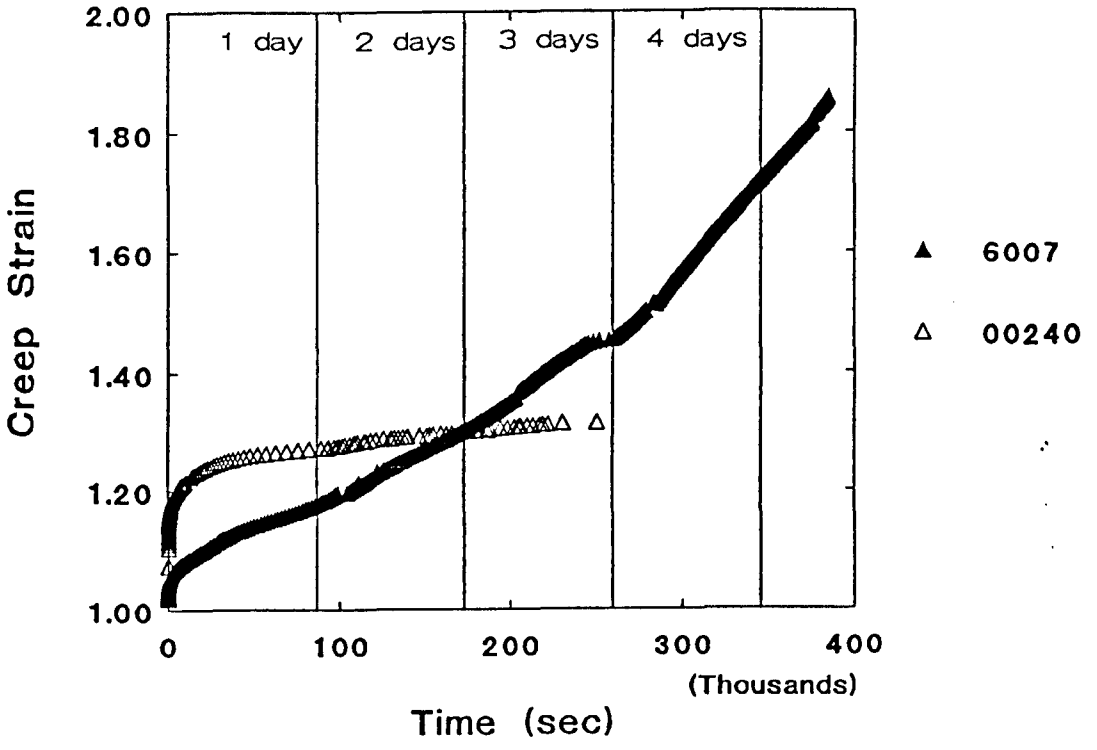

Since the initial cross-sectional area, gauge length, initial strain, (draw ratio) and applied stress were known for the sample, the current length, strain, (draw ratio), true strain rate and true stress could be calculated for the sample for any of the collected data points. It was assumed that the volume of the sample was conserved when making these calculations. In actual fact there would have been a small change in volume as the test progressed, due to the change in crystallinity as the strain increased, however this change was neglected. The method used to determine the true strain rate was a simple arithmetic one, equation 2·5

$$\dot{\varepsilon} = \frac{1}{l_2}\left(\frac{l_1 - l_2}{t_1 - t_2}\right) \qquad (2\cdot5)$$

Where $l_1$ is the initial length, $l_2$ the final length, $t_1$ the initial time and $t_2$ the final time.

A graphics package, (Easyplot), was used to place cross-hairs on data points in the graphs produced in order to read off either strain rate at a chosen strain, or strain at a chose strain rate. This method for picking out individual data points was as quick and efficient as any other method.

**2·8 Recovery**

Creep recovery experiments were conducted on the creep rigs described earlier and the specimens for recovery were prepared in the same manner as a creep specimen and were then loaded into the grips of a creep rig, and the system set running.

When a pre chosen strain, (draw ratio), had been reached, (the control programme of the computer monitoring the creep rigs was set up so that the data could be reviewed periodically), the mass applied via the load pan was removed. This left the sample effectively unloaded, (there was still a small load of around 35 to 40g left on the sample due to the bottom grip assembly and transducer core). The computer continued to monitor the output of the transducer throughout recovery.

The experiments were halted when the recovery strain rate approached the lower limit of the creep rig's strain rate range.

All the initial variables, (gauge length, initial stress level, initial strain and initial cross sectional area), were known before the test was started, so that data analysis could be carried out in the same way as for ordinary creep.

Deformation was assumed to be homogeneous. Any isotropic samples which necked were not analysed since the stress and strain rate within the neck could only be monitored by photographic methods beyond the scope of this work.

The amount of slippage that takes place in the grips during the initial deformation section of the test is important in recovery work. It places a limit on the resolution of the machine. This limit was calculated and tests which recovered to this limit were treated as having recovered fully. Tests which did not recover to this limit were treated as having been deformed permanently.

**2·9 Instron Experiments**

On occasion it was required to perform experiments either to determine yield stresses or provide stress data at strain rates outside the envelope of strain rates covered by the creep rigs. In these situations an Instron tensile testing machine was used.

The load cell on the Instron was calibrated by hanging known masses on to the grip attached to it, and these were used either to set the full scale deflection of the chart recorder, (once the zero point had been adjusted), or to provide reference data points for the computer.

When using a chart recorder the drive speed of the paper was known, and hence the time elapsed since the test was started at any point on the output curve could be calculated, and from this the position of the crosshead could be derived.

The computer recorded the data at specified time intervals, so the same determination of crosshead position could be made.

To provide yield stress data a crosshead speed was selected and an isotropic sample loaded into the machine. The data were collected from the load output of the load cell, which was recorded either on computer or chart recorder.

To provide stress data at a particular strain and strain rate was more complicated. The test specimen was prepared in the usual way, (i.e. it was cold drawn for an oriented sample).

When an older Instron with fixed selectable speeds was used the specimen was marked with the appropriate gauge length, (determined by correcting the length obtained from equation 2·1 to take into account the necessary increase in strain of the sample), to which it was loaded into the Instron in order to achieve the required strain rate.

When a newer Instron with electronic control and infinitely variable speed control was used the gauge length was measured and the speed set accordingly to give the required strain rate.

Stress data were obtained by first determining the load output at the required point of the test. This load was then converted to a stress by using the following formula.

$$\sigma = \frac{Load}{Area} \qquad (2\cdot7)$$

The load in kg was converted to Newtons by multiplying by g. The area was corrected from the known initial cross sectional area of the test specimen to take into account the increase in strain. Conservation of volume was again assumed.

## 2·10 Transient Stress Dip Tests

These were performed using the method of Fotheringham and Cherry[4], and involved first straining a sample and then immediately removing some of the applied strain and allowing it to relax.

The test specimens, either isotropic or oriented, were prepared and loaded into the grips of an Instron tensile testing machine.

Isotropic samples were prepared in the usual manner as for a creep test. Oriented samples were prepared by cold drawing the dumbbell on the same Instron as the test was to be performed on, but after the desired draw ratio had been achieved the crosshead was returned a known amount and the sample left in an unstrained state for 10 minutes before starting the test. This allowed a more accurate determination of the draw ratio. Comparison of the applied stress and strain rate data with equivalent data from creep work where the sample had been left for 24 hours to recover showed no appreciable difference, (stress relaxation experiments showed that practically all relaxation occurred in the first minute).

The crosshead speed of the Instron was selected and movement of the crosshead was started. When the sample had reached a predetermined value of strain the crosshead was reversed for a known distance. The speed at which the crosshead was reversed was set at five times the speed at which it had been travelling down.

The crosshead was then brought to a halt and the behaviour of the load output from the load cell was observed. The tests involved searching for the point at which the load output remained constant with time. The reason for this has been discussed earlier, (section 1·3·3). The distance over which the crosshead was returned was varied in order to achieve this. A schematic representation of the load output against time, and the necessary corrections to the return distance of the crosshead are shown in figure 2·3.

Figure 2-3

Schematic representation of the chart recorder output of an Instron during a transient stress dip test, and the action taken to obtain the condition of $\sigma_r = \sigma_t$.

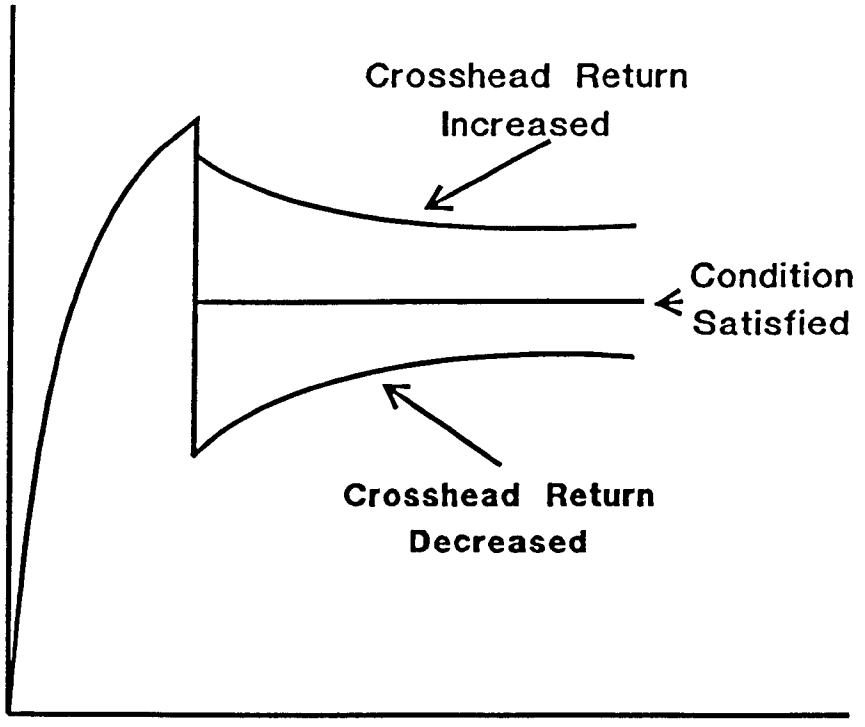

## 2·11 Creep Data Analysis And Sherby Dorn Plots

Once the values of true stress, strain and true strain rate had been calculated using a spreadsheet, for all the time data points collected during a test conducted using the technique described previously, the data were plotted in the manner of Sherby and Dorn[5].

The resulting Sherby Dorn plots were then transferred into a graphics package which had a facility to place crosshairs on the graph to give the values of the x and y co-ordinates at their centre. This facility was used to collect the strain rate data at specific strains or strain data at specific strain rates and proved to be faster, more accurate and more reliable than any alternative method.

## 2·12 Reproducibility

The reproducibility of the experiments was very good. An example of this is shown in the Sherby Dorn plots of figure 2·4, where the only special care taken was to ensure that the applied stress levels were as close to each other as possible.

Figure 2-4

A check of the reproducibility of creep experiments for oriented 6007 in the quenched morphology.

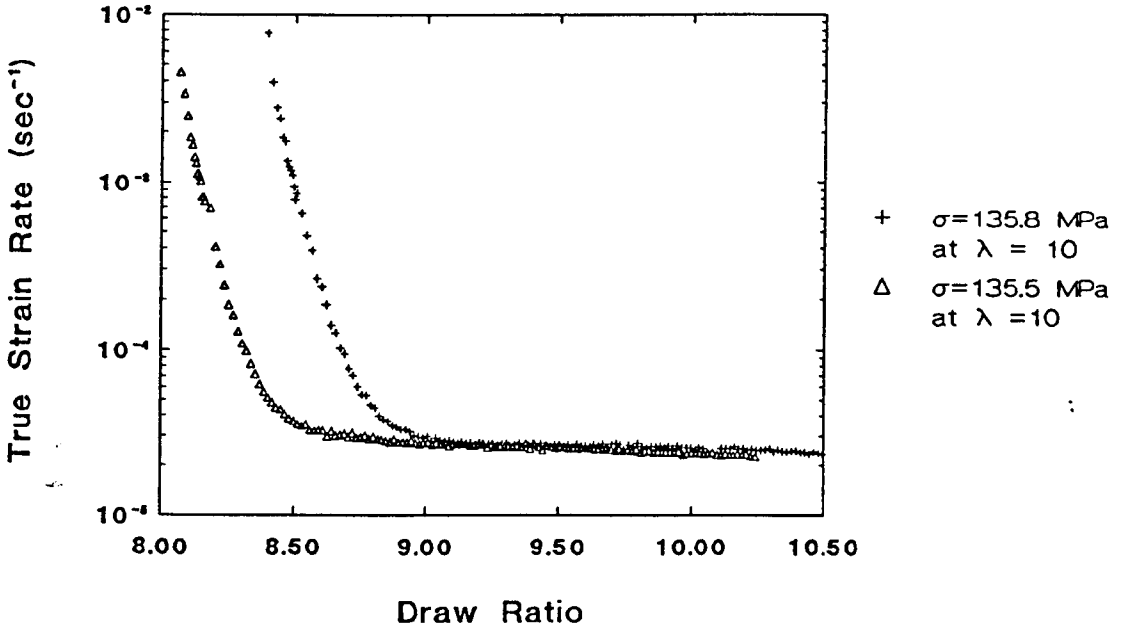

## 2·13 References

1. Capaccio, G. and Ward, I.M., Polymer, **15**, (1974), 233
2. Coates, P.D. and Ward, I.M., J. Mat. Sci., **13**, (1978), 629
3. Alberola, N., Cavaille, J.Y. and Perez, J., J. Polym. Sci., Part B, **28**, (1990), 569
4. Fotheringham, D.G. and Cherry, B.W., J. Mat. Sci., **13**, (1978), 951
5. Sherby,O.D. and Dorn, J.E., J. Mech. Phys. Solids, **19**, (1956), 165

# Chapter 3

## The Oriented State

## 3·1 Introduction

The plastic deformation behaviour of a polymer is an important consideration for engineers and designers, since it governs the long term viability of any structure which experiences constant or even cyclic loading. For example it would be foolhardy to manufacture something as expensive and essential as a bridge out of a material which is going to extend to many times its original length under the kinds of loads associated with just supporting its own weight. Thus there is a great deal of need for the designer to have this long term plastic deformation behaviour data to hand. And by the same token there is a need for the scientist to understand the underlying physical principles and molecular mechanisms which influence and control this deformation, in order that better and more able materials can be produced in the future.

The oriented state of polymers is important in engineering terms because it can generally support greater loads than the isotropic state, that is the force required to break the polymer is higher. There is an increasing desire to support loads and reinforce materials using materials that are less bulky than the traditional engineering materials, such as iron and steel.

In addition it has been shown that oriented fibrils of material[1] form when an isotropic material, (such as that found in a gas pipe), fail by slow crack growth. Because of this the plastic deformation behaviour of the oriented states of three grades of polyethylene supplied by BP has been studied using the constant dead loading creep experiments and constant crosshead velocity Instron experiments detailed earlier. This chapter will also discuss the general differences between the creep responses of the quenched and slow cooled morphologies of each grade and of the grades themselves. The idea of a unique relationship between true stress, true strain and true strain rate for the oriented materials will also be discussed.

In order to investigate the underlying mechanisms of creep both the Eyring process model and the Fotheringham and Cherry co-operative jump model have been applied to this oriented material, and the resulting activation parameters will be discussed. For this comparison the modelling was performed on the quenched morphology of 6007. This was simply because this particular grade and morphology provided the most complete data set with which to work.

## 3·2 Data Handling

Once the values of true stress, strain and true strain rate had been calculated for all the data points collected during a test using the technique described previously, the data were plotted in the manner of Sherby and Dorn[2].

The resulting log (strain rate) vs. strain data plots were then transferred into a graphical application on a personal computer, where they could be printed out. This package also had a facility to place crosshairs on the graph to give a read-out of the co-ordinates at any position. This facility was used to interpolate by eye and so collect the strain rate data at specific strains or strain data at specific strain rates. This method proved to be faster, more accurate and more reliable than any alternative method.

As was shown previously, (section 2·12 and figure 2·4), the reproducibility in the experiments is good. This adds confidence both to the existence of a unique relationship between true stress, strain and true strain rate and to the derived values of the activation parameters.

## 3·3 Form Of Sherby Dorn Plots

The Sherby Dorn plots for these materials in the oriented state all show the same basic form. They mostly have two distinct regions, (figure 3·1).

Region 1. In this region the true strain rate falls off rapidly with increasing strain.

Region 2. In this region the true strain rate is more nearly constant with strain.

It can be seen that although 6007, (figure 3·2), and 5502, (figure 3·3), show these two types of behaviour very clearly, 00240, (figure 3·4), does not.

For 00240 region 1 was generally characterised by a nearly constant true strain rate. This was an artefact of the experimental method. Given the conditions the tests were conducted under, the 00240 had an extremely high strain rate at the stress levels that were being imposed upon it. Hence during the initial part of the experiment, when the weights were first being lowered, the limiting factor was the speed at which the weights were lowered, which appears to be constant.

None of the materials studied exhibited a true plateau region on the Sherby Dorn plot. This would be a region where, if the tests were conducted under constant true stress conditions, the true strain rate would remain constant with increasing strain. Since the tests were conducted under constant dead load, the conditions were actually of increasing true stress. In this case an increase in the true strain rate of the sample with increasing strain would be expected in contrast with the constantly decreasing strain rate observed.

Figure 3·1

Schematic representation of the Sherby Dorn plot as used in creep experiments.

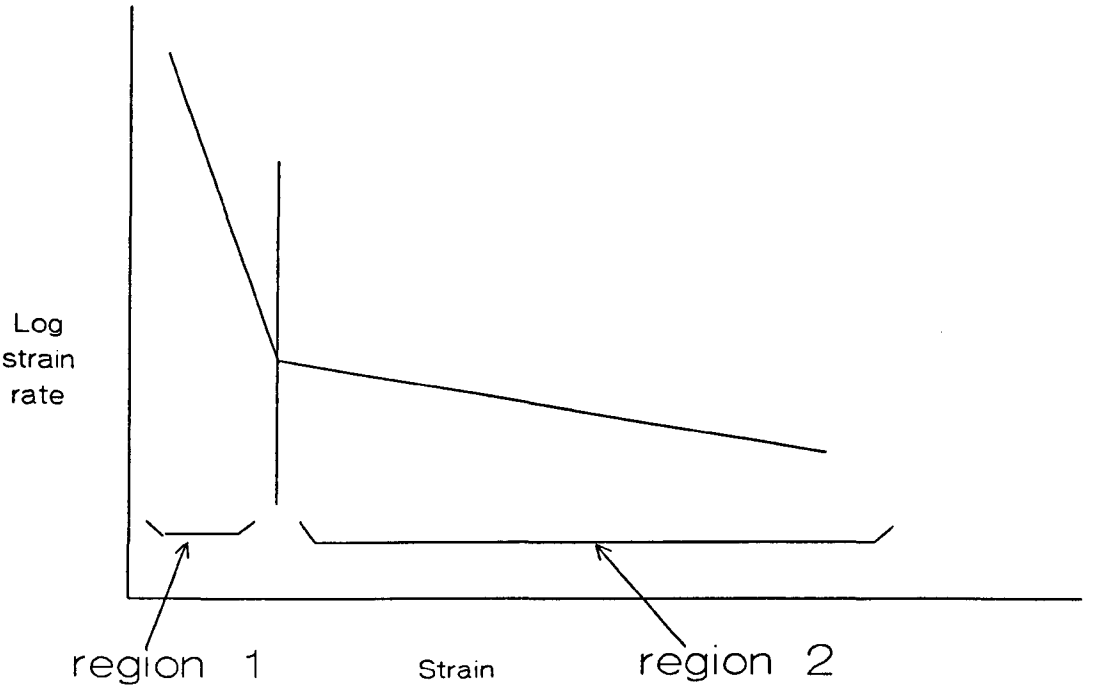

Figure 3-2

Sample Sherby Dorn plot for the quenched morphology of oriented 6007 at an initial stress of 159 MPa.

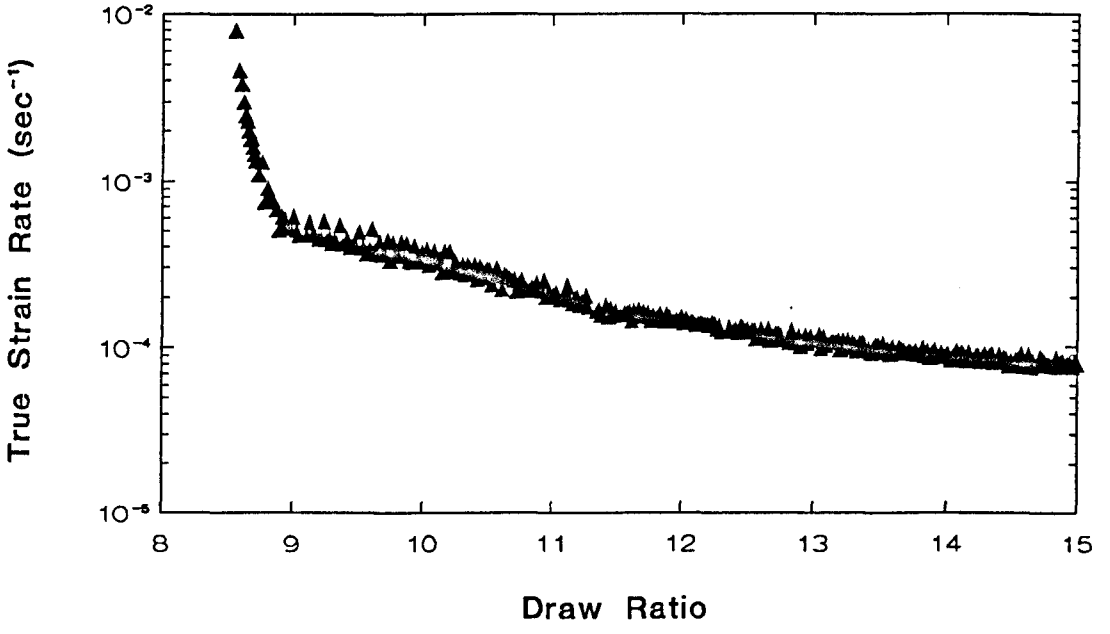

Figure 3-3

Sample Sherby Dorn plot for the quenched morphology of oriented 5502 at an initial stress of 150 MPa.

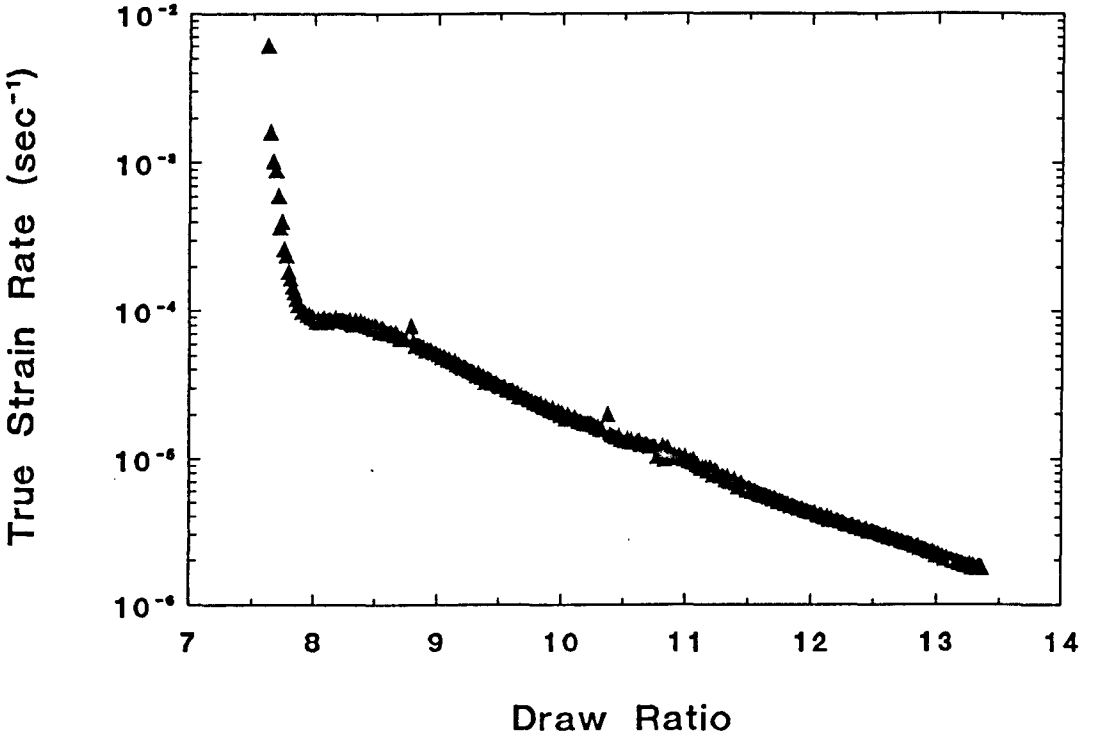

Figure 3-4

Sample Sherby Dorn plot for the quenched morphology of oriented 00240 at an initial stress of 128 MPa.

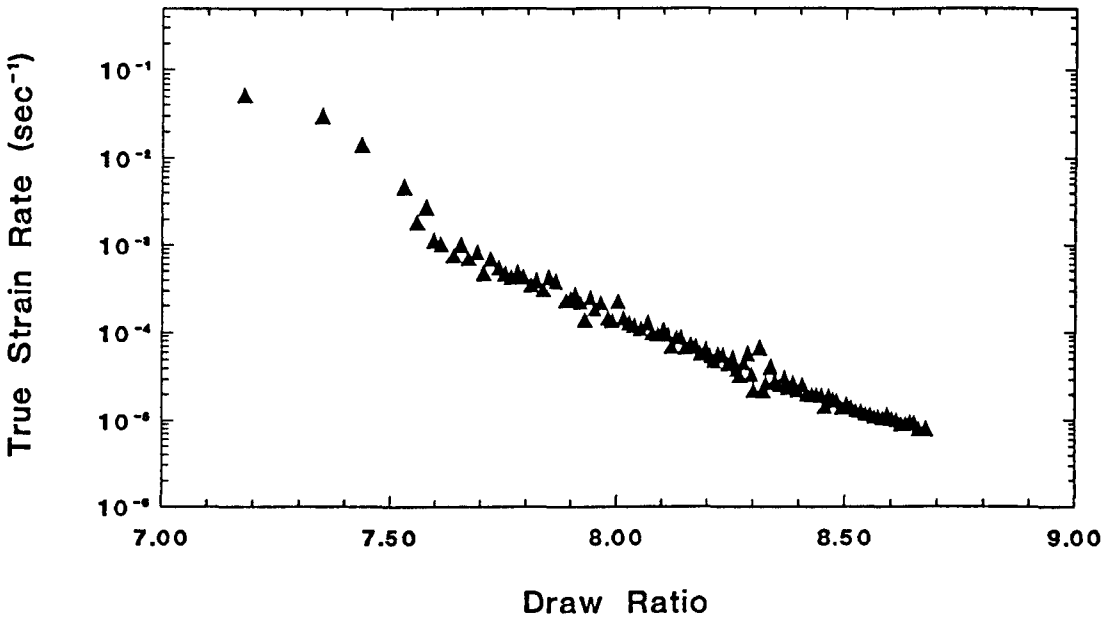

Figure 3·5

Example Sherby Dorn plots to illustrate different rates of strain hardening in the three grades.

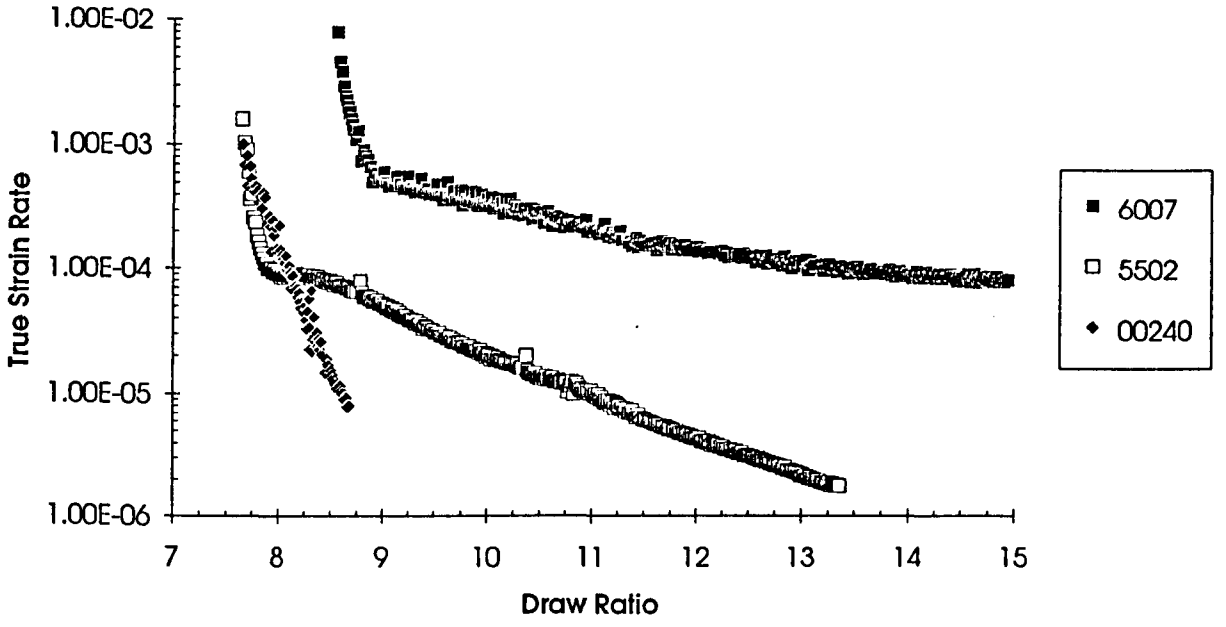

The observed decrease in the strain rate with increasing strain during the test indicates that strain hardening occurred in the samples. The quenched 00240 displayed the most rapid decrease in strain rate with strain, and hence exhibited the greatest amount of strain hardening. The quenched 6007 had the lowest decrease of strain rate with strain of the quenched materials, and hence the least strain hardening of the three materials in the quenched state. The quenched 5502 is intermediate between these two extremes. The increase in the number of side chain branches increases the viscosity of the amorphous region and also provides more "pinning points", which restrict the movement of the chains through the crystal regions. This may explain the increased resistance to creep. In order to view the different strain hardening performance of the three grades sample Sherby Dorn plots have been plotted on the same axis in figure 3·5.

Failure of the samples in the creep rig was characterised by a sharp and sudden increase in the true strain rate on the Sherby Dorn plot, and this is generally not plotted.

### 3·3·1 The origin of region 1

The reason for the rapid decrease in strain rate of the sample during the initial part of the test was investigated. It was noted that every specimen produced underwent recovery after being released from the grips of the Instron tensile testing machine after cold drawing, and that the magnitude of this recovery was of the same order of magnitude as the strain that occurred in the creep samples at the transition for region 1 to region 2.

To study this the maximum draw ratio achieved in the Instron was recorded, and was compared to the strain at which the tests made the transition from region 1 of the Sherby Dorn plot to region 2. It was found that there was good agreement between the two strains, (an example is plotted in figure 3·6). It was therefore proposed[3] that this region of the Sherby Dorn plots is caused by the polymer having a molecular network which retains a memory of its prior strain history, with region 1 simply being caused by the network reextending up to the maximum strain it had already experienced.

## 3·4 Unique Stress-Strain-Strain Rate Relationship

It has been possible to plot data from individual tests on to a master plot containing true stress, true strain and true strain rate information. As indicated earlier this is achieved by simply reading off the true strain rate at a given strain, (or vice versa), from the Sherby Dorn plots, and calculating the true stress at that point. In all three grades these plots (figures 3·7,3·8,3·9 and 3·10) appear to indicate the existence of a unique relationship between true stress, true strain and true strain rate, similar to those found by Coates and Ward[4] for PE and POM, and by Coates, Gibson and Ward[5].

Figure 3·6 .

Investigation into the cause of region 1.

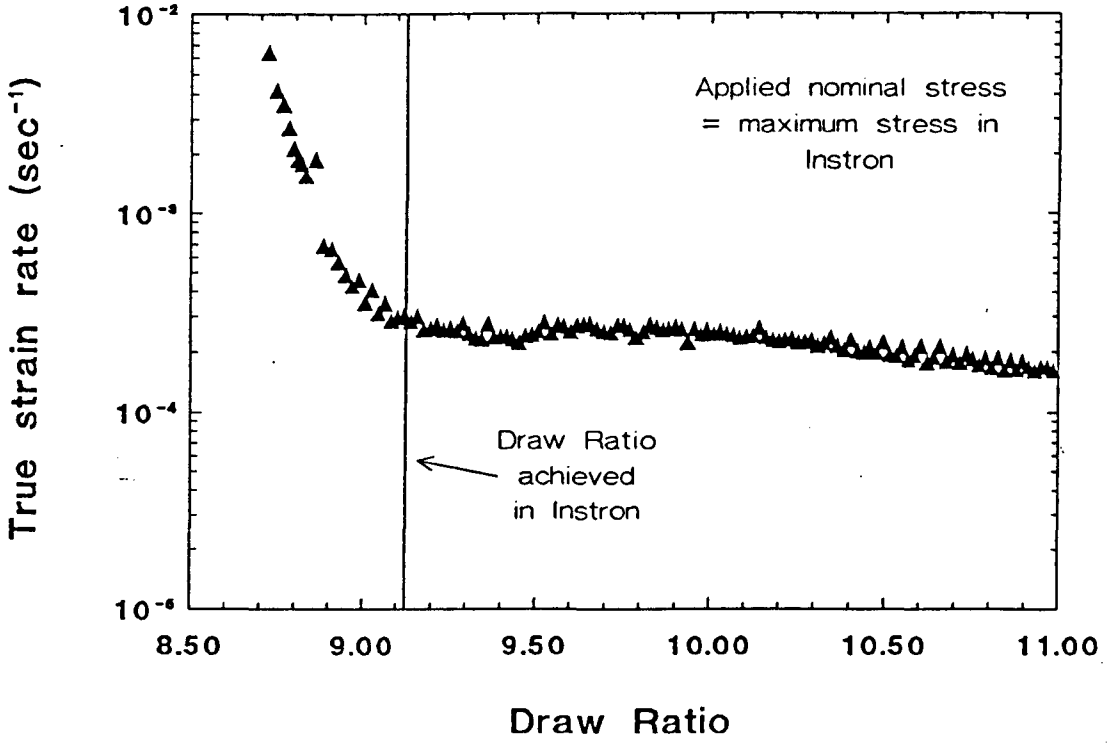

Figure 3·7

True stress versus strain at constant true strain rate for the quenched morphology of oriented 6007.

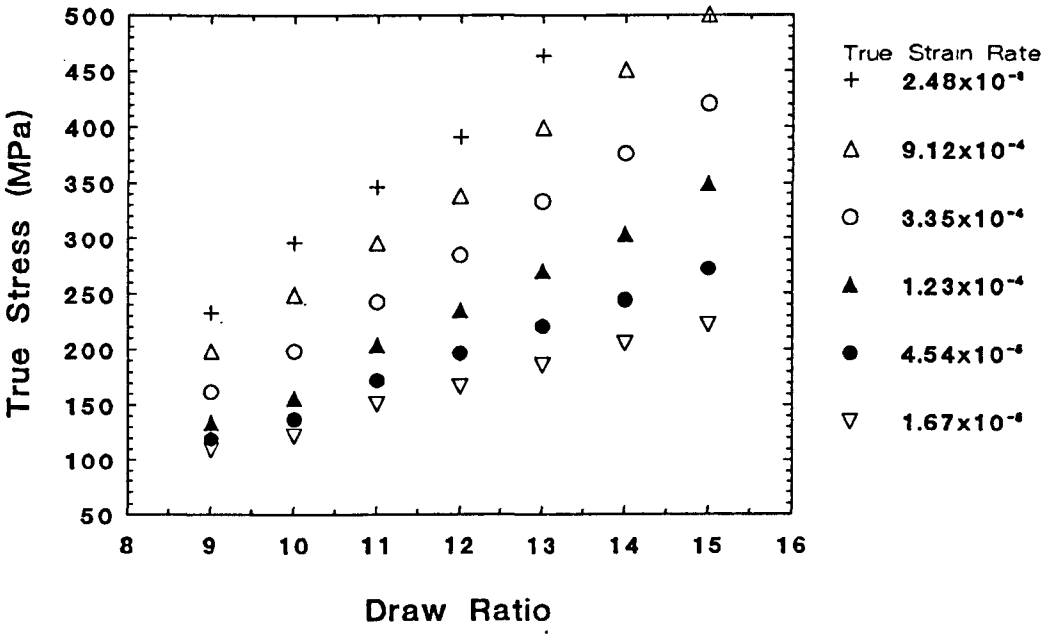

Figure 3·8

True stress versus strain at constant true strain rate for the quenched morphology of oriented 00240.

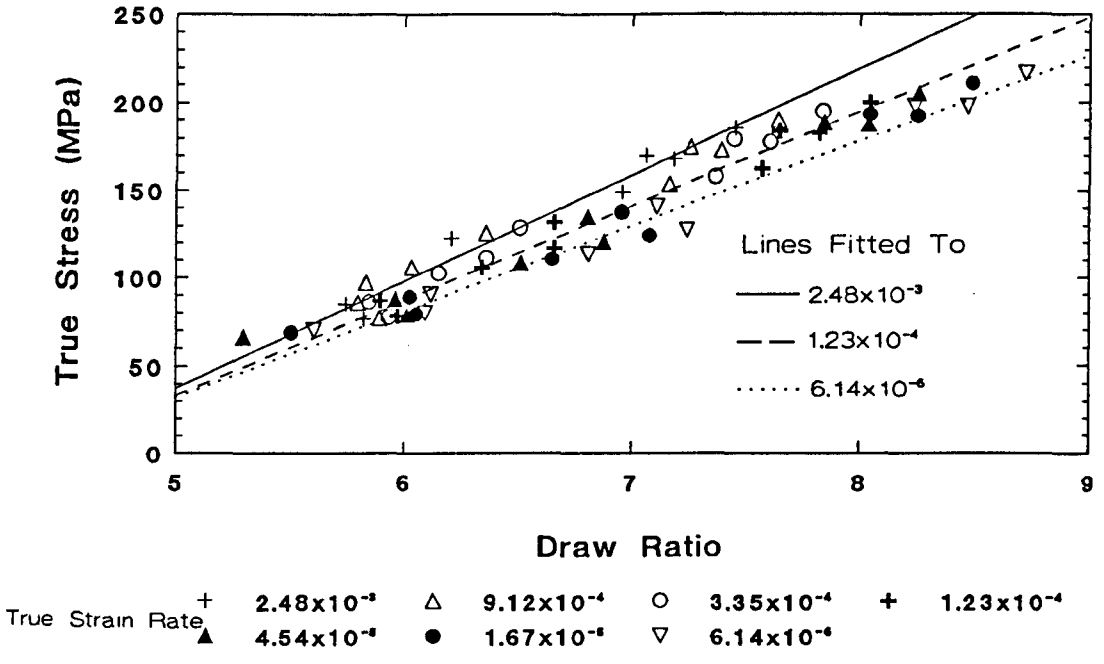

Figure 3-9

True stress versus strain at constant true strain rate for the slow cooled morphology of oriented 00240.

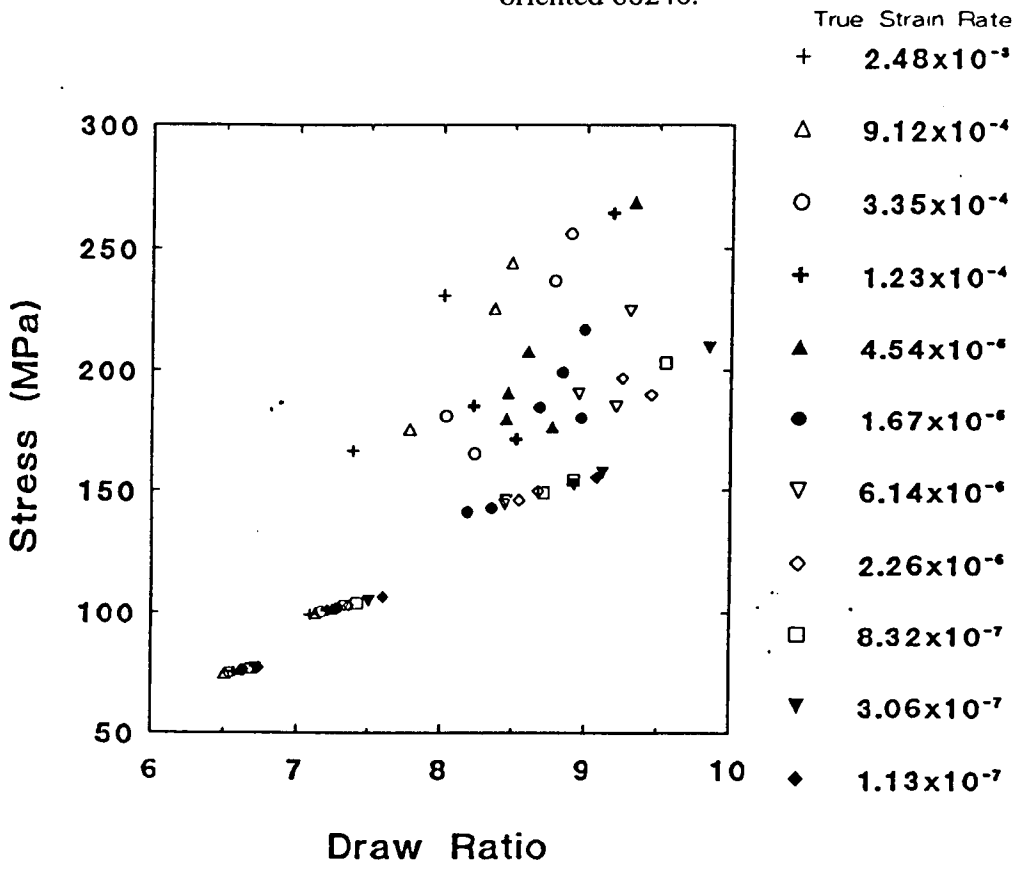

Figure 3-10

True stress versus strain at constant true strain rate for the slow cooled morphology of oriented 5502.

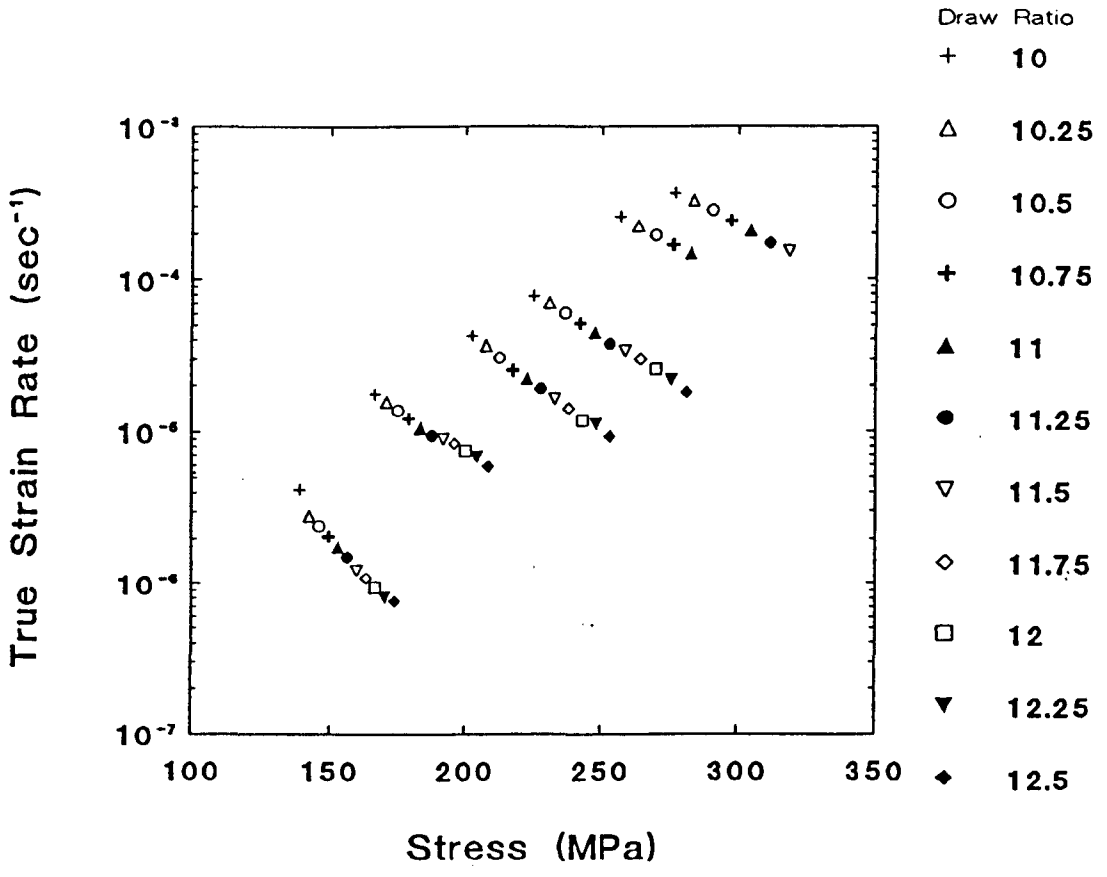

This relationship appears to exist once the material has been oriented, that is at draw ratios in excess of the natural draw ratio, and above a critical stress. Below this critical stress the strain rate data collected from an Instron diverges from strain rate data collected by creep. For example in 6007 at draw ratio 9, (figure 3·11), the critical stress is approximately 100 MPa. Reasons for this apparent divergence from a unique surface will be considered later.

With the absence of a true plateau the tests are not being conducted under equilibrium conditions. Previous work to evaluate these relationships was based on the strain rate in the plateau region. It appears, therefore, that these relationships are also present in non-equilibrium situations.

Further evidence for a unique relationship between true stress, strain and true strain rate above the critical stress is provided by work carried out on Instron tensile testing machines with quenched 6007. In this work samples were prepared in the same method as for creep, that is they were cut from compression moulded sheets and then cold drawn, which were then loaded into the Instron, and were strained at constant crosshead velocity. Once again since the initial conditions, (gauge length, sample area, crosshead speed and chart recorder speed), were known, the values of strain, true stress and true strain rate could be calculated at any point. Data from these experiments matches the data obtained from creep experiments well, (figures 3·11 to 3·16).

Although the experiments in the Instron are not radically dissimilar to creep experiments, they are not exactly the same. Thus it would appear that it is possible for us to reach the same point via several different routes on the true stress, strain, true strain rate surface. That is if we fix two values, (stress and strain for example), then when we reach those values the third value, (true strain rate), will be the same no matter how we proceed to the fixed values, but provided that we start with equivalent morphologies.

For quenched 6007 it was decided to run a series of creep tests using samples that had been cold drawn at various nominal strain rates, loaded in such a way that the same stress level would be present on each sample at draw ratio 10. The nominal strain rates used covered an order of magnitude in range, and the resulting Sherby Dorn plots are shown in figure 3·17.

In order to interpret the data, the standard nominal strain rate for cold drawing, 0.005 $sec^{-1}$, was taken as the reference. Looking at the two samples drawn at nominal strain rates lower than this it can be seen that neither lie exactly on the same curve.

Figure 3·11

Creep and Instron data for the quenched morphology of 6007 at draw ratio 9.

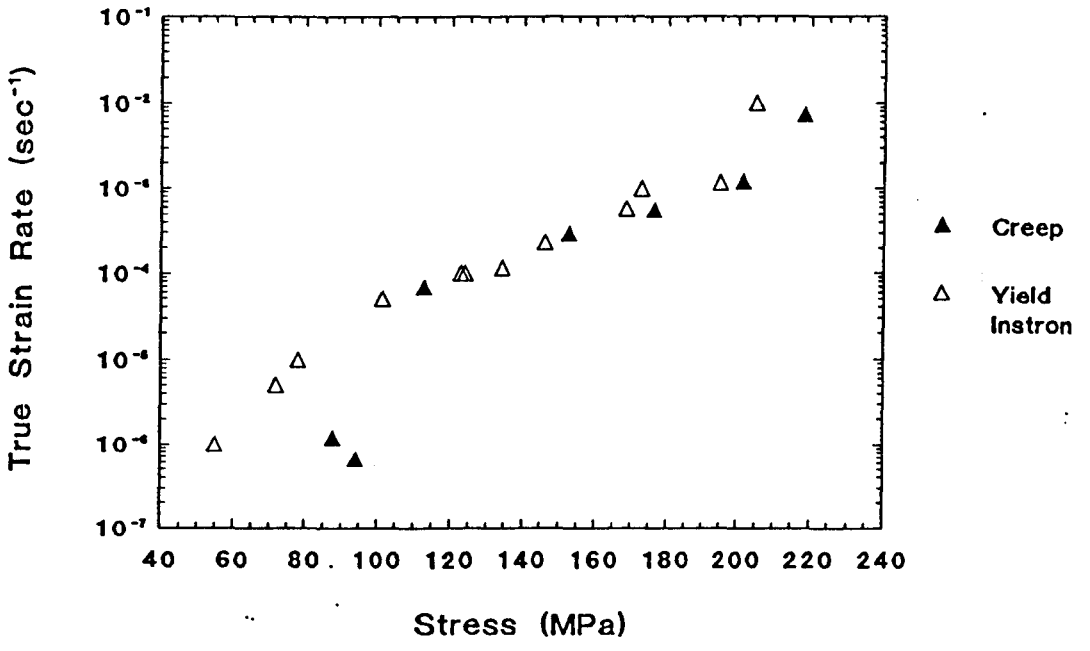

Figure 3·12

Creep and Instron data for the quenched morphology of 6007 at draw ratio 10.

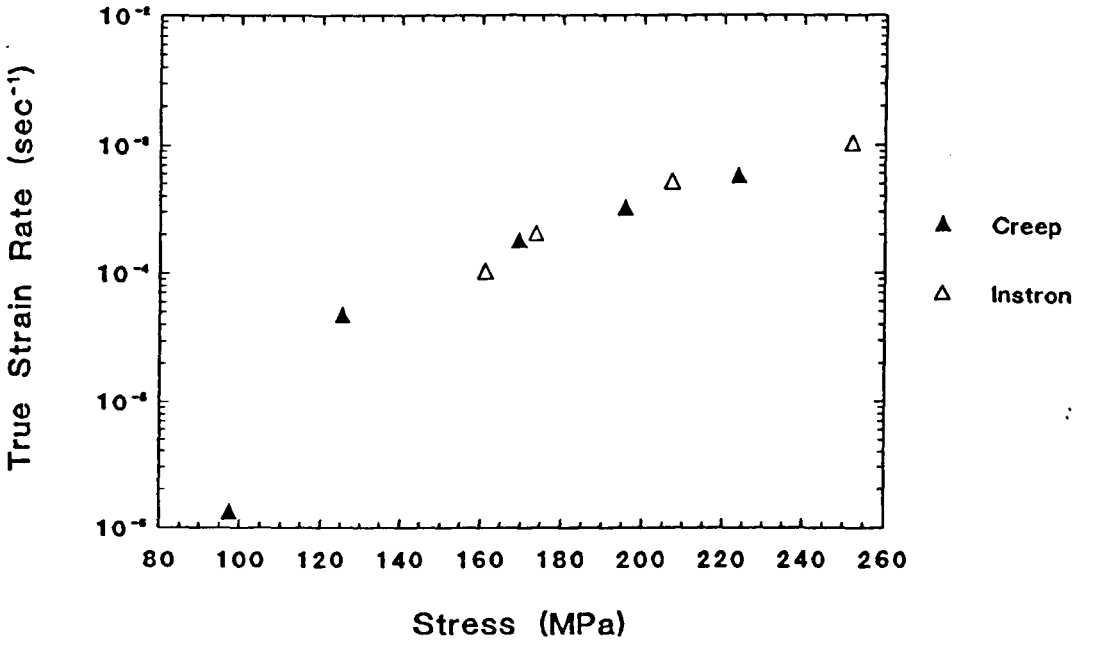

Figure 3·13

Creep and Instron data for the quenched morphology of 6007 at draw ratio 11.

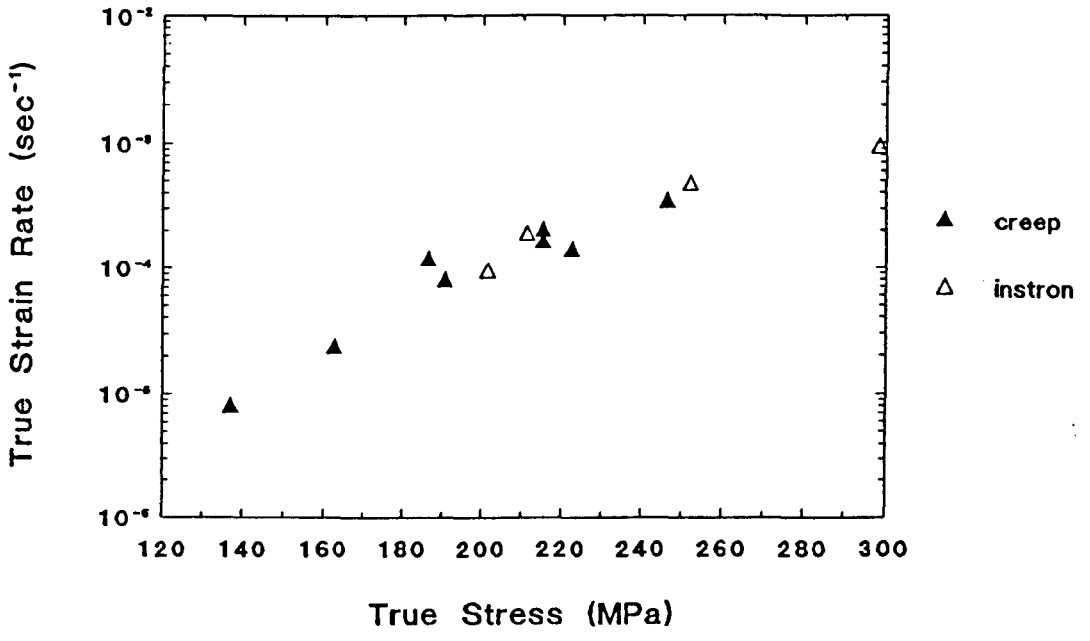

Figure 3·14

Creep and Instron data for the quenched morphology of 6007 at draw ratio 12.

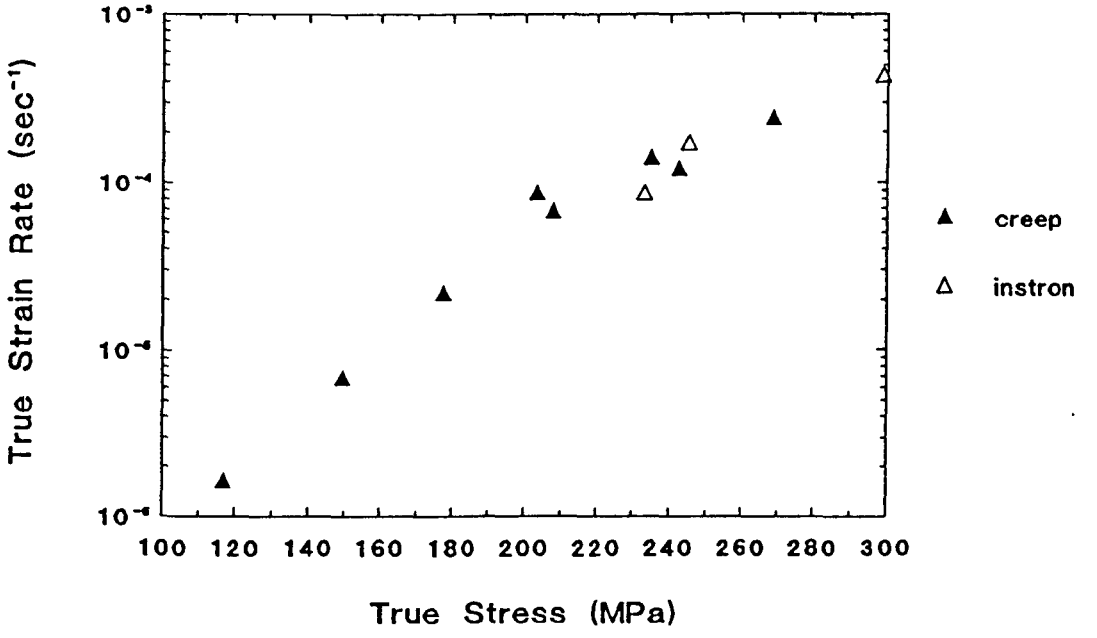

Figure 3·15

Creep and Instron data for the quenched morphology of 6007 at draw ratio 13.

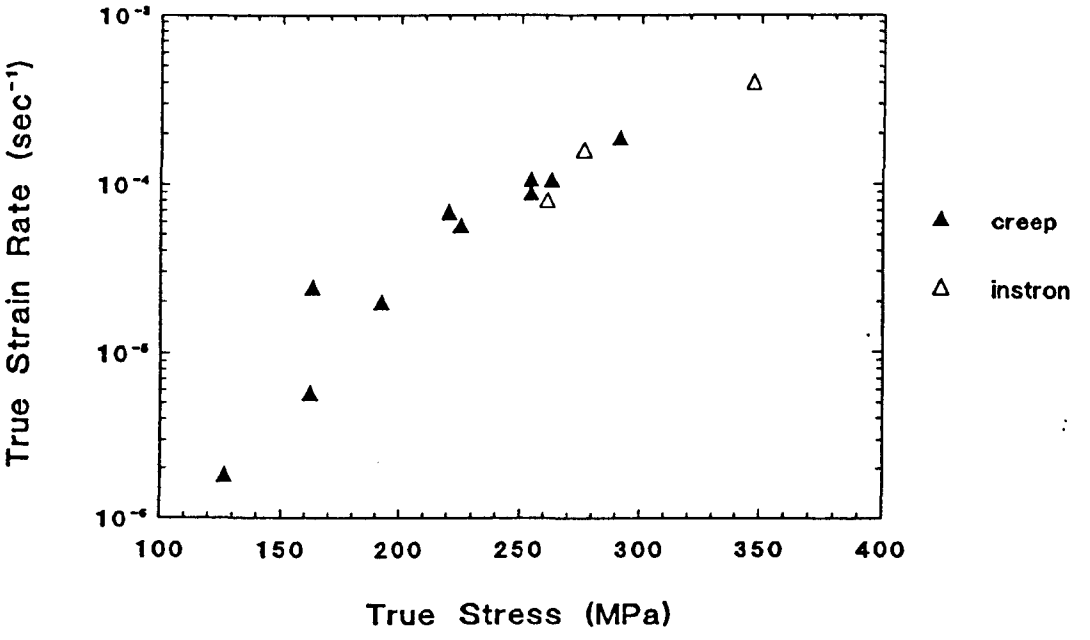

Figure 3-16

Creep and Instron data for the quenched morphology of 6007 at draw ratio 14.

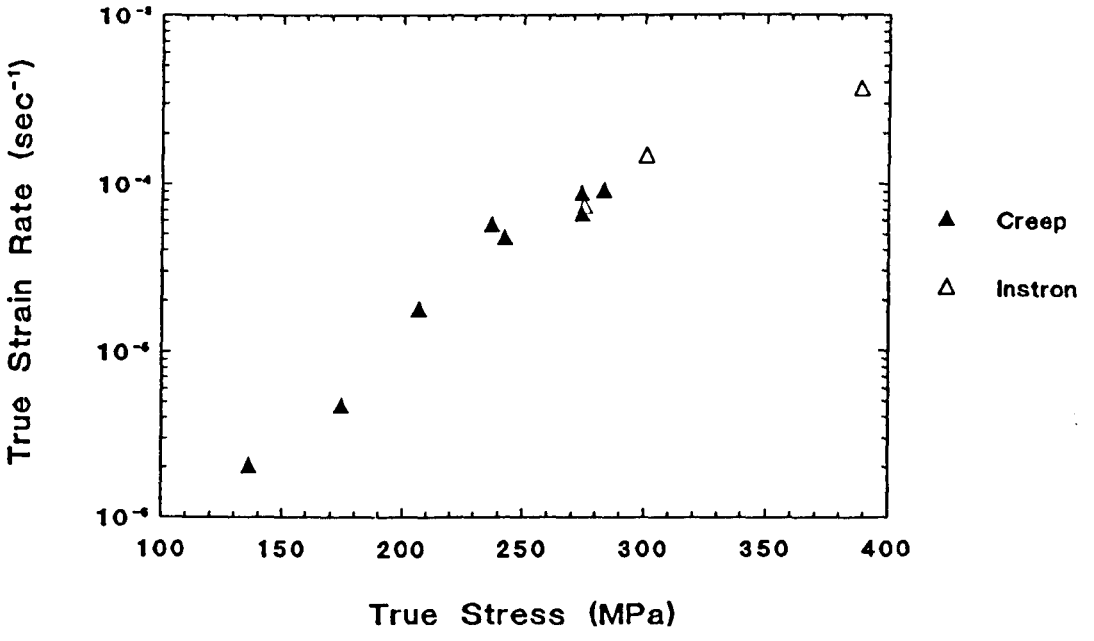

Figure 3·17

Sherby Dorn plots for the quenched morphology of oriented 6007 drawn at different initial strain rates.

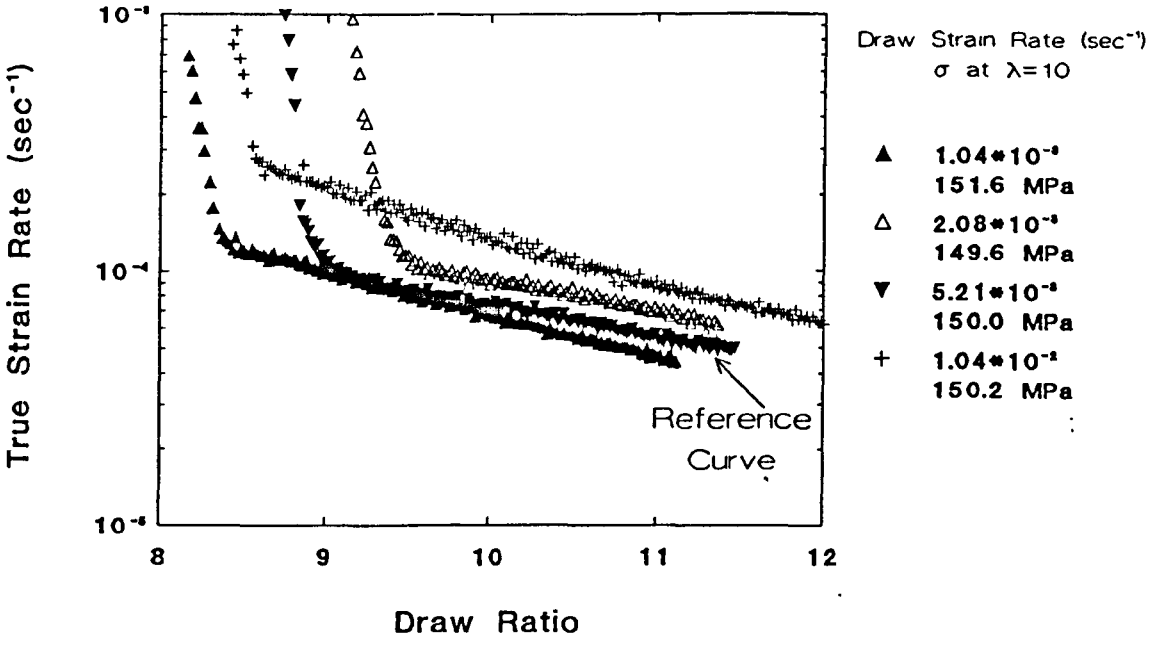

However in region 2 of the Sherby Dorn plots a true strain rate can be chosen, and then the value of strain at which this occurs obtained. When this is done it is found that the strain is within 10% of the strain at which the reference curve obtains the same true strain rate for both samples. The likely error in measuring the initial draw ratio was approximately 5%, with other errors in measuring the cross sectional area and the applied mass placing an error of around 5% on the applied stress. Thus the difference of only 10% in the strains is likely to be within the experimental accuracy.

For the sample drawn at 0.01 $sec^{-1}$ the difference in strains is 20%, or double the likely experimental errors. This sample was noticeably more opaque than the other three, indicating the presence of voids. Other evidence of void formation during drawing at nominal strain rates higher than 0.05 $sec^{-1}$ has been observed, where the cross sectional area after drawing was not that which was predicted assuming conservation of volume. Thus it seems likely that void formation had taken place in this sample, giving it a different initial structure from the other three.

Consequently it would appear that provided the initial structure of the material was kept constant, the same true stress, true strain rate, strain relationship will apply regardless of how any given point is reached.

### 3·4·1 Difference in initial morphologies

All three materials have been studied by creep experiments in both the quenched and slow cooled forms.

These two cooling rates were chosen since they produced two differing morphologies, as shown by the crystallinities reported in chapter 2 Table 2·2.

All three materials have higher natural draw ratios in the slow cooled form. The natural draw ratios obtained are shown in Table 3·1 below, (the samples were drawn at the standard nominal strain rates for the thermal treatment).

| | Quenched | Slow Cooled |
|---|---|---|
| 6007 | 8·4 | 10·5 |
| 5502 | 6·8 | 9·2 |
| 00240 | 5·2 | 6·4 |

**Table 3·1**

Table showing the natural draw ratio of the three grades for both thermal treatments used during processing.

This is consistent with the work of Capaccio et al.[7,8], who demonstrated that although an optimum initial morphology exists to produce oriented material with the maximum possible draw ratio, a general trend is for the maximum achievable draw ratio and the natural draw ratio to increase with increasing crystallinity.

The 5502 showed no appreciable difference in creep performance between the two cooling rates, (figures 3·18, 3·19, and 3·20). That is the true strain rate at any given true stress and strain, (provided that the material is above its natural draw ratio and has extended beyond the largest strain previously applied to it), were approximately the same: that is the curves were identical within the likely errors.

This work has shown that the 5502 is an intermediate grade in terms of its performance when compared to 6007 and 00240. In the isotropic state the more crystalline 6007 performs better, in the drawn state the more viscous 00240 performs better. Because it is neither highly crystalline nor highly viscous, the apparent equivalence in performance of the two morphologies of 5502 may be due to a competition between the crystallinity and viscosity in resisting creep; where the loss of viscosity in the slow cooled morphology is compensated for by the increased crystallinity.

The other two grades studied, 6007, (figure 3·21), and 00240, (figure 3·22), both show radically differing creep performance between the quenched and slow cooled state. In both cases, (provided that the material is above its natural draw ratio and has extended beyond the largest strain previously applied to it), the quenched material has superior creep performance to the slow cooled material, that is the true strain rate at any given stress and strain is lower for the quench cooled material than the slow cooled material. This difference is extremely marked in the case of 00240.

This result may be explained by studying the initial morphologies of the slow cooled and quenched samples.

As shown by Capaccio et al.[7,8] the quenched samples undergo very rapid cooling, effectively locking in the structure of the melt, resulting in a large amount of molecular tangling in the amorphous regions. In addition long molecules are more likely to be incorporated into several different lamellae, forming a large number of effective tie chain molecules.

During slow cooling the polymer has much longer to form crystal lamellae. Because of this more of the high molecular weight polymer will be incorporated into the lamellae, resulting in a less tangled amorphous region and a lower number of long molecules available to form tie chain molecules.

Figure 3·18

Comparison in the creep performance of the quenched and slow cooled morphologies of 5502 with a stress loading of 150 MPa at draw ratio 9.

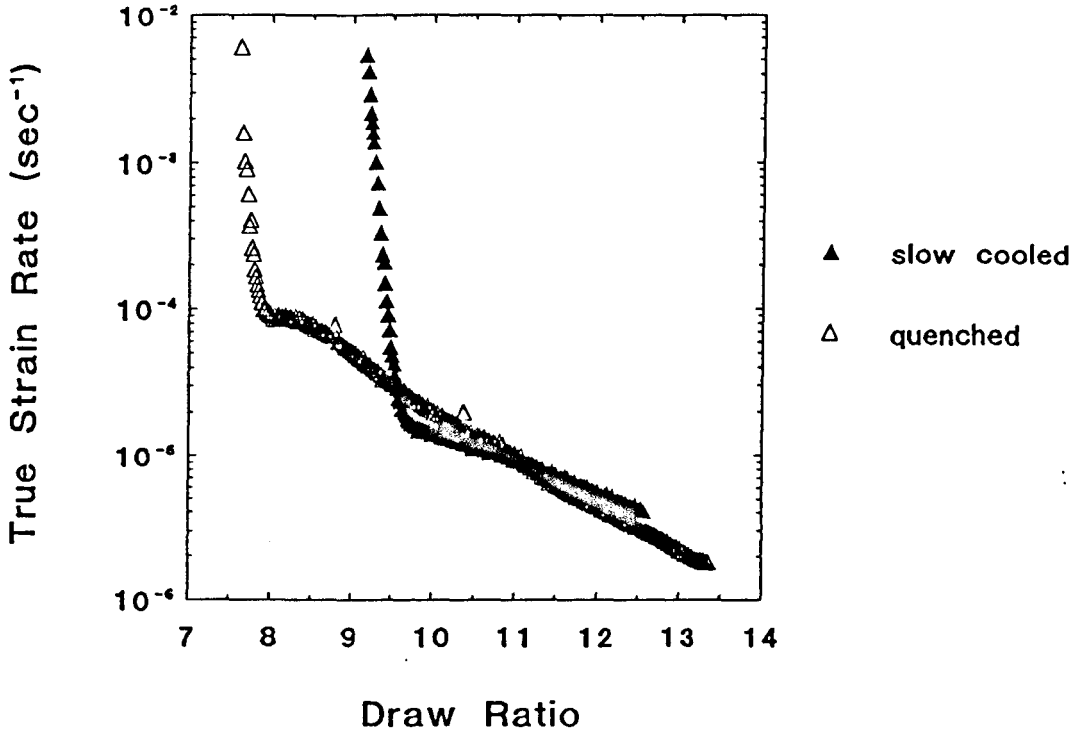

Figure 3·19

Comparison in the creep performance of the quenched and slow cooled morphologies of 5502 with a stress loading of 175 MPa at draw ratio 9.

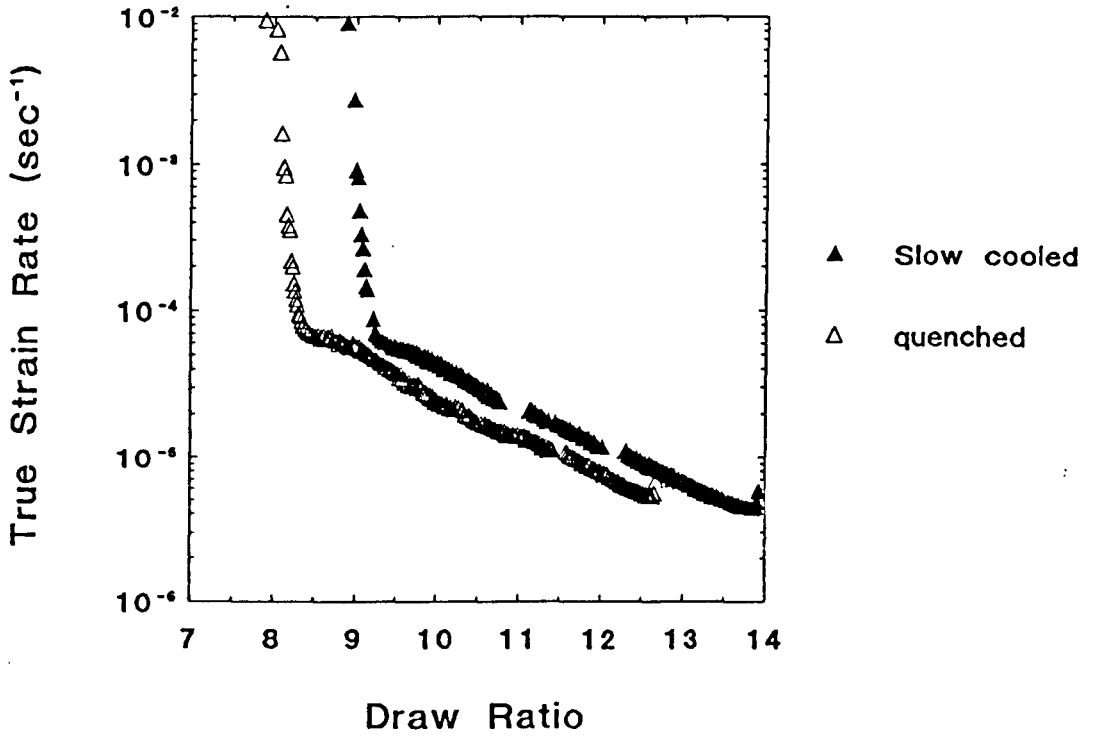

Figure 3·20

Comparison in the creep performance of the quenched and slow cooled morphologies of 5502 with a stress loading of 200 MPa at draw ratio 9.

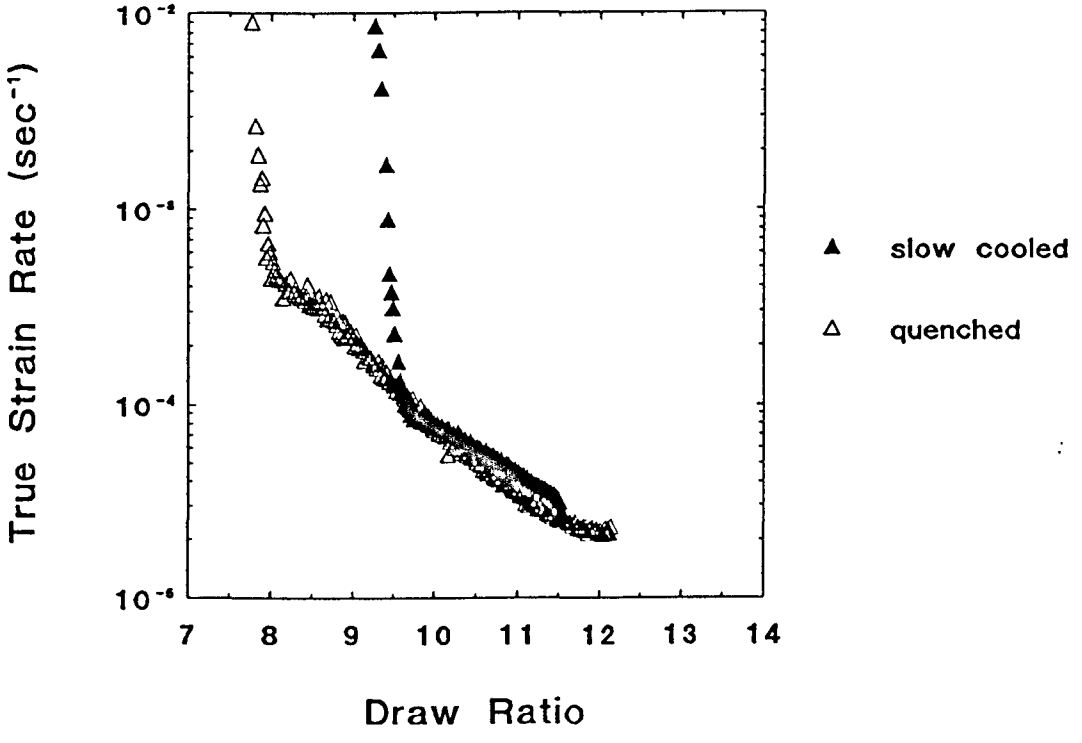

Figure 3·21

Comparison in the creep performance of the quenched and slow cooled morphologies of 6007 at draw ratio 14.

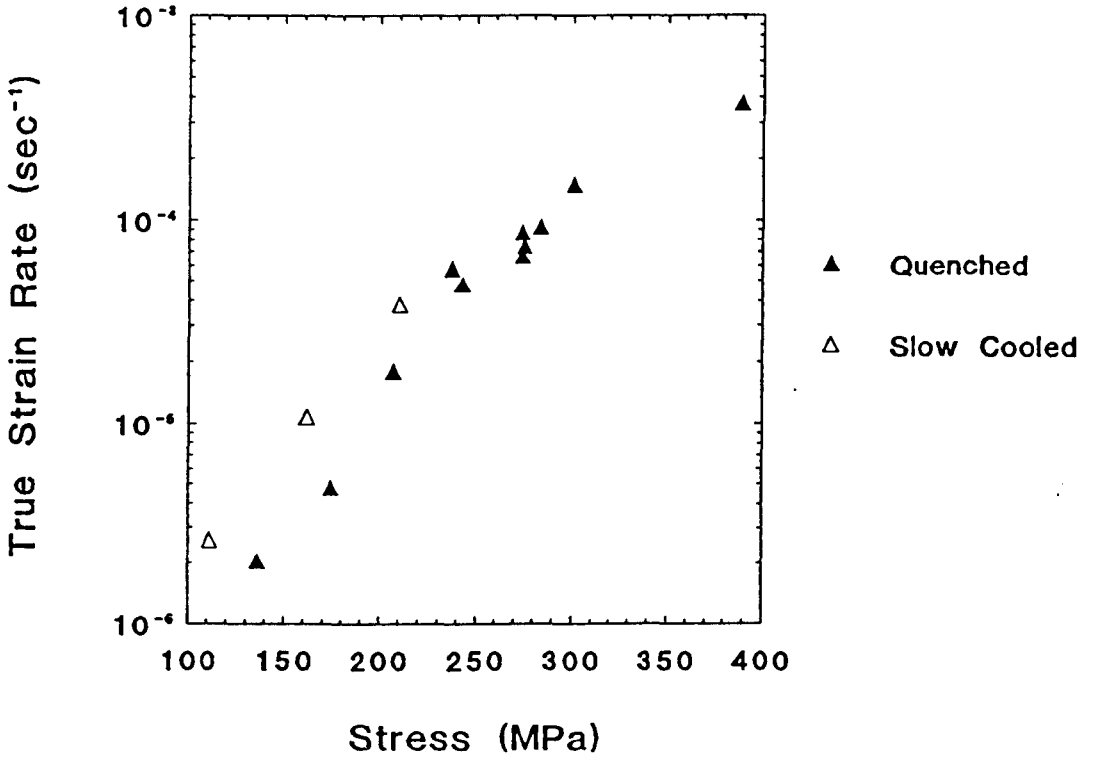

Figure 3-22

Comparison in the creep performance of the quenched and slow cooled morphologies of 00240 with a stress loading of 120 MPa at draw ratio 7.

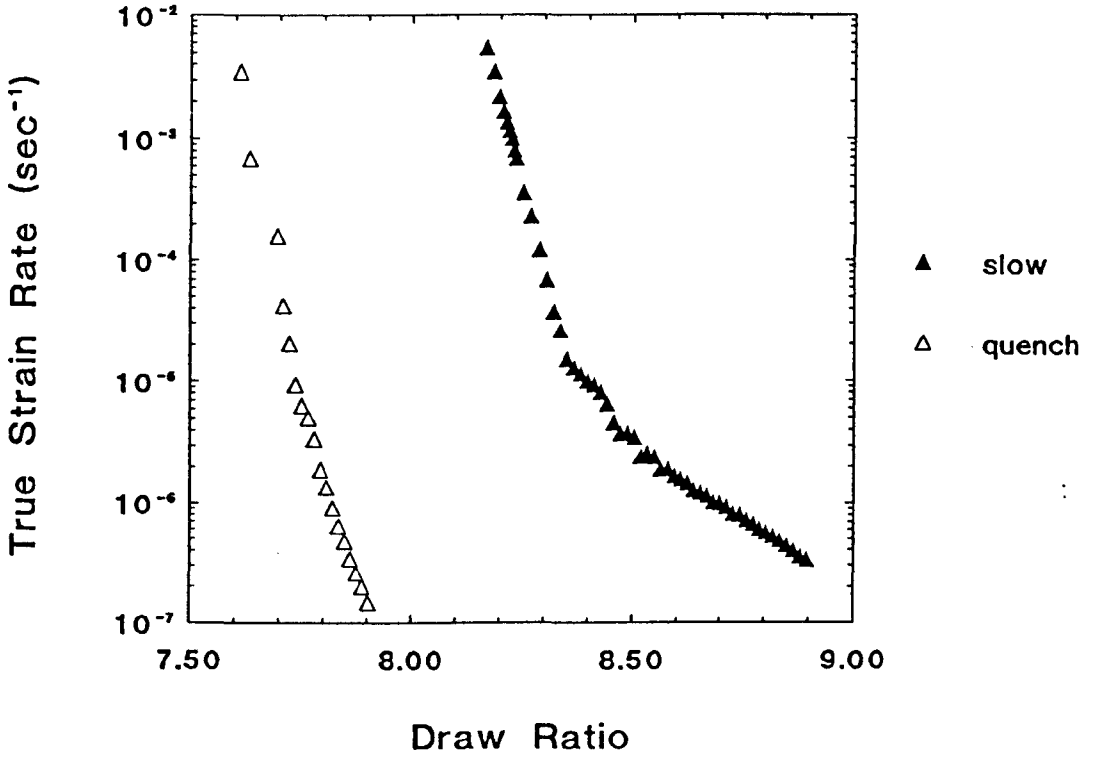

The difference in the relative amounts of tie chain molecules and amorphous entanglement can be used to explain the difference in creep behaviour of 6007 and 00240 between the two thermal treatments, provided that this is not destroyed during the initial stages of drawing.

During deformation two processes are thought to occur[7]. One is a deformation of the crystal lamellae. The other is a deformation and orientation of the amorphous regions. These occur simultaneously and compete and interact.

The more highly entangled amorphous regions with a greater number of tie chain molecules in the quenched material will present more resistance to deformation than those of the less entangled slow cooled material, resulting in an improved creep performance.

In addition to the differing creep performance and natural draw ratios, 6007 and 5502 both suffered an increased tendency to rupture during cold drawing in the slow cooled state. It was for this reason that the nominal strain rate used for cold drawing was reduced for slow cooled samples.

Samples of slow cooled 5502 failed predominantly at the neck which forms in the sample during drawing. As demonstrated in chapter 2 the slow cooled material has a higher crystallinity than the quenched material, and hence has an increased yield stress at any given temperature and strain rate. It has been shown[9] that the brittle failure stress of isotropic polyethylene is dependent upon the tie molecule concentration. As has already been stated the slow cooled material had a lower concentration of tie molecules, and hence would posses a lower brittle failure stress than the quench cooled material. Consequently the slow cooled material is more likely to encounter situations where the yield stress exceeds the brittle failure stress, and hence it is more likely to fracture than to yield and draw.

This explains why the 5502 failed predominantly in the region of the neck, where yielding was occurring. Any unnoticed or internal flaws in the material could act as stress concentrators and raise the local effective stress above the brittle failure stress. It also explains why a reduction in nominal strain rate for drawing was required, since the yield stress is dependent upon the strain rate, and by lowering the strain rate at which the material is cold drawn, the yield stress is lowered. Thus it is more likely that the yield stress will remain below the brittle failure stress at low strain rates and the sample will draw rather than fail.

Samples of slow cooled 6007 failed predominately in the section of the material that had already been drawn. This was attributed to the reduced creep performance of the material allowing the drawn section to creep to failure within the time period of drawing. Further evidence that this was the main cause for failure comes from the fact

that a high proportion of samples that did not fail could not be used because the draw ratio of the drawn section had too large a spread of values, with the highest draw ratios being observed at the end which passed through the neck first.

Samples of slow cooled 00240 failed very rarely during drawing. This may be explained by the nature of the grade of polymer. 00240 has a relatively high sidechain content, (≈7 side groups per 1000 carbon atoms in the backbone), and was the most creep resistant grade studied in this work. The good creep resistance of this grade means that failure in the drawn section due to creep to failure is unlikely. The high side group content provides a large number of "background" tie molecules, which are independent of the tie molecules formed during the compression moulding to form sheets, and hence which are independent of thermal history. Thus the brittle failure stress will always be relatively high, and hence more likely to exceed the yield stress.

## 3·5 The Eyring Model

The Eyring model described in chapter 1 will now be discussed in relation to its application to the drawn material.

### 3·5·1 Activation Volume

Activation volumes have been calculated for the quenched morphologies of 6007 and 00240. These were obtained by considering that the true strain rate versus stress data falls into low stress and high stress regions, (figure 3·23), and by assuming that in each of these regions the data rapidly converges to a single Eyring process. Thus the data are assumed to approximate to a single Eyring process and equation 1·4 was used in the calculation. In the low stress region the contribution from the second process was considered to be negligible, in the high stress region effective activation volumes have been calculated, where the effective activation volume is given by equation 1·9.

An example of this is shown in figure 3·24 for quenched 6007. The variations of effective activation volume derived in this manner with strain for both quenched 6007 and quenched 00240 are shown in Table 3·2 below, and graphically in figures 3·25 and 3·26. It can be seen that the effective activation volume reduces exponentially with strain as previously reported by Coates[10].

Figure 3-23

Schematic representation of the low and high stress regions of a true strain rate versus true stress plot.

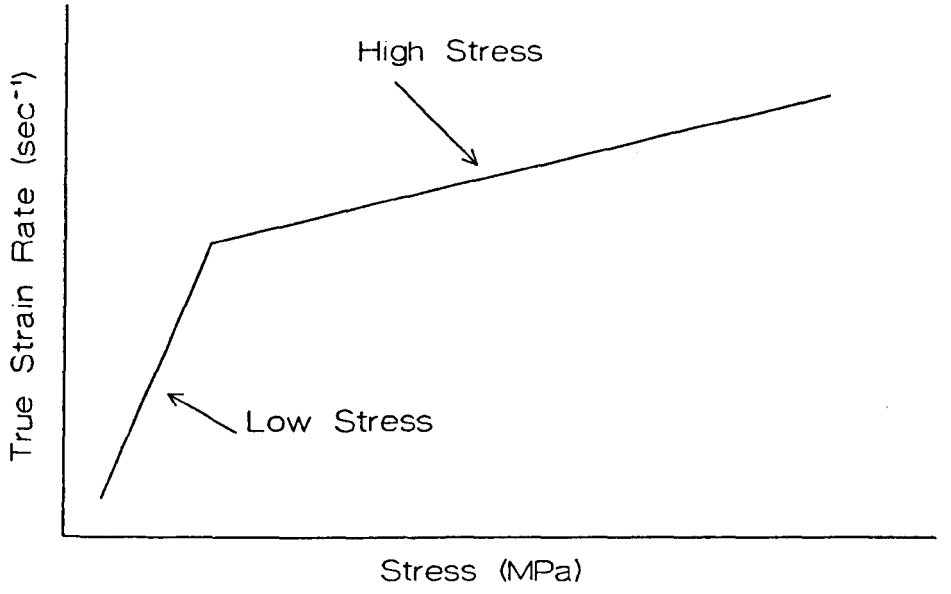

Figure 3-24

Activation volume derivation for the quenched morphology of 6007 at draw ratio 10.

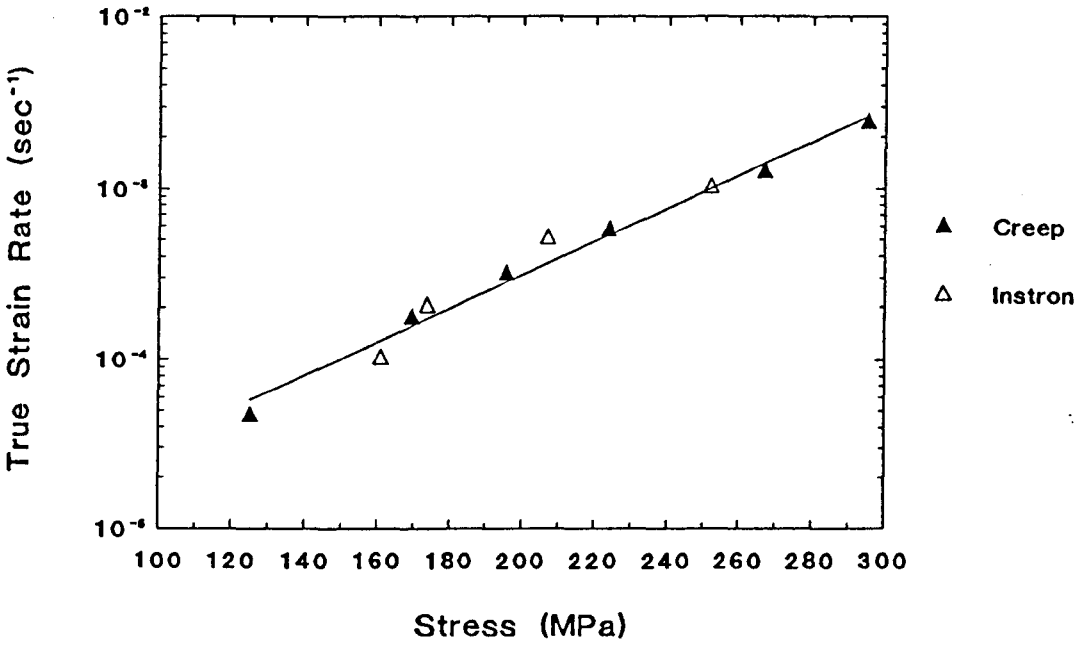

Figure 3·25

Activation volume of process 2 for the quenched morphology of oriented 6007.

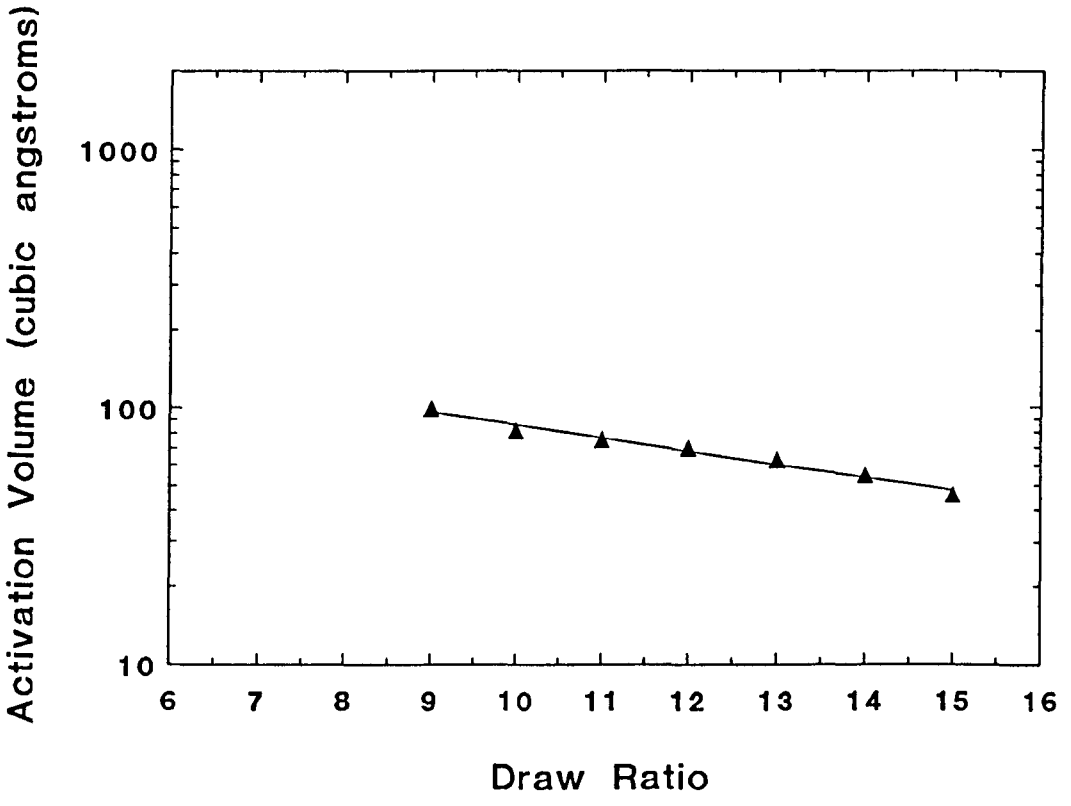

Figure 3·26

Activation volume of process 2 for the quenched morphology of oriented 00240.

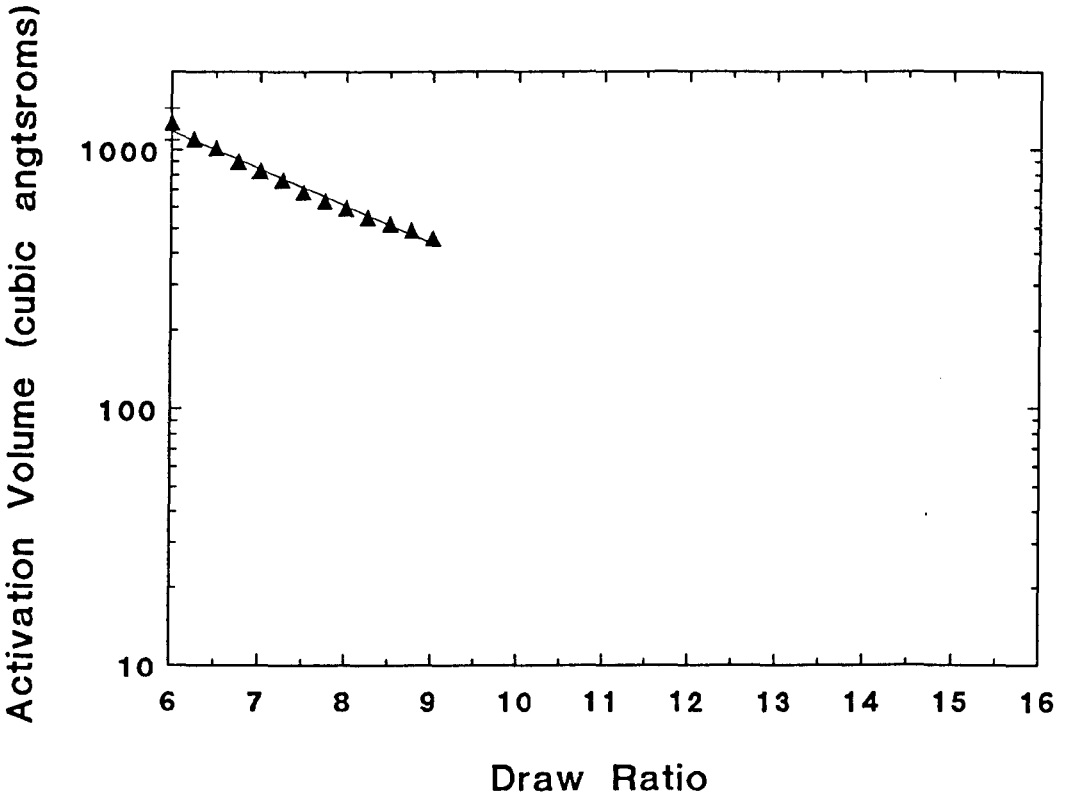

The effective activation volumes derived compare favourably with those reported previously for polyethylene. The range of activation volumes calculated for 6007 varies between 100 Å$^3$ and 40 Å$^3$ as the strain is increased from draw ratio 9 to draw ratio 14. Previously Coates and Ward[6] found activation volumes of around 100 Å$^3$ for Rigidex 50, (a related high density polyethylene of $\overline{M}_W$=101,450 and $\overline{M}_N$=6,180), at 100°C, (because of the higher temperature the stresses used would have been much lower than those used in this study). Coates[10] also found activation volumes ranging from 300 Å$^3$ to 100Å$^3$ in Rigidex 50 between draw ratios of 10 and 25 at 100°C. Also Wilding[11] reported activation volumes ranging from 121 to 104 Å$^3$ at 20°C for Rigidex 50 between draw ratios 10 and 20.

### 3·5·2 Activation Energies

These were also determined by assuming that in the high and low stress regions the data approximated to a single Eyring type process, using equation 1·5.

An example of the plot used to determine this activation energy is shown in figure 3·27 for the quenched morphology of 6007.

The activation energies determined in this manner are shown in Table 3·2 in section 3·6·4.

### 3·5·3 Mechanisms Controlling Creep

The activation volumes derived using the assumption that the high stress region of the strain rate against stress curves can be approximated to a single Eyring type process with constant effective activation parameters are plotted in figures 3·25 and 3·26. It can be seen that there is a simple relationship between effective activation volume and strain. In addition three activation volumes have been calculated for quenched 6007 in the low stress region. However there are large uncertainties associated with these due to the lack of available data. These three activation volumes are listed in Table 3·2.

The activation energies have been calculated as described previously, and are listed in Table 3·2. These have been derived for quenched 6007 for both processes, and for the high stress process for quenched 5502.

Figure 3-27

Activation energy for the second process of the quenched morphology of 6007 at draw ratio 12 and 200 MPa.

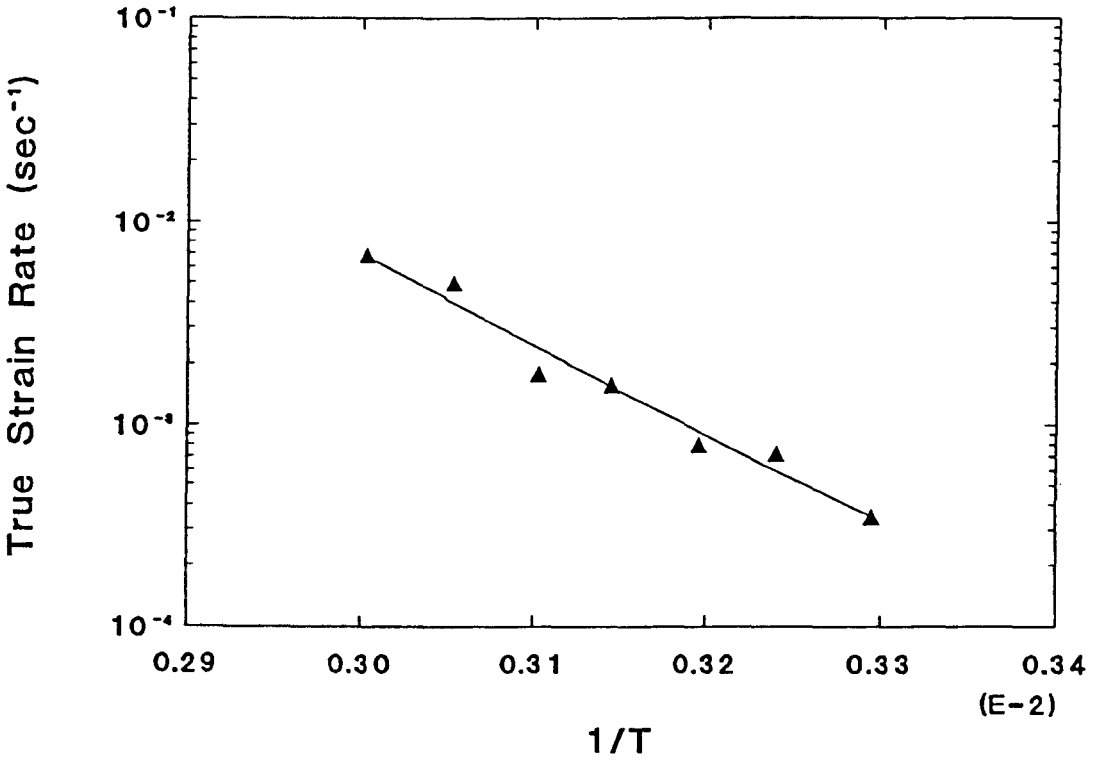

| Grade | Process | Draw Ratio | Stress (MPa) | Activation Volume ($Å^3$) | Activation Energy (kJ/mol) | Activation Energy (kcal/mol) |
|---|---|---|---|---|---|---|
| 6007 | 2 | 11 | 183 | 74·8 | 89·3 | 21·3 |
| 6007 | 2 | 12 | 200 | 69·6 | 92·6 | 22·1 |
| 6007 | 2 | 13 | 217 | 62·7 | 93·1 | 22·2 |
| 5502 | 2 | 9 | 150 | 153·9 | 143·7 | 34·3 |
| 5502 | 2 | 10 | 166 | 128·7 | 143·1 | 34·2 |
| 6007 | 1 | 9 | | ≈730 | | |
| 6007 | 1 | 10 | 100 | ≈582 | ≈117 | ≈28 |
| 6007 | 1 | 11 | 110 | ≈450 | ≈115 | ≈27 |

**Table 3·2**

Table showing derived activation volumes and activation energies assuming that the gathered data can be approximated to a single Eyring type expression.

These activation energies lie in the region reported for the activation energy of the $\alpha$ process.

There have been numerous reports[12,13] of two $\alpha$ processes, $\alpha_1$ and $\alpha_2$. The $\alpha_1$ activation energy has been reported[12,13] as being 28 to 31 kcal $mol^{-1}$, the $\alpha_2$ activation energy[12,13] as 46 kcal $mol^{-1}$, although Alberola et al.[13] indicate that there may be a dependence of the activation energy on lamellar thickness.

Most of the activation energies derived using the effective activation volume for the oriented material lie in the region of the $\alpha_1$ activation energy.

The $\alpha$ process is generally associated with c-shear in the crystals of the polymer, although the location of the mechanism of the individual $\alpha_1$ and $\alpha_2$ processes is still not clear, see for example Kajiyama et al.[12] and Alberola et al.[13]. Thus it would appear that the mechanism controlling creep in these polyethylene grades is c-shear.

The most remarkable feature is the fact that the activation energy appears to change so little between the process governing the high stress response and the low stress response in quenched 6007, and can be attributed to a c-shear mechanism in both cases.

For 6007 at draw ratios 9, 10 and 11 it is possible to calculate the true value of the activation volume for the second process by using equation 1·9, since the value of the activation volume of the first process has been calculated. These activation volumes

are shown in Table 3·3 below and are significantly higher than the effective activation volumes.

| Draw Ratio | Effective Activation Volume ($Å^3$) | Actual Activation Volume ($Å^3$) | Effective Activation Energy (kcal/mol) |
|---|---|---|---|
| 9 | 98·3 | 114 | 21·3 |
| 10 | 81·3 | 95 | 22·1 |
| 11 | 74·8 | 90 | 22·2 |

**Table 3·3**

Comparison of the effective and activation parameters at draw ratios 9, 10 and 11 for the quenched morphology of 6007

### 3·5·4 Variable Activation Volume

The activation parameters derived in the previous sections have assumed that the activation volume varies in a simple manner. There are four possibilities as to how it may vary and it is instructive to consider what the effects of these variations would be.

The possibilities are:

1. V is constant.
2. V is a function of stress only.
3. V is a function of strain only.
4. V is a function of both stress and strain.

The activation volume is defined from equation 1·4 as

$$V = 2 \cdot 3kT\left(\frac{d\log\dot{\varepsilon}}{d\sigma}\right) \qquad (3\cdot1)$$

It is now possible to examine each of the four possibilities, and determine which fits the gathered data the best.

1. V = constant. If this is the case then plots of $\sigma$ against $\log(\dot{\varepsilon})$ at constant strain will be parallel straight lines.
2. $V = V(\sigma)$. If V is, for example, directly proportional to stress then as the stress is increased the gradient of the curves will increase. However, if there is no dependence of V on strain the activation volume should be constant at any given

stress. Therefore a simple linear shift parallel to the $\log(\dot{\varepsilon})$ axis should superimpose the curves of $\sigma$ against $\log(\dot{\varepsilon})$.

3. $V = V(\varepsilon)$. If V is dependent on the strain and there is no variation of V with stress the curves of a $\log(\dot{\varepsilon})$ against stress graph will be straight lines, but the gradient of the lines will change with the strain. For example, if V decreases as the strain increases then the gradient of the curves will decrease.
4. $V = V(\varepsilon,\sigma)$. This is the most complex case. With the activation volume depending on both stress and strain the plots of $\sigma$ against $\log(\dot{\varepsilon})$ will be curves which will not superimpose by a simple translation parallel to an axis.

In figure 3·28 $\log(\dot{\varepsilon})$ versus $\sigma$ data for the quenched morphology of 6007 at three different draw ratios have been plotted. The first observation is that at draw ratio 10 there is a definite curve to the data. This implies a complex dependence of V on both stress and strain. However, above a critical stress the data lie on lines which are to effectively straight lines, and the lines plotted on the graph are simple linear fits to the data, which indicates little dependence on stress. The gradients of these lines varies with draw ratio, which indicates a much stronger dependence of V on strain than stress.

### 3·5·5 Multiple Activation Volumes

There are two explanations for a non-linear relationship between log(true strain rate) and stress.

Firstly there could be a single activated process with a variable activation volume dependent upon stress, strain or both stress and strain.

Secondly there could be more than one activated process taking place. The simplest possible case in this situation would be for there to be two processes participating in the straining of the material.

In this situation it is envisaged that the two processes are dominant at different stress levels. At high stress levels both processes occur, but one would be dominant. At low stress levels the process which is dominant at high stress levels can effectively be considered not to participate, leaving the process which is secondary at high stress levels to be dominant.

As mentioned previously this approach has been used extensively by Wilding and Ward[11], and it has been detailed in chapter 1, and it is the approach that has been used throughout this investigation.

Figure 3-28

True strain rate versus true stress for the quenched morphology of 6007 at room temperature.

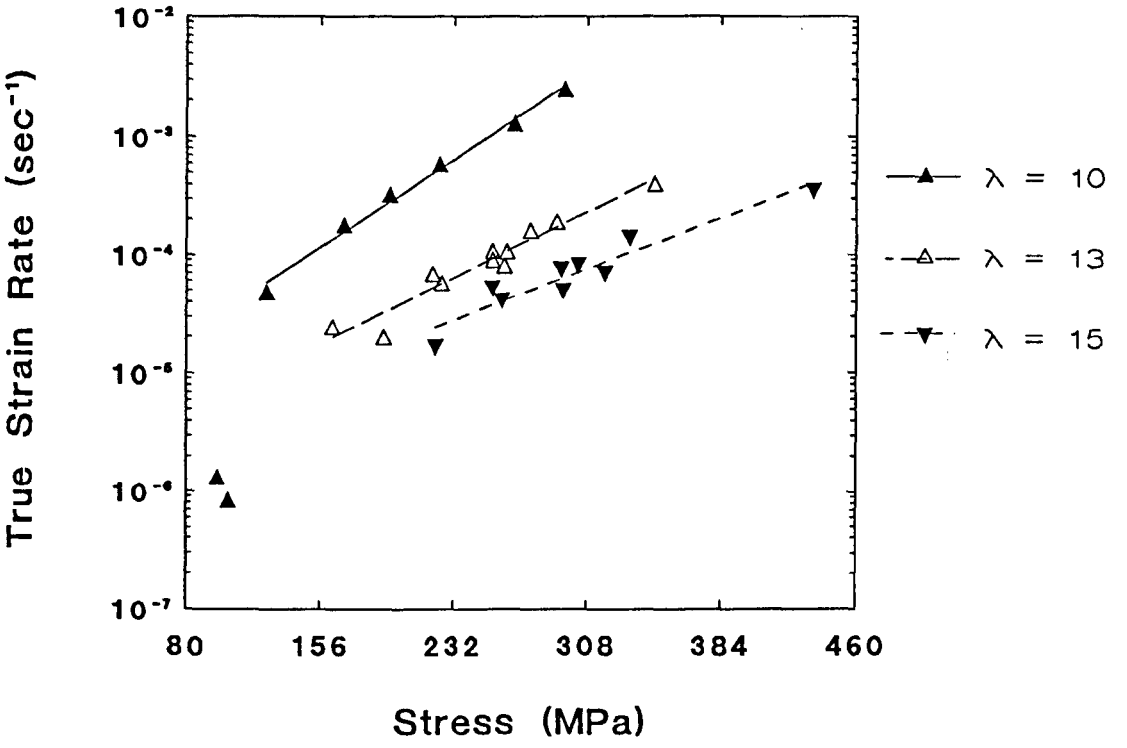

### 3·5·6 Fitting The Two Process Model

Equation 1·7 has been fitted to creep data obtained for quenched 6007 at draw ratio 9. This is the only grade and draw ratio for which there is sufficient data available in the low stress region to allow fitting to both processes. It would be possible to produce detailed creep data for the low stress region, (see Rasburn[14]), in order to conclusively prove the ability of this model, but this is extremely time consuming, requiring a minimum of 3 to 4 weeks per test to collect data points lower than those reported in this work. Given the amount of time that would have been required it was decided not to concentrate on extending the creep data to this low stress region for all grades and draw ratios.

The fitting was carried out using a least squares procedure, with the parameters $V_1$, $V_2$, $[\dot{\varepsilon}_0']_1$ and $[\dot{\varepsilon}_0']_2$ unconstrained. The resulting values are shown in Table 3·4 below and the curve calculated from these values was plotted on the same graph as the experimental results, figure 3·29. In this figure the open triangles are the data points to which the equation was fitted, and the line is the fitted curve. The filled inverted triangle is a data point which was gathered after the fitting was performed, indicating that the fit is able to predict the values of true stress or strain rate with good accuracy.

| | Activation Volume | $[\dot{\varepsilon}_0']$ |
|---|---|---|
| Process 1 | 984 Å$^3$ | $2{\cdot}47\times10^{-27}$ |
| Process 2 | 143 Å$^3$ | $8{\cdot}69\times10^{-5}$ |

**Table 3·4**

Activation parameters for quenched 6007 at draw ratio 9.

The value of the high stress, (process 2), effective activation volume derived previously is of the same order of magnitude as the one derived by this more complete treatment, ( 98 Å$^3$ compared with 143 Å$^3$). This gives a reasonable level of confidence in the other results obtained by assuming the presence of a single process with effective activation parameters based on a combination of the real parameters.

However the agreement between the actual activation volume derived earlier, by using the effective value and the value of the activation volume of the first process, is better, with a volume of 114 Å$^3$ compared to the 143 Å$^3$ of the complete method.

Figure 3·29

Best Eyring fit for the quenched morphology of 6007 at draw ratio 9.

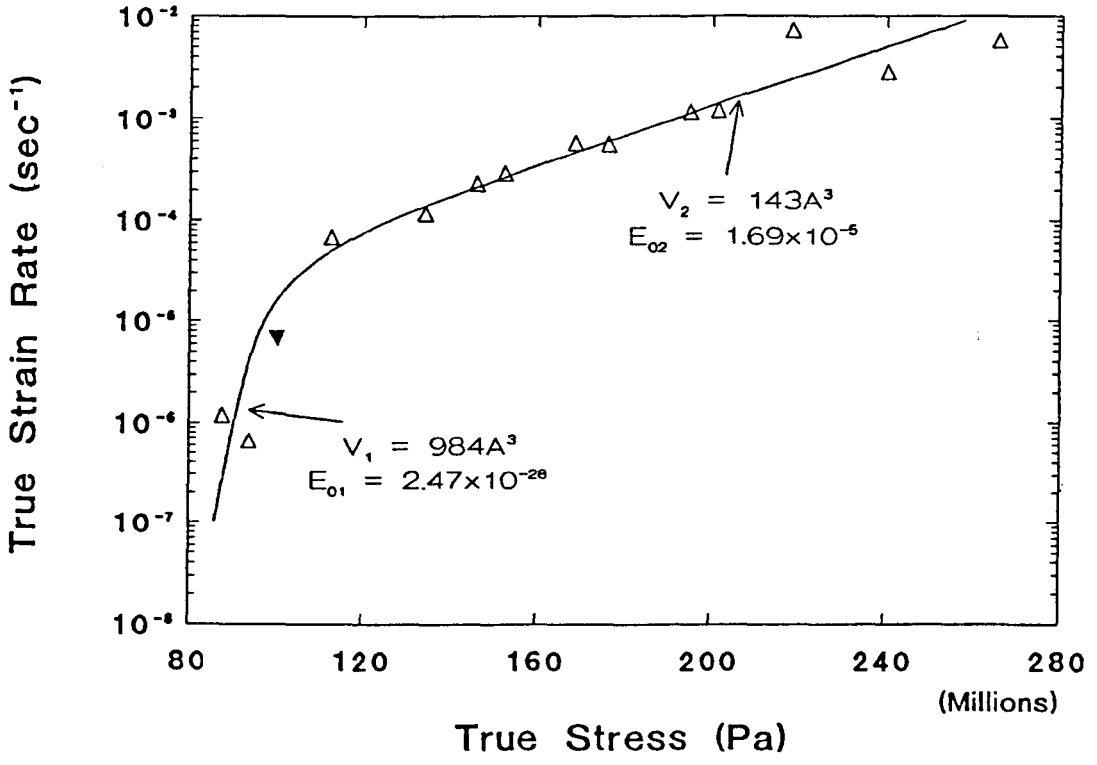

### 3·6 Fotheringham and Cherry Approach

Transient stress dip tests were performed on the quenched morphology of 6007 at draw ratio 9 and room temperature. This material and strain were chosen because this was the material and strain used with the two Eyring process model discussed earlier. The results from these transient stress dip tests are shown in figure 3·30. It can be seen from this graph that the recovery stress decreases steadily as the strain rate is increased. This is a surprising result, and is not thought to be caused by experimental technique. It may indicate that there is a breakdown in the network within the polymer as the strain rate is increased.

The effective stress data were fed into a fitting routine used to fit equation 1·18 of this co-operative jump model. The resulting fit is shown in figure 3·31.

It can be seen that for the data in the strain rate region covered by the transient stress dip tests the fit obtained is reasonable. However the values of the variables required to produce the fit are not.

The value of $K_T$ is very low, $\sim 10^{-5}$.

The value of n is less than one. This is physically unreasonable.

The activation volume is a factor of 6 larger than the activation volume for the second, high stress, process derived using the two Eyring process model. It is also larger than the activation volume derived for the isotropic material using this co-operative jump model, (687 $Å^3$ at $\lambda = 9$, 151 $Å^3$ at $\lambda = 1{\cdot}1$). It does not seem likely that orientation would cause the activation volume to increase in this manner.

Also when the co-operative jump approach is fitted to all the data gathered for the quenched morphology of 6007 at draw ratio 9 it is not possible to produce a good fit in the low stress region. In addition the values of the fitted parameters get even worse, ($K_T \sim 10^{-5}$, n = 0·234 and V = 1070 $Å^3$). In order to produce this fit it was assumed that the three lowest stress data points had effective stresses of 2% of the applied stress for the 100 MPa data point and 1% of the applied stress for the two lowest stress data points. This does not seem to be unreasonable given the low effective stress for the data point just below the $1 \times 10^{-4}$ $sec^{-1}$ strain rate. It can be seen from figure 3·32 that while a good fit is still obtained for the high stress region, the turn over for the fitted curve is less sharp than the experimental curve, and from figure 3·33 it can be seen that the values of $\frac{\sigma_e}{T}$ for the fitted curve at each experimental strain rate are not stable in the low stress region and oscillate below the experimental data. However this may be an artefact of the fitting procedure used.

Figure 3·30

Recovery stress data for the quenched morphology of 6007 at draw ratio 9 and room temperature.

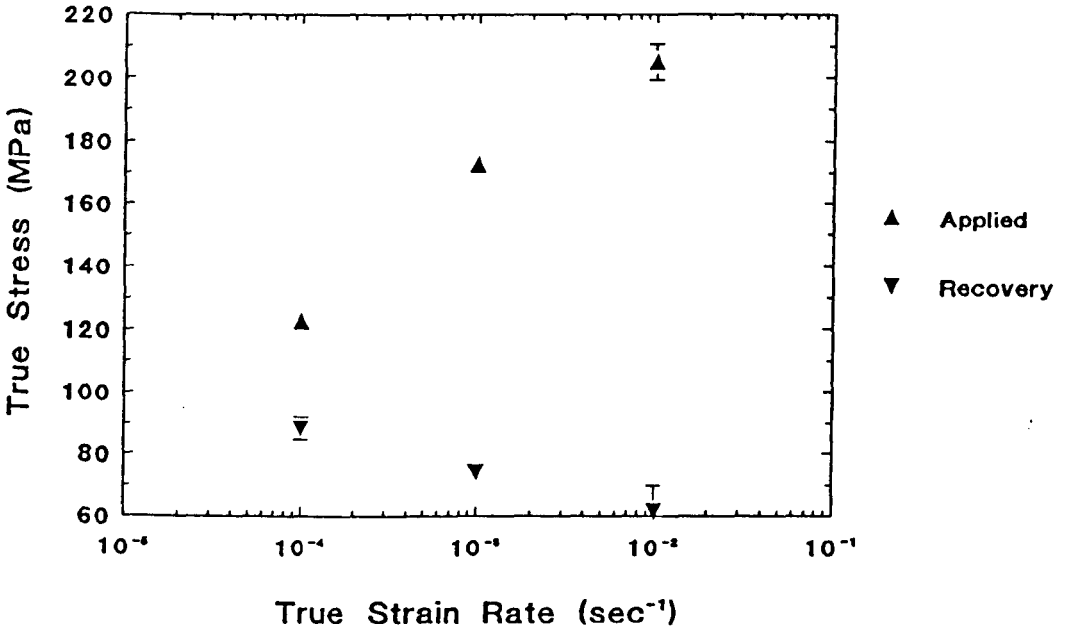

Figure 3-31

Fotheringham Cherry fit for the quenched morphology of 6007 at draw ratio 9 and room temperature, fitted to the high stress data only.

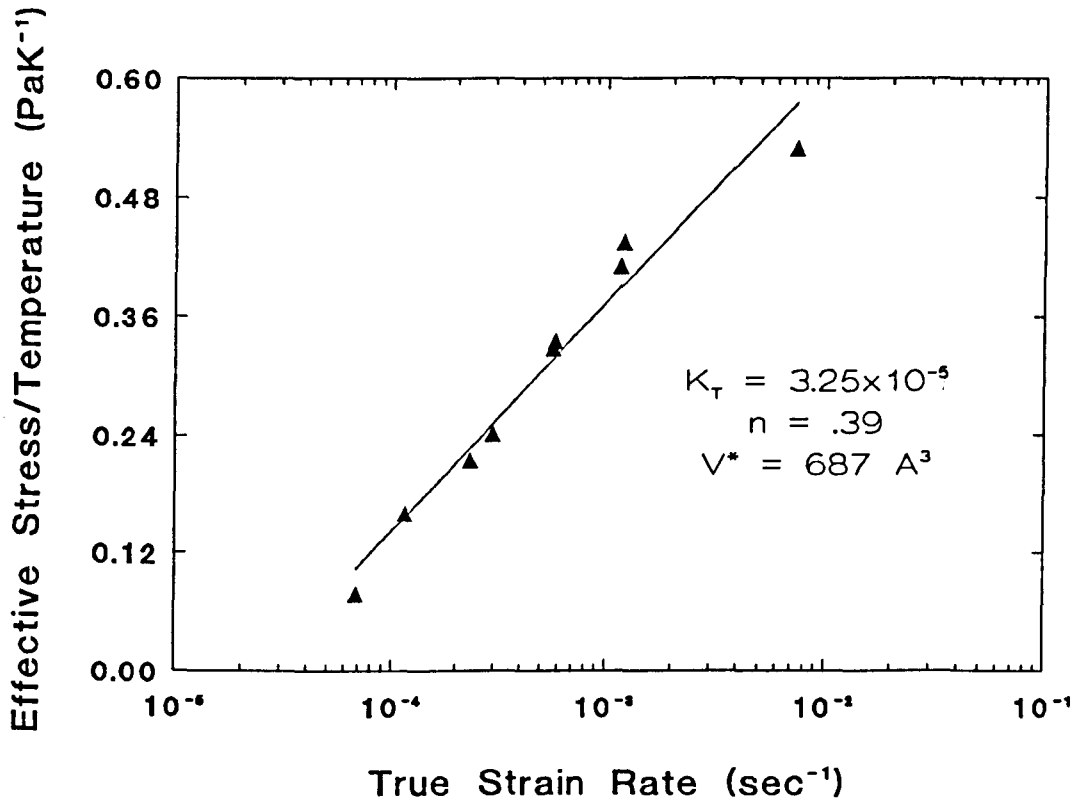

Figure 3-32

Fotheringham Cherry fit for the quenched morphology of 6007 at draw ratio 9 and room temperature, using all available data.

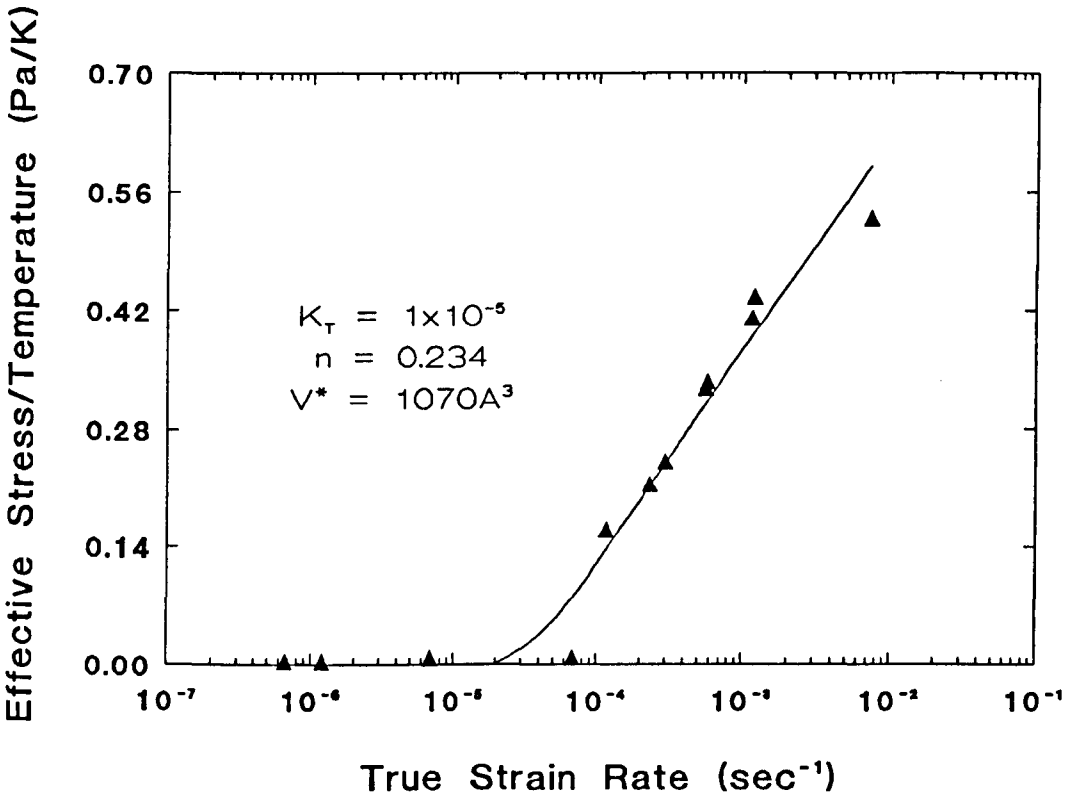

Figure 3·33

An expansion of the low stress region of the Fotheringham Cherry fit for the quenched morphology of 6007 of 6007 at draw ratio 9 and room temperature, using all available data.

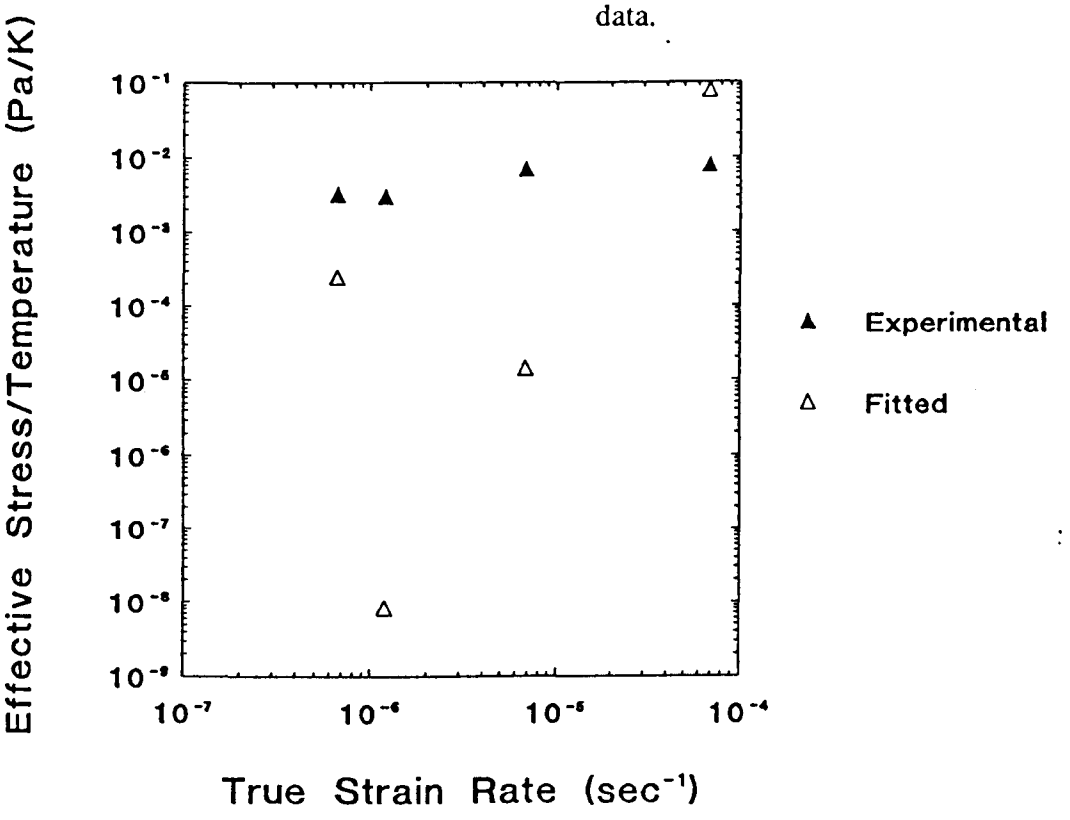

Because this work was begun at the end of the project there was insufficient time to perform a thorough investigation into the effects of temperature, so no master curve was produced and no activation energy has been calculated. However, the master curve is simply all the data shifted by eye to lie on the room temperature curve. Thus if a good fit with reasonable values of the fitted parameters cannot be obtained for the curve at room temperature itself, it does not seem likely that the addition of more data points will alter the fit, because for the model to work at all, the shape of the curve must be the same when these extra data points are added.

## 3·7 Validity Of Unique True Stress, True Strain And True Strain Rate Relationship

In order to obtain more data in the low stress region for quenched 6007 at draw ratio 9 a series of tests were conducted on an Instron tensile testing machine running at constant crosshead velocity.

These tests were conducted in an Instron because the available creep data indicated that there would be a very strong stress dependence, and as such it was easier to choose the crosshead speed to set the strain rate, rather than select stress levels which would require loads of just a few tens of grams difference.

The samples were drawn at the standard draw rate to their natural draw ratio, and were then allowed to relax. The crosshead velocity was then selected to provide the required true strain rate at draw ratio 9.

The two data sets are shown in figure 3·11. The discrepancy is obvious. It is thought that one possible reason for this discrepancy is dashpot 1. It was stated earlier that this dashpot has a very high viscosity, and could be considered to have infinite viscosity at low stress. This is obviously only an approximation.

It may be that equilibrium has not been reached. At short times, (or low stress levels), the dashpot does not yield and flow because the spring $E_1$, figure 3·34, does not reach an equilibrium extension. Thus no stress is transferred to dashpot 1 and hence all the extension in this side of the model is caused by the elastic extension of the spring $E_1$. At long times, (or high stresses), the dashpot will flow since the spring $E_1$ does reach an equilibrium extension, thus stress is transferred to dashpot 1 and it will begin to flow, consequently the extension of this side of the model is now caused by both the elastic extension of the spring $E_1$ and the plastic extension of dashpot 1.

Since under recovery dashpot 1 can be assumed to have essentially infinite viscosity, because $\eta_1 >> \eta_2$, dashpot 1 will carry the permanent strain, and with longer time will flow more and hence a greater permanent strain will be developed.

Figure 3·34

Schematic representation of the mechanical interpretation of the two Eyring process model.

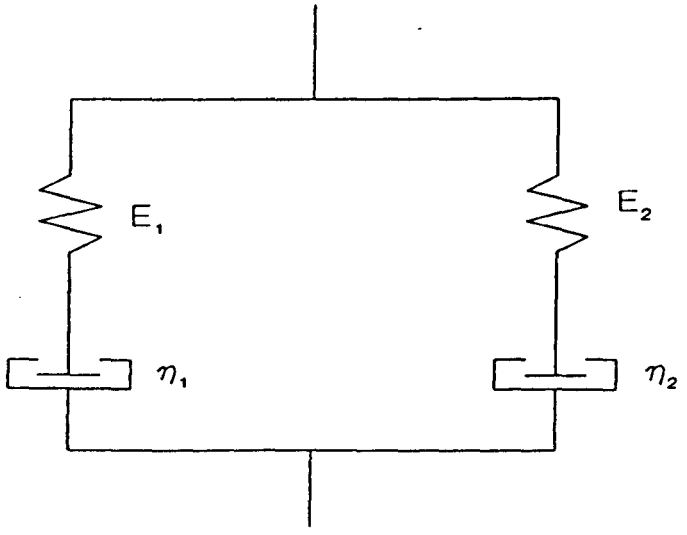

In the creep tests the material can develop to an equilibrium situation over a long time period. Thus dashpot 1 will flow in an equilibrium manner, leading to true plastic flow.

In a test conducted in an Instron the material is both being forced to extend at an artificially high rate, and is not loaded in a step sequence as in a creep test. Thus dashpot 1 will not flow as much, since it has had less time under load, and hence a large proportion of the applied strain rate will be due to the recoverable elastic extension of the spring $E_1$ as it attempts to reach an equilibrium extension rather than permanent plastic flow.

### 3·8 Conclusions

The transition from region 1 to region 2 of the Sherby Dorn plots is caused by the reextending of a polymer network, which has a memory of the strain history applied to it.

Even though the creep experiments did not reach a state of strain rate equilibrium, (a situation where the strain rate remained constant with increasing strain), a unique true stress, true strain rate, strain relationship still exists for the three materials, provided that the initial morphology of the oriented material is equivalent.

The difference in creep performance between the quenched and slow cooled morphologies of the 6007 and 00240 can be explained in terms of an increase in tie molecule content and general entanglement of the amorphous regions in the quenched state. The lack of difference in creep performance of the 5502 between the slow cooled and quenched morphologies is surprising, and has not as yet been explained.

A two process model based on the viscous flow ideas of Eyring can be used to described the behaviour of the oriented material over the entire stress range covered.

The assumption that the behaviour of the material can be approximated to a single Eyring type process with constant activation parameters is valid providing that the area under investigation is not in the region where both processes make approximately equal contributions, that is provided the area under investigation is solely composed of the high stress or low stress regions. In the intermediate region this approximation will not hold.

From values of the activation energies derived it is concluded that c-shear is the mechanism which controls creep in oriented quenched 6007 and 5502.

It is concluded that the Fotheringham and Cherry co-operative jump approach is not a successful method for the modelling of oriented polyethylene.

### 3·9 References


1. Bhattacharya, S.K. and Brown, N., J. Mat. Sci., **19**, (1984), 2519
2. Sherby, O.D. and Dorn, J.E., Journal of the Mechanics and Physics of Solids, **19**, (1956), 165
3. Capaccio, G. private communication, 1992
4. Coates, P.D., and Ward, I.M., Journal of Materials Science, **13**, (1978), 629
5. Coates, P.D., Gibson, A.G. and Ward, I.M., Journal of Materials Science, **15**, (1980), 359
6. Coates, P.D. and Ward, I.M., Journal of Materials Science, **15**, (1980), 2897
7. Capaccio, G. and Ward, I.M., Polymer, **15**, (1974), 233
8. Capaccio, G, Crompton, T.A. and Ward, I.M., Journal of Polymer Science: Polymer Physics Ed., **14**, (1976), 1641
9. Brown, N. and Ward, I.M., Journal of Materials Science, **18**, (1983), 1405
10. Coates, P. D., PhD Thesis, University of Leeds, 1976
11. Wilding, M. A. and Ward, I. M., Polymer, **22**, (1981), 870
12. Kajiyama, T., Okada, T., Sakoda, A. and Takayanagi, M., J. Macromol. Sci.-Phys., **B3**, (1973), 583
13. Alberola, N. Cavaille, J. Y. and Perez, J., J. Polymer Sci. B, **28**, (1990), 569
14. Rasburn, J., Klein, P. G. and Ward I., M., J. Polymer Sci. B, **32**, (1994), 1329

# Chapter 4

# The Isotropic State

## 4·1 Introduction

For the same reasons that the long term plastic deformation, (or creep), behaviour is important in the oriented state, it is important in the isotropic state. It is especially important in situations where a load acts constantly upon a material, as this will tend to cause the material to extend. In this chapter the creep behaviour of the isotropic material will be considered, with attention paid to the apparent effects of the crystallinity of the material. It will also be shown that within the creep data there is evidence for the existence of two yield points in the three grades studied. This supports the ideas and results of Brooks et al.[1].

The creep data that will be presented have been analysed using two different models. The first model used was the two Eyring type process approach, which has been shown to be successful in describing the behaviour of the oriented material in this work, (see chapter 3), and oriented material in numerous other studies[2,3]. The second model was a co-operative jump model based upon the work of Fotheringham and Cherry[4], and which has been successfully used by Brooks et al.[1] in their work on isotropic polyethylene. In both cases the data for the quenched morphology of 6007 was used when fitting the model, since this was the most complete data set available. The results of fitting the two models will be presented, and the activation parameters will be compared to those previously published.

An explanation as to what causes the discrepancy between the position in strain at which second yield point occurs in creep tests and conventional Instron experiments will also be proposed.

## 4·2 Creep Behaviour

The creep behaviour of all three grades in both quenched and slow cooled morphologies was investigated using the dead loading creep apparatus designed within this department, as described previously in chapter 2. The data were transferred from the monitoring computer to a spreadsheet and then plotted as Sherby Dorn plots, as described previously in chapter 1 for the oriented material. The resulting Sherby Dorn plots for the three grades are shown in figures 4·1 to 4·6.

It is apparent from these figures that the Sherby Dorn plots have the same general shape as those for the oriented material, chapter 3. That is they have a sharp decrease in strain rate with strain followed by a "plateau" region where the strain rate remains relatively constant.

Figure 4·1

Sherby Dorn plots for the quenched morphology of isotropic 00240.

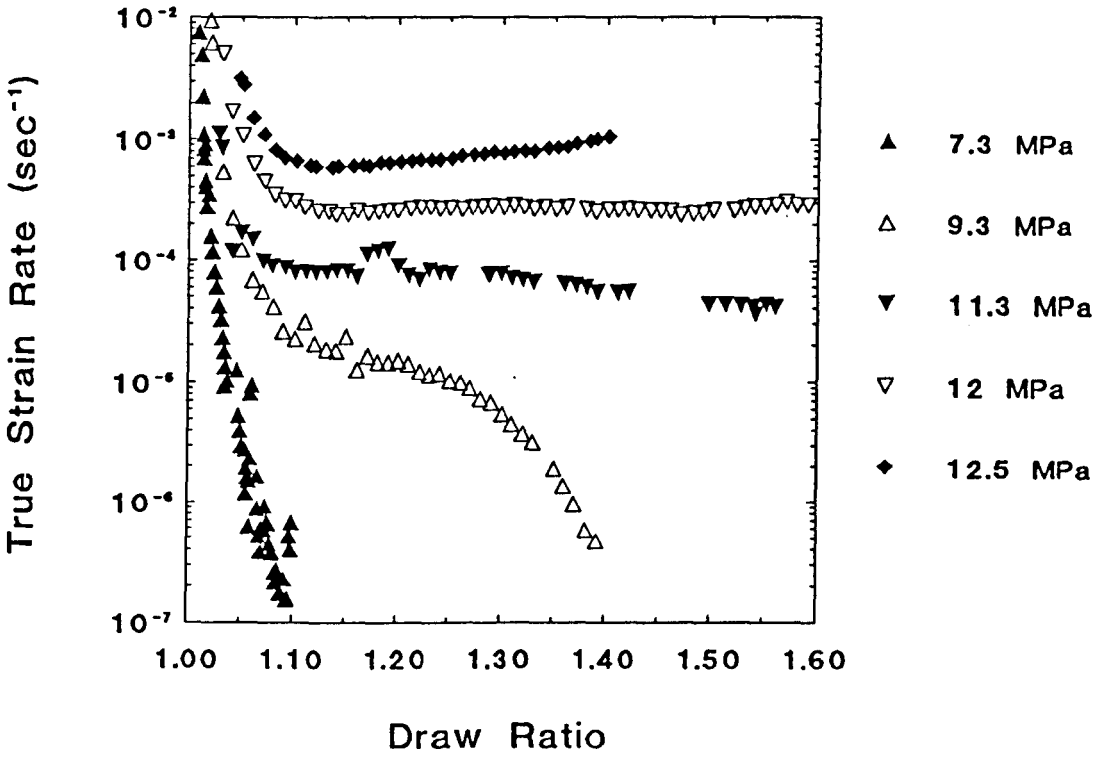

Figure 4.2

Sherby Dorn plots for the slow cooled morphology of isotropic 00240.

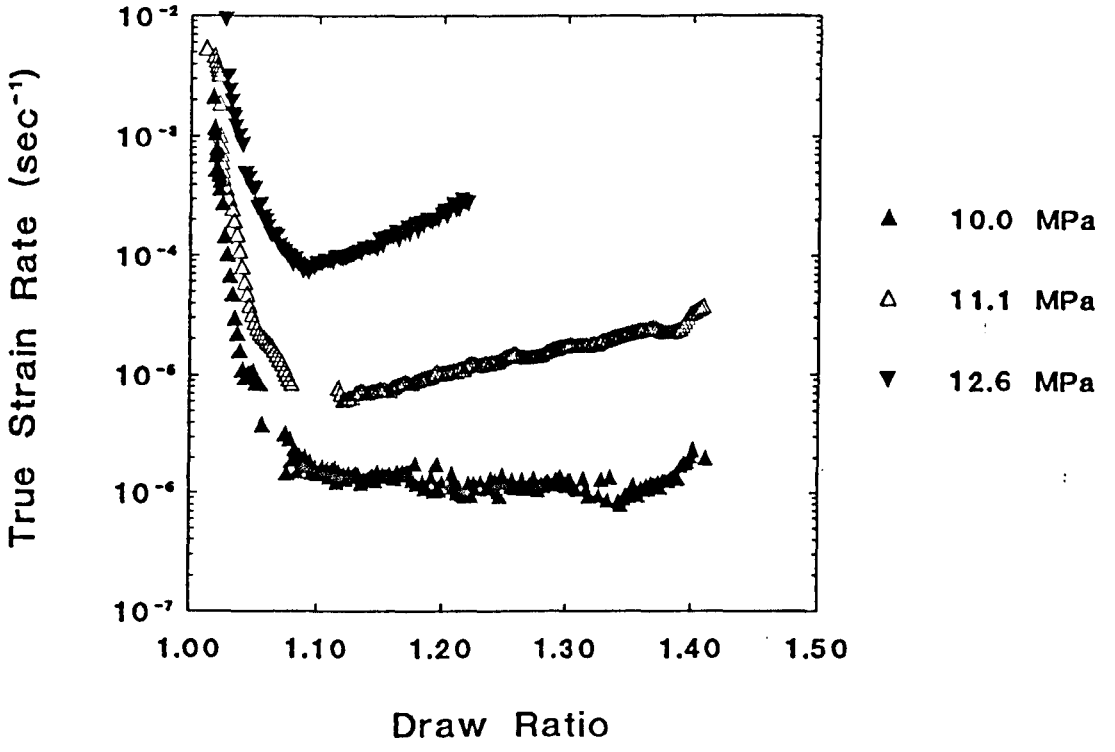

Figure 4-3

Sherby Dorn plots for the quenched morphology of isotropic 5502.

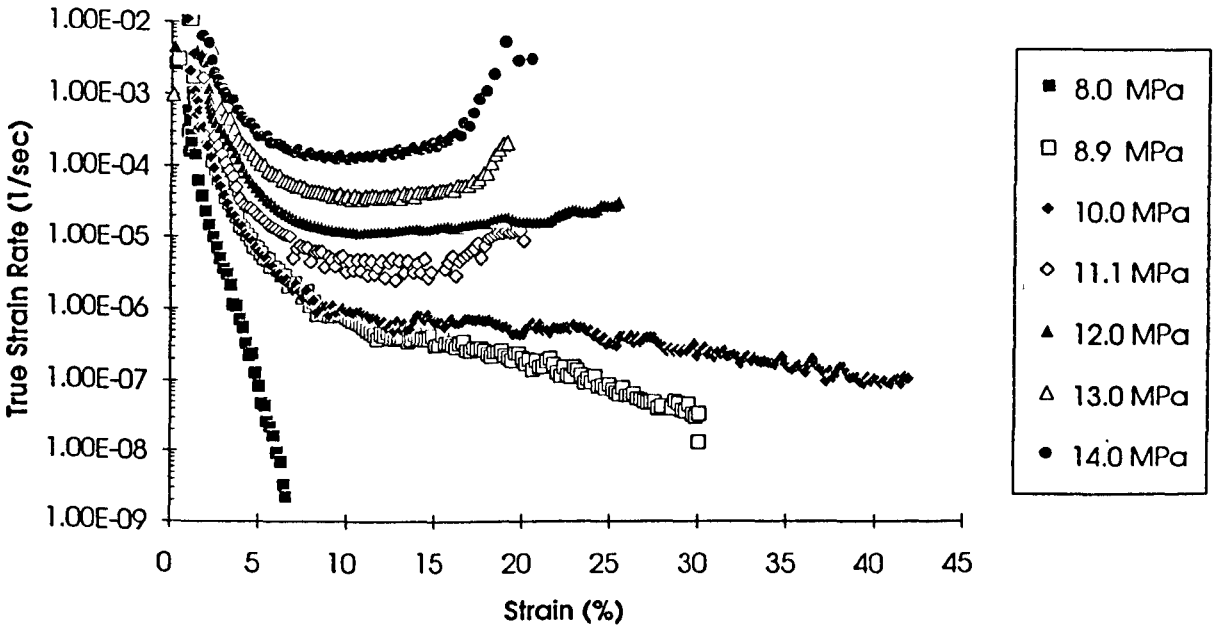

Figure 4-4

Sherby Dorn plots for the slow cooled morphology of isotropic 5502.

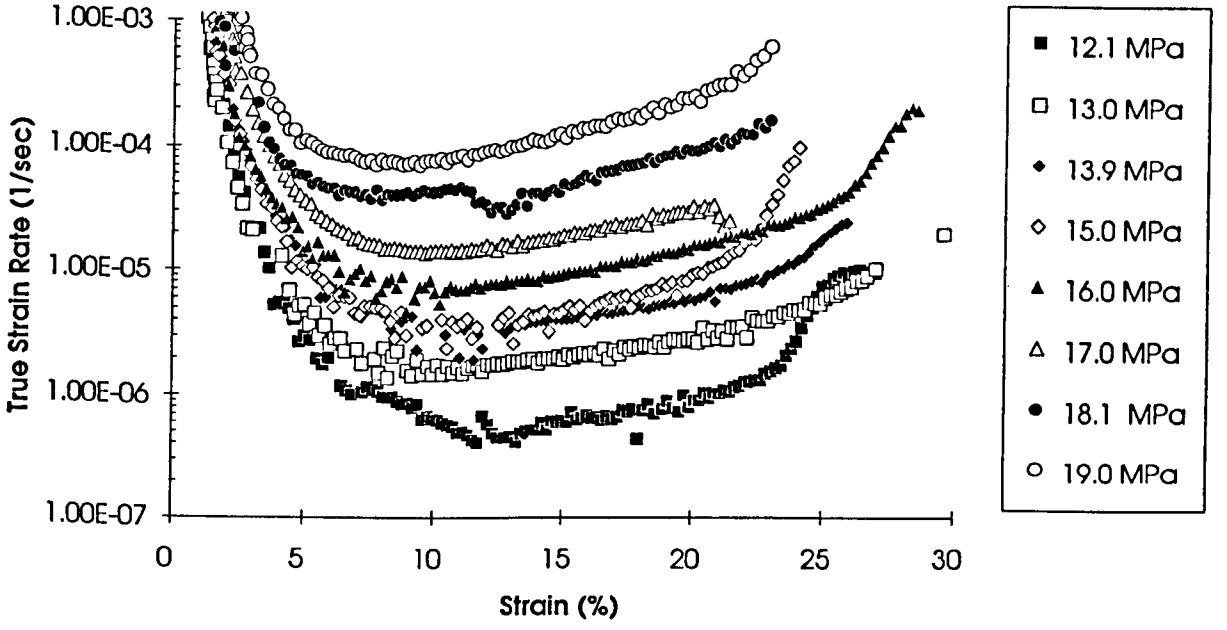

Figure 4-5

Sherby Dorn plots for the quenched morphology of isotropic 6007.

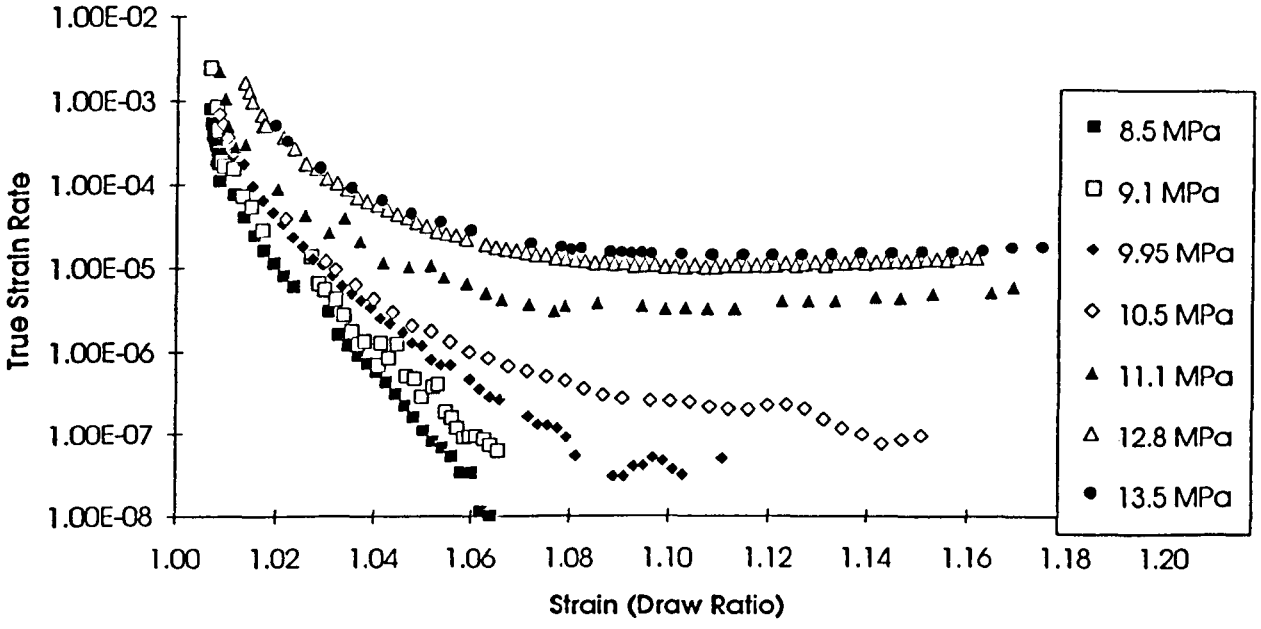

Figure 4-6

Sherby Dorn plots for the slow cooled morphology of isotropic 6007.

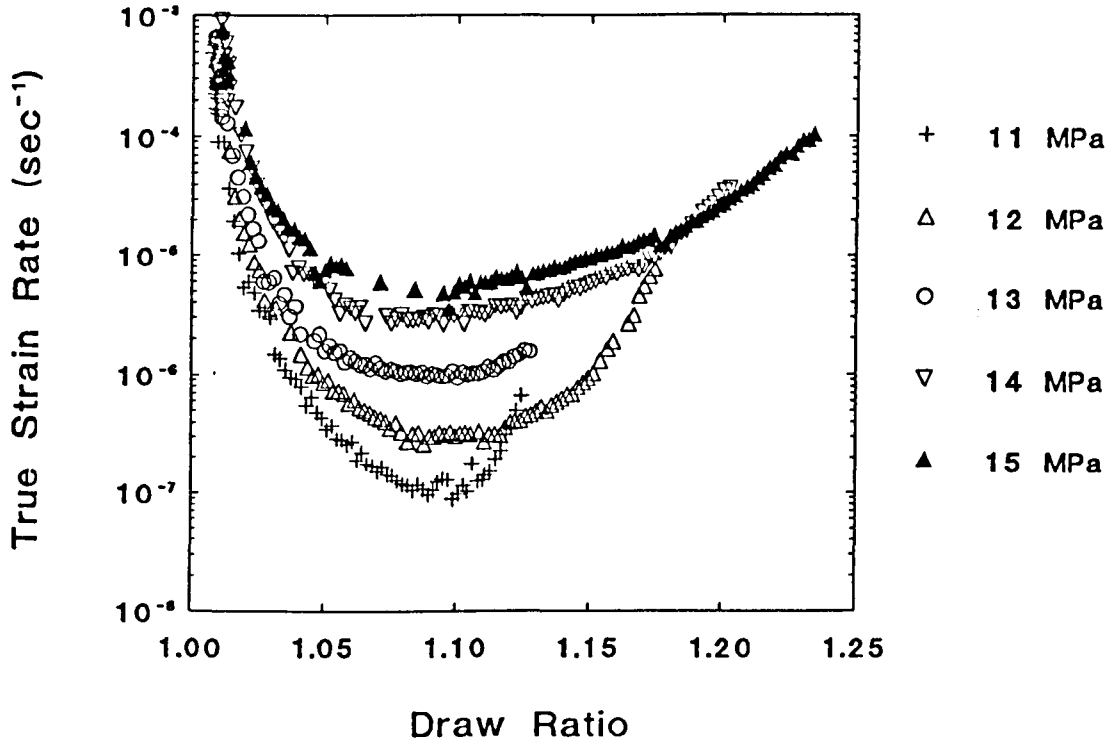

In order to show more clearly the difference in creep performance that arises from the change in morphology from quenched to slow cooled, a set of Sherby Dorn plots showing the behaviour of both the quenched and slow cooled material at a single stress were produced. These are shown in figures 4·7 to 4·9. It is apparent that in all cases the slow cooled morphology has a better creep resistance than the quenched morphology. The reason for this is likely to be complex. It is apparent from figures 4·7 to 4·9 that, provided that the samples are loaded at equivalent nominal stresses, all three grades show at least an order of magnitude improvement in the creep performance of the slow cooled material, and in the case of 5502, figure 4·8, the improvement is by two orders of magnitude. This indicates a major change in the morphology of the material, which cannot be explained simply on the basis of an increase in the crystallinity, which in the case of 5502 has a relative change of less than 15%, (from 60·1% to 68·4%).

However there is a large change in the crystallite thickness, for example in 5502 the thickness of the crystallites increases from 172 Å to 249 Å when the sheet is slow cooled rather than quenched. This may account for the improved properties of the slow cooled materials, since the yield stress is dependent on the lamellar thickness, as can be seen from Table 2·2 in chapter 2. Also when isotropic samples are loaded to equivalent fractions of their yield stress, (figures 4·8 and 4·9), then the creep performance is essentially equivalent.

The conventional yield point provides an easy way of ranking the creep behaviour of the material. At the conventional yield point the strain rate of the machine matches the plastic strain rate of the material. In a creep test it is the plastic strain rate which is being monitored, and, as can be seen in figure 4·10, there is a good agreement between the two sets of data, one obtained from yield work on an Instron, (with the strain rate and stress at the conventional yield point), and one from creep data taken immediately after the transition from region 1 to region 2 of the Sherby Dorn plot, (figure 4·11).

The ranking provided by yield stress, creep performance or natural draw ratio is the same as the percentage crystallinity. Thus we can conclude that at least for the molecular weight range covered by the polyethylenes this work has studied, percentage crystallinity is an important factor in determining the mechanical properties of polyethylene.

Figure 4·7

Comparison of creep in the quenched and slow cooled morphologies of isotropic 00240 at a nominal stress of 12·5 MPa

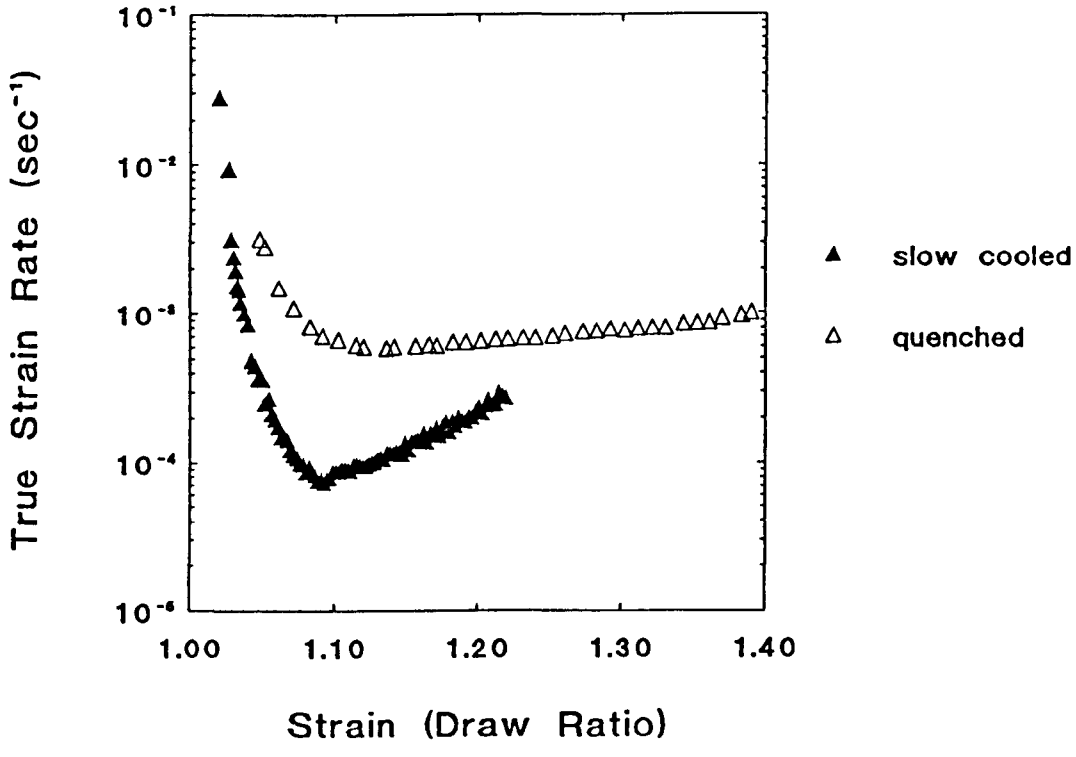

Figure 4·8

Comparison of creep in the quenched and slow cooled morphologies of isotropic 5502.

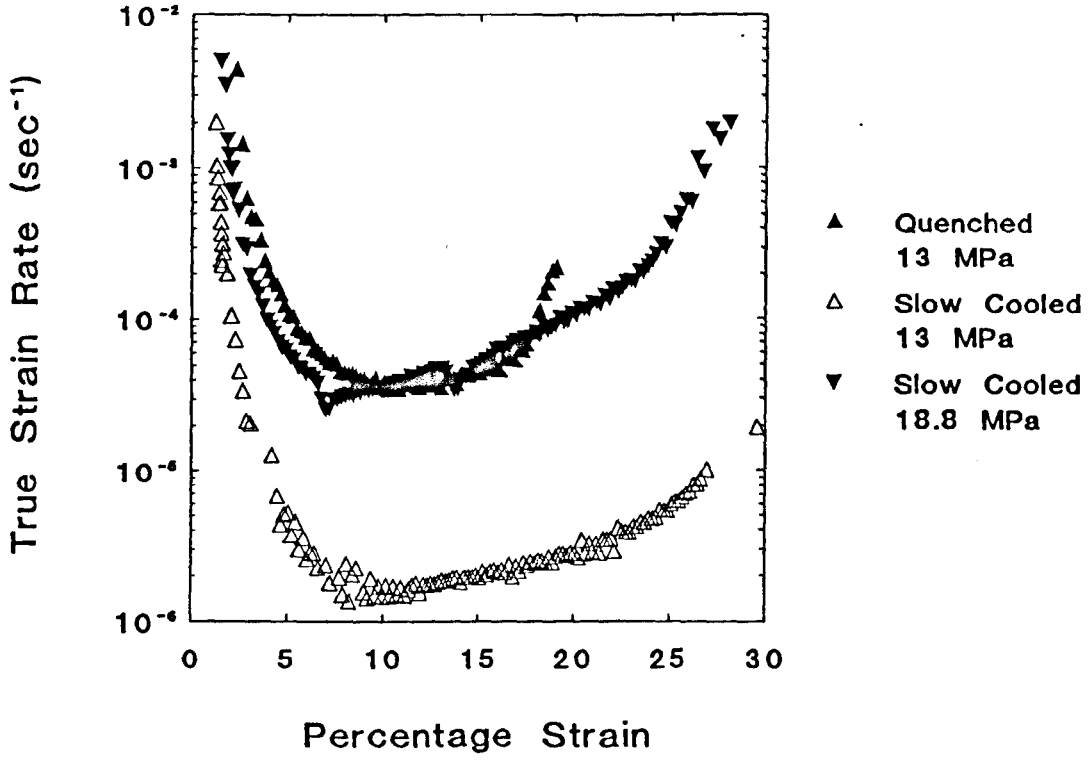

Figure 4-9

Comparison of creep in the quenched and slow cooled morphologies of isotropic 6007.

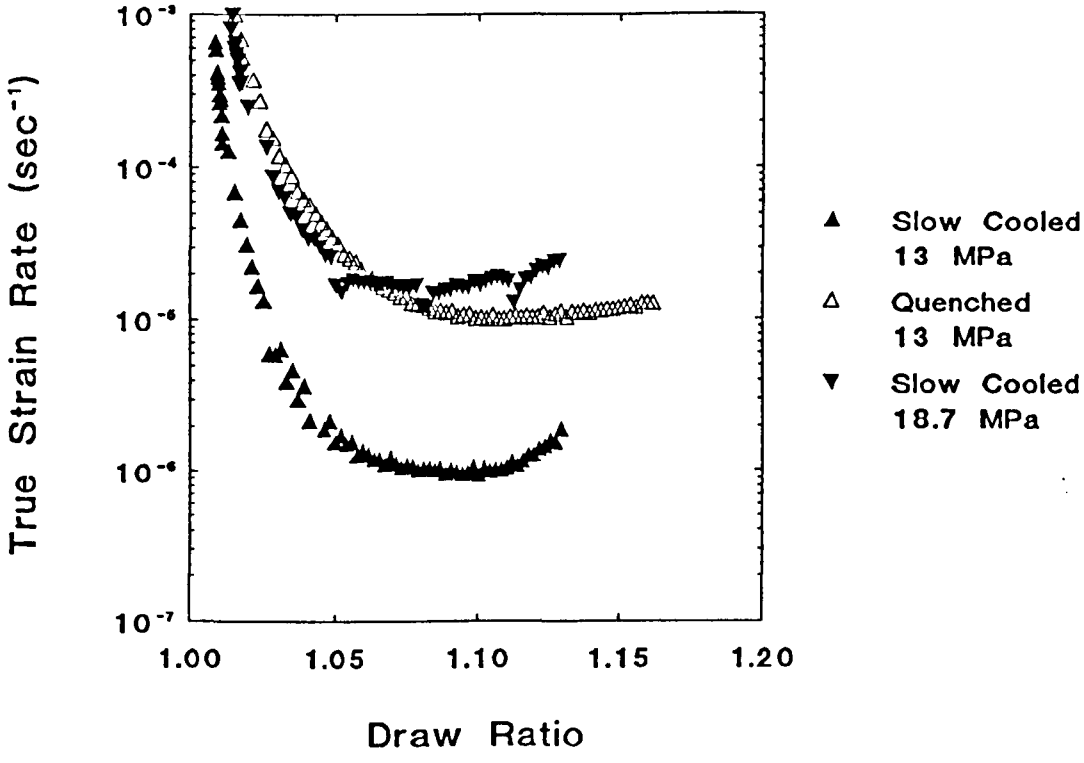

Figure 4·10

Comparison of creep and yield behaviour in the quenched morphologies of isotropic 00240 and 6007.

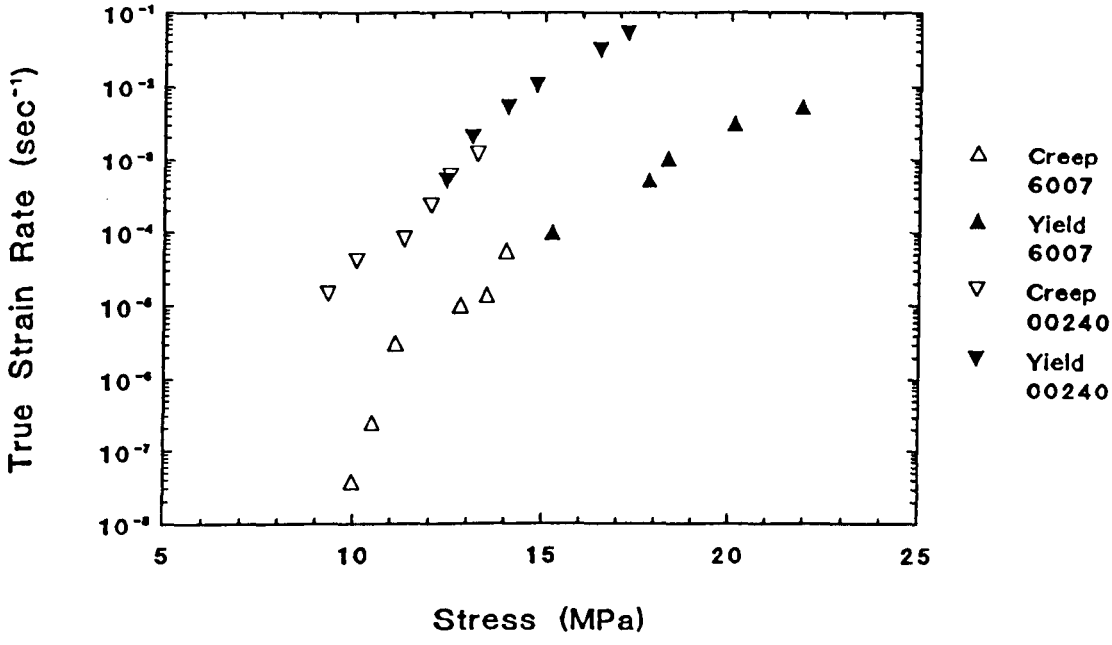

Figure 4·11

Schematic representation of the Sherby Dorn plot as used in creep experiments.

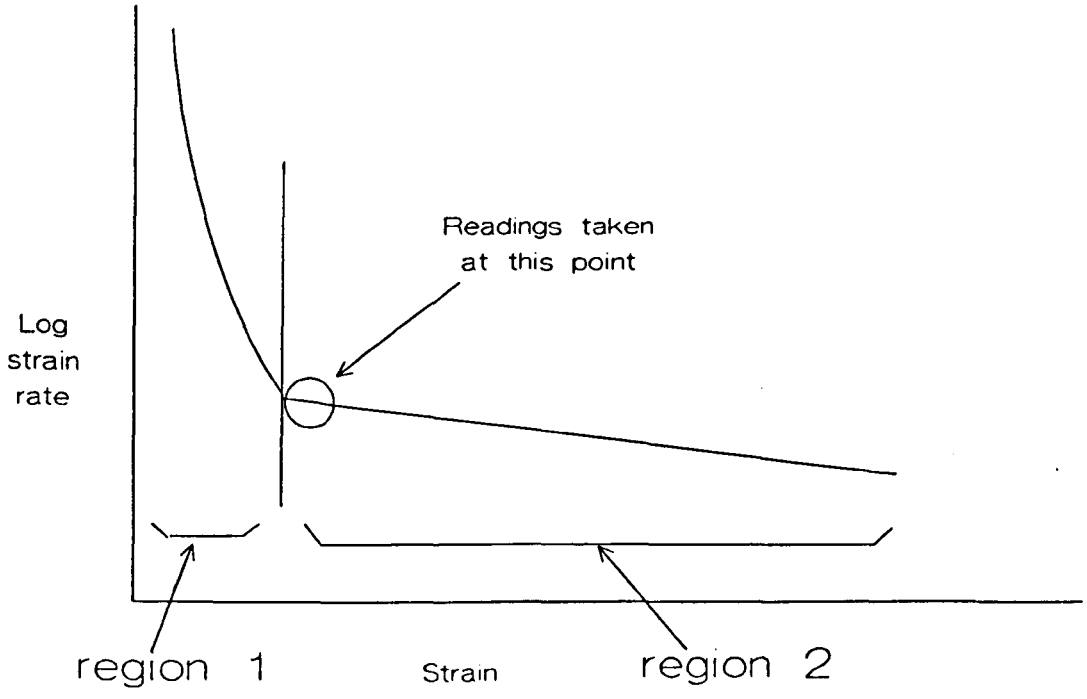

## 4·3 Form Of The Sherby Dorn Plots - Double Yield Points

The work of Brooks et al. within this department on double yield points in polyethylene meant that at an early stage it was realised that when the creep data for the isotropic material was plotted in a Sherby Dorn format it provided additional evidence of the existence of these two yield points.

This initially occurred when it was noted that the transition from region 1 to region 2 of the Sherby Dorn plot, (see figure 4·11), occurred at the same strain values as the first yield detected by Brooks, (between 5 and 10%). The values of strain at which this transition occurs are presented in Table 4·1.

| Grade | Range of Strain at First Yield Point (%) |
|---|---|
| 00240 Quenched | 8 |
| 00240 Slow Cooled | 9 |
| 6007 Quenched | ≈7 |
| 6007 Slow Cooled | 5 → 9 |
| 5502 Quenched | 6 → 8 |
| 5502 Slow Cooled | 5 → 8 |

**Table 4·1**

Table showing the strain values associated with the transition from region 1 to region 2 of Sherby Dorn plots, (the first yield point), for isotropic polyethylene.

It can be seen from figures 4·1 to 4·6 that the more crystalline materials exhibit a stress dependence of this first yield point, with the strain at which the first yield point occurs decreasing as the stress is increased.

The second yield point of Brooks work was associated with a sharp necking of the sample when tests were conducted in tension on an Instron tensile testing machine. The creep experiments were terminated when necking of the sample occurred. The strains at which this happened are similar to the strains quoted by Brooks for the second yield point in his work.

Brooks quotes a value of approximately 35% for the second yield point in his work. Using creep experiments it was found that the quenched 00240 necked around 40%, slow cooled 00240 around 30%. Both quenched and slow cooled 6007 necked around 15 to 20%, and quenched and slow cooled 5502 necked around 25%.

Although in general the strain values for the second yield point, (necking), in this work are lower, Brooks conducted his work mainly under compression, and hence did not have the problems associated with a flaw or notch in the material causing a stress concentration and subsequent premature yielding.

However there is also evidence from tensile experiments conducted in an Instron tensile testing machine that there may be a time dependence or stress history effect that needs to be considered when comparing the two sets of results. This will be discussed in greater detail later.

These two yield points were found by Brooks using residual strain experiments. As described previously these involved placing a known compressive strain on the sample and then allowing it to recover in an unconstrained state for three days, before measuring the amount of residual strain it still held. It was found that recovery was complete up to the first yield point, partial between the first and second yield point, and irrecoverable after the second yield point.

Obviously in tension when the samples neck and yield, orientation begins to take place and the deformation is largely plastic and irrecoverable. However a series of recovery experiments, figures 4·12 and 4·13, were conducted at strains up to the second yield point, in order to test whether the same behaviour would be apparent in tension. It was discovered that for strains up to the first yield point recovery was complete to within the resolution of the machine. Between the first and second yield points recovery took place, but was not complete. Whilst Brooks speculated that given sufficient time the recovery would be complete, data acquired from these creep recovery experiments indicates that a fraction of the applied strain will always remain irrecoverable. This will be discussed in more detail later.

### 4·4 The Two Process Approach

The creep data presented previously for the quenched morphology of 6007, was used to provide the data plotted in figure 4·14. This plot is similar to the form of those shown in figures 3·12 to 3·17. Thus it was thought to be reasonable to use the two process model discussed previously to attempt to describe the behaviour of this material.

#### 4·4·1 Parameterising The Model

This model is the Eyring two process model discussed previously for the oriented material. The mechanical interpretation is shown in figure 4·15.

It was decided to attempt to determine the real values of $E_1$, $E_2$, and $\eta_2$ in the model. In order to accomplish this a series of recovery and transient stress dip tests were undertaken. It is not possible to determine a value for $\eta_1$ by the simple methods used to derive values for the other three parameters, ($E_1$, $E_2$, and $\eta_2$), so no values for this have been calculated.

Figure 4-12

Strain versus time for the quenched morphology of isotropic 6007. .

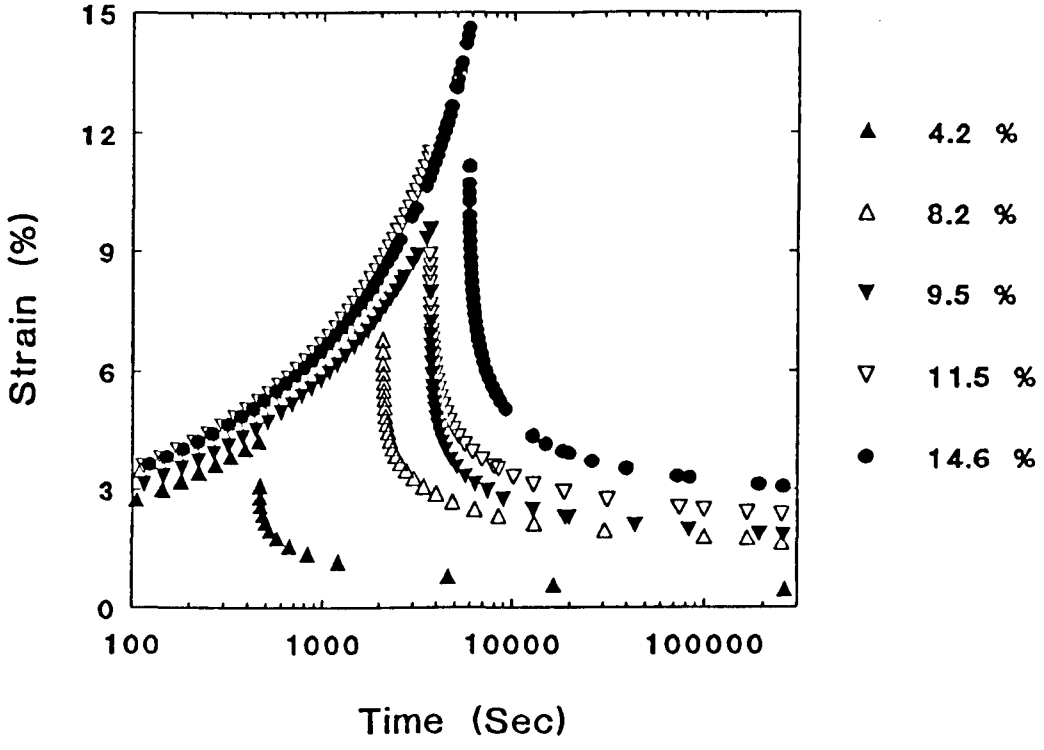

Figure 4·13

Strain versus time for the quenched morphology of isotropic 00240.

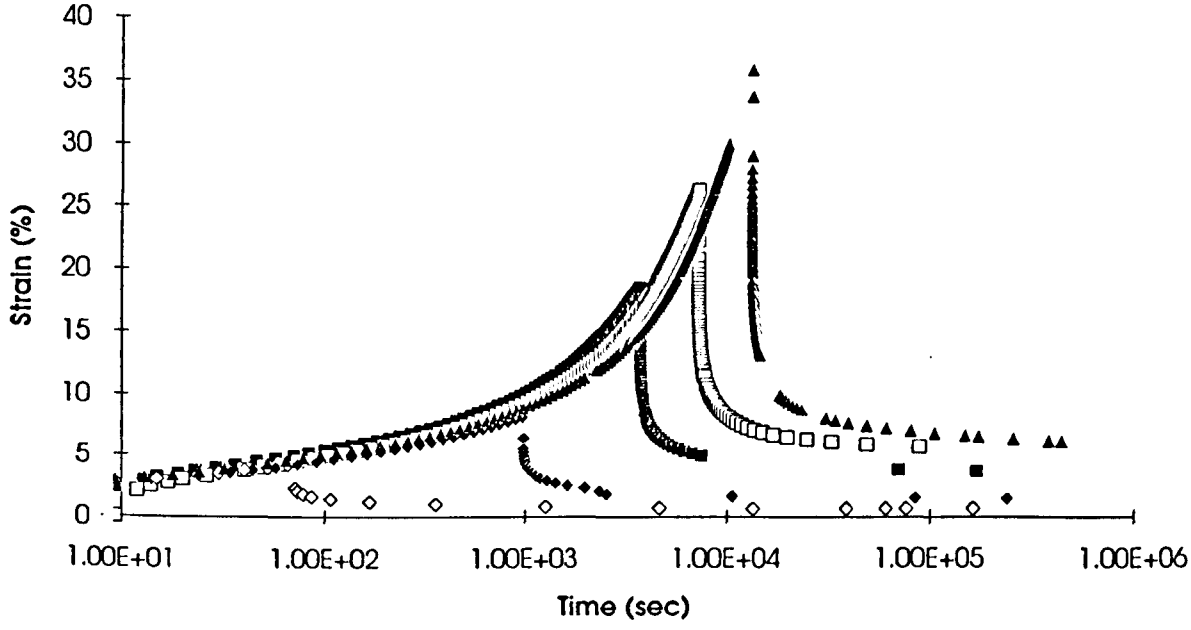

Figure 4·14

True strain rate versus true stress data for the quenched morphology of 6007 at draw ratio 1·1.

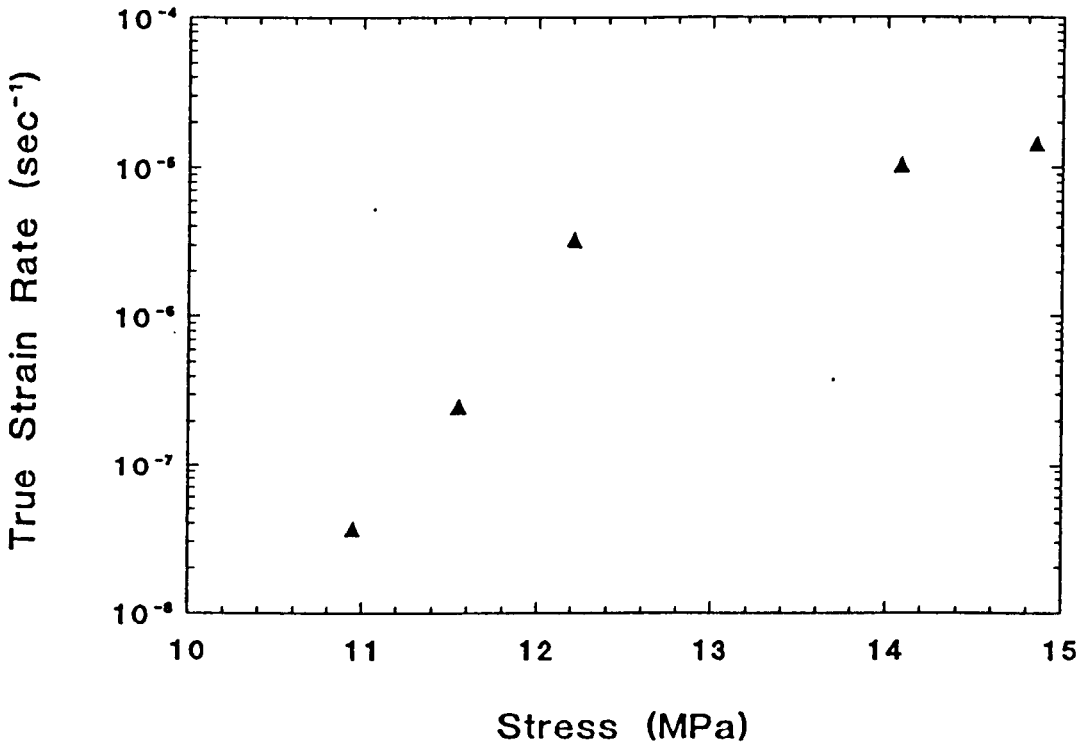

Figure 4·15

Schematic representation of the mechanical interpretation of the Eyring two process model.

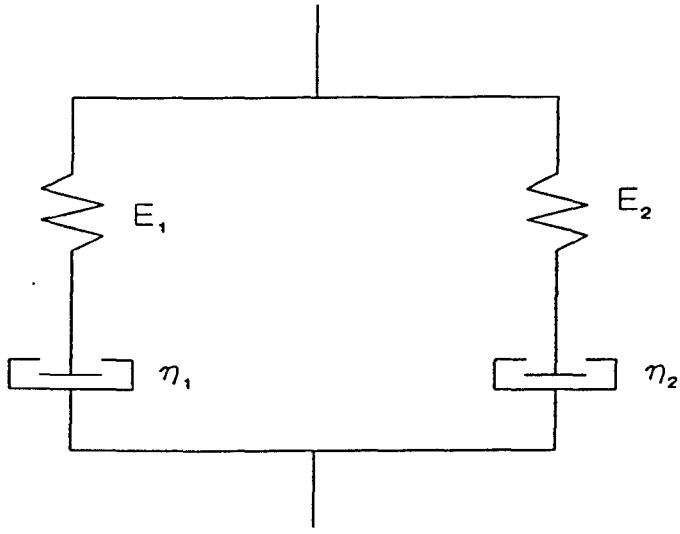

### 4·4·2 Recovery

The data from recovery experiments carried out as detailed in chapter 2, for quenched 6007 and quenched 00240 is shown in figures 4·12 and 4·13. These two grades were studied primarily because they were the most widely different available.

As stated earlier, up to the first yield point these experiments show complete recovery to the limit of resolution of the apparatus. They also show that at strains in excess of the strain at which the first yield point occurs there is a "permanent" strain developed in the material.

This permanent strain, $\varepsilon_p$, may well recover if left unconstrained for a sufficient period of time, however the creep rigs have a lower strain rate limit of around $1\times10^{-9}$ $sec^{-1}$, and because of this the recovery experiments were terminated when the recovery strain rate decreased below $9\times10^{-9}$ $sec^{-1}$. The strain still left in the sample at this point was defined as the permanent strain.

The magnitude of the permanent strain as a percentage of the applied strain is shown in Table 4·2, (in this table $\varepsilon_p$ is the permanent strain as defined above and $\varepsilon_a$ the applied strain defined as the strain to which the test was allowed to progress before the recovery was initiated).

| Grade | $\varepsilon_a$ (%) | $\varepsilon_p/\varepsilon_a$ |
|---|---|---|
| 00240 | 35·7 | 0·19 |
| 00240 | 26·2 | 0·21 |
| 00240 | 18·5 | 0·21 |
| 00240 | 8·1 | 0·18 |
| 6007 | 15·6 | 0·21 |
| 6007 | 11·5 | 0·22 |
| 6007 | 9·5 | 0·22 |
| 6007 | 8·2 | 0·22 |

**Table 4·2**

Table showing the ratio of the permanent strain to the applied strain at varying applied strains for the quenched morphologies of 00240 and 6007.

An interesting feature of the permanent strain is the fact that if considered as a percentage of the applied strain, then it remains remarkably constant after the first yield point.

### 4·4·3 Transient Stress Dip Tests

Values of the ratio of $\sigma_r$ to $\sigma_a$ as a percentage for all three grades in both the quenched and slow cooled morphologies are shown below in Table 4·3.

| Strain | 5502 Q | 5502 S | 6007 Q | 6007 S | 00240 Q | 00240 S |
|---|---|---|---|---|---|---|
| 2 % | 90 | --- | 90 | --- | 90 | --- |
| 5 % | 93 | 95 | 94 | 92 | 93 | 94 |
| 10 % | 94 | 95 | 93 | 93 | 95 | 95 |
| 15 % | 96 | 95 | 93 | 93 | 96 | 95 |
| 20 % | 96 | --- | 94 | --- | 95 | 96 |
| 25 % | --- | --- | 93 | --- | 95 | 95 |
| 30 % | --- | --- | --- | --- | 95 | --- |
| 35 % | --- | --- | --- | --- | 94 | --- |

**Table 4·3**

Table showing the ratio of $\sigma_r$ to $\sigma_a$ as a percentage for all three grades in both the quenched and slow cooled morphologies.

It can be seen from these values that beyond the first yield point the value of the ratio of $\sigma_r$ to $\sigma_a$ does not change, (the tests were conducted at a constant crosshead speed, so the actual change in true strain rate over the range of strains shown is 25% in the case of 00240).

It is also apparent that neither grade or thermal treatment has a significant effect on the ratio. This is a surprising result in view of the very dramatic changes that take place in creep response, yield stress and natural draw ratio. The applied stress did scale to the yield stress, but it can be seen that the recovery stress remained the same fraction of the applied stress.

The fact that the recovery stress is always the same fraction of the applied stress, (at a given strain rate and strain), independent of grade or thermal treatment, indicates that the recovery process must take place in a region of the polymer where the morphology is relatively the same under widely varying conditions.

The only area where this condition will be satisfied is within the crystallites. The side chain branches of the copolymers will restrict the thickness of the crystallites, but the interaction between the main chain segments within the crystallites will be the same in all three grades. The slow cooled material has more crystalline material, and this accounts for the applied stress increasing, but if the recovery is due to a process occurring in the crystalline regions then its magnitude will also increase by the same amount, and hence the ratio of $\sigma_r$ to $\sigma_a$ will remain constant.

The amorphous sections of the material will differ between grades since the copolymers will be more viscous due to their side chain branches. Also on slow cooling there will be less amorphous material, so a recovery process located in this region would mean that the ratio $\sigma_r$ to $\sigma_a$ would decrease with slow cooling.

From these values of $\sigma_r$ it is a simple matter to determine $E_1$, (assuming that the spring is Hookean, which is not particularly likely), since

$$E_1 = \frac{\sigma_r}{\varepsilon} \qquad (4\cdot1)$$

It is assumed that the recovery stress is provided completely by the spring $E_1$, and that dashpot 1 does not yield.

It is also possible to calculate a value for $E_2$, given $E_1$. Plotting the creep data in the form of strain against time, as in figure 4·16, shows a rapid linear increase in strain followed by a more gentle non linear increase in strain. This initial linear increase in strain at short times is due to the elastic response of the material, before either dashpot has yielded. Hence a total modulus, $E_T$, for the system can be determined, and $E_2$ derived from

$$E_T = E_1 + E_2 \qquad (4\cdot2)$$

since the springs are in parallel.

The values of $E_1$ and $E_2$ thus derived at the transition from elastic to plastic response are shown in Table 4·4 below, (it was assumed that neither dashpot had yielded).

| | Quenched 6007 | Quenched 00240 |
|---|---|---|
| $E_T$ | 880 MPa | 475 MPa |
| $E_1$ | 425 MPa | 250 MPa |
| $E_2$ | 455 MPa | 225 MPa |

**Table 4·4**

Table showing the values of the moduli of the springs in the two process model at the transition from elastic to plastic response.

It is not possible to calculate $E_2$ directly from the transient stress dip tests, since dashpot 2 will have yielded, and the exact strain of the spring $E_2$ is impossible to determine.

Figure 4-16

Example of the initial creep of the quenched morphology of isotropic 6007.

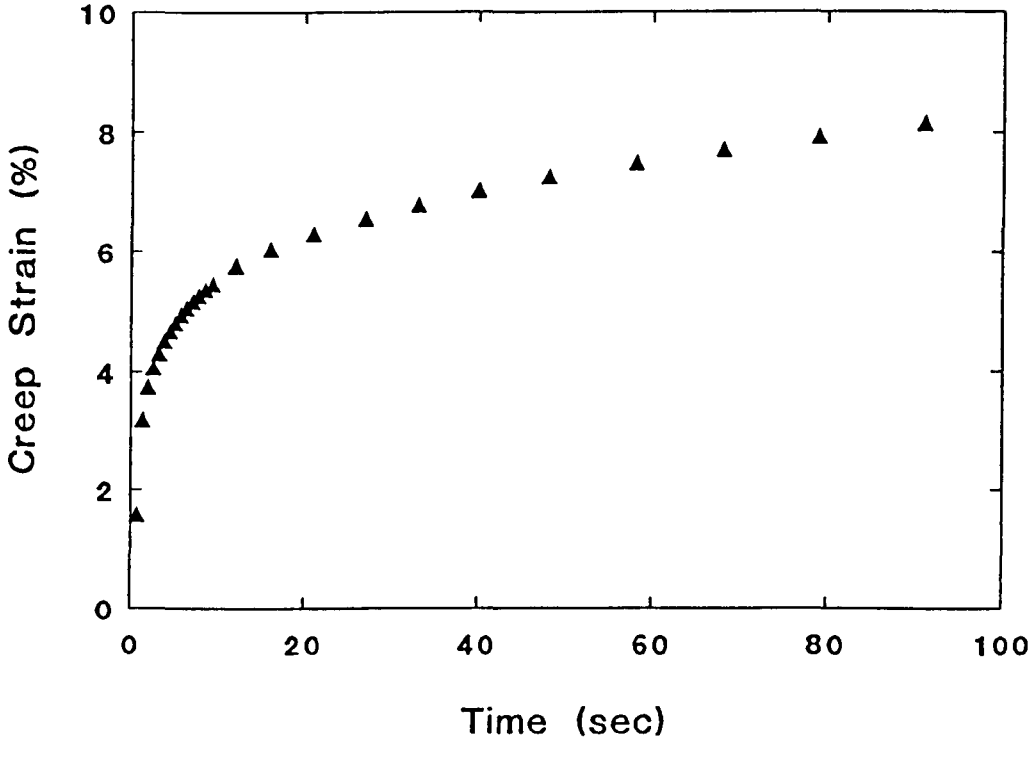

The final parameter of this simplified model is the viscosity of dashpot 2. This can be found in two ways.

The first way to calculate $\eta_2$ is directly from the recovery experiments, using

$$\eta_2 = \frac{\sigma_r}{\dot{\varepsilon}_r} \tag{4·3}$$

where $\dot{\varepsilon}_r$ is the recovery strain rate taken directly from the recovery experiment, and the recovery stress, $\sigma_r$ is taken at the same strain as the recovery strain rate by interpolating between the measured recovery stress values.

The second way to calculate this is from the effective retardation time of the recovery experiments. It should be noted that a real polymer system has an entire range of retardation times, so the effective retardation time used here is a large simplification. This effective retardation time can be defined as the time required for the sample to recover to 1/e of the applied strain, and is denoted by the symbol $\tau$. The value of $\tau$ can be calculated using the following equation, assuming a standard linear solid approach.

$$\tau = \left( \frac{E_1 + E_2}{E_1 E_2} \right) \eta_2 \tag{4·4}$$

Thus since $E_1$ and $E_2$ have been calculated, and $\tau$ can be measured, $\eta_2$ can be calculated using either equation 4·3 or 4·4. The values of $\eta_2$ derived from both methods are shown below in Table 4·5 in the next section.

### 4·4·4 Permanent Strain

There is a large discrepancy between these two methods, equations 4·3 and 4·4, of determining $\eta_2$. Because of this the effect of the permanent strain was investigated.

Dashpot 1 was now assumed to yield and all of the permanent strain that developed during a recovery test was placed in it. This assumption was made since it is likely that the spring, $E_2$, would be unable to drive the recovery of the strong dashpot, (dashpot 1). Thus the value of $E_1$ could still be calculated, since the strain upon it was simply the applied strain minus the permanent strain.

$$E_1 = \frac{\sigma_r}{\varepsilon - \varepsilon_p} \tag{4·5}$$

The fact that dashpot 1 was assumed to flow is also valid, since the dashpot is not a switch, the contribution is merely small, and once the system begins recovery dashpot 1 effectively locks up and the system becomes a standard linear solid, figure 4·17.

It can be seen from Table 4·5 that when the permanent strain is treated in this manner the calculated values of the viscosity agree more. Given the simplicity of the model, (both the assumption that the behaviour of the springs is Hookean and the single retardation time rather than an entire spectrum of retardation times), the agreement between the values calculated using experimental data and the predicted data is reasonable.

In Table 4·5 below $\varepsilon_\tau$ is the strain corresponding to $\frac{\varepsilon_a}{e}$, at which strain all calculations of the value of $\eta_2$ were made, where $\varepsilon_a$ is the applied strain, defined as the strain which was allowed to develop in the sample before recovery was initiated.

| Grade | $\varepsilon_\tau$ (%) | $\eta_2$ (eqn 4·4) ($\eta_1$ fixed) | $\eta_2$ (eqn 4·4) ($\eta_1$ yields) | $\eta_2$ (eqn 4·3) |
|---|---|---|---|---|
| 00240 | 13·1 | $7{\cdot}9\times10^{10}$ | $1{\cdot}2\times10^{11}$ | $5{\cdot}0\times10^{11}$ |
| 00240 | 9·6 | $7{\cdot}8\times10^{10}$ | $1{\cdot}2\times10^{11}$ | $5{\cdot}3\times10^{11}$ |
| 00240 | 6·8 | $6{\cdot}2\times10^{10}$ | $8{\cdot}6\times10^{10}$ | $4{\cdot}8\times10^{11}$ |
| 00240 | 3·0 | $3{\cdot}6\times10^{10}$ | $4{\cdot}0\times10^{10}$ | $3{\cdot}4\times10^{11}$ |
| 6007 | 5·7 | $3{\cdot}7\times10^{11}$ | $4{\cdot}8\times10^{11}$ | $2{\cdot}7\times10^{12}$ |
| 6007 | 4·2 | $3{\cdot}5\times10^{11}$ | $4{\cdot}6\times10^{11}$ | $2{\cdot}6\times10^{12}$ |
| 6007 | 3·5 | $2{\cdot}6\times10^{11}$ | $3{\cdot}2\times10^{11}$ | $1{\cdot}9\times10^{12}$ |
| 6007 | 3·0 | $2{\cdot}8\times10^{11}$ | $3{\cdot}3\times10^{11}$ | $2{\cdot}0\times10^{12}$ |

**Table 4·5**

Table showing the values of viscosity, (in Pa.sec), for quenched isotropic 6007 and quenched isotropic 00240 at varying values of strain.

It is proposed that dashpot 1 has a stress history or time dependence to its yielding, and that this is responsible for the discrepancy between the strain at which the second yield point is seen in the creep tests and the strain at which it was seen by tests conducted on an Instron tensile testing machine.

If we integrate the stress acting on the dashpot with respect to time, then this time dependence can be thought of as a minimum value of this integral which must be exceeded if the dashpot is to yield.

Figure 4·17

Schematic representation of the mechanical interpretation of the standard linear solid model.

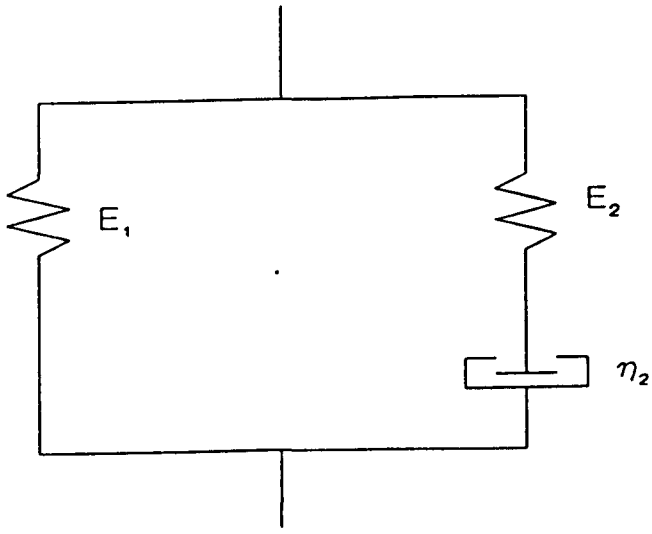

As reported previously the creep experiments show the second yield point around 16% strain in quenched 6007. However by performing tests on an Instron where the sample is strained at constant crosshead velocity until necking occurs, (the physical process associated with the second yield point), which appears to occur around 35% strain at low strain rates, moving to lower strains as the strain rate is increased, (figure 4·18). This value of 35% is much closer to the value of 30 % to 40% quoted by Brooks[1] in his work.

This proposal implies that in the creep experiments, with step loading stress histories, the situation is such that dashpot 1 will yield earlier than in an Instron based experiment, where the stress history is such that the stress increases progressively from zero.

At higher crosshead velocities the stress is greater and increases more rapidly than in the low crosshead velocity tests. This rapid rise in stress approaches the step loading pattern of a creep test, and hence the strains at which the second yield point occurs will approach those found in creep tests.

Further evidence for this time dependence of the flow of dashpot 1 is found in figure 4·19. In these recovery tests the material was loaded at various stress levels but recovery was always initiated at 10% applied strain. Thus the lowest stress levels took longest to reach 10% applied strain, and hence had longer for dashpot 1 to flow, resulting in a higher proportion of plastic deformation and less elastic deformation.

**4·4·5 Activation Volume**

It can be seen from figure 4·14 that the form of the strain rate versus stress plot is reminiscent of those produced by the oriented material. There appear to be two distinct regions within it, a low stress region and a high stress region, both with linear responses on this plot.

From this type of plot the activation volume can be calculated in the same manner as the oriented material, (using equation 1·4). Due to the lack of data in the low stress region the activation volume of the low stress region has not been calculated with any degree of certainty for any grade or morphology. For the quenched morphology in 6007, (where most data exists), the activation volume at 10% strain in this low stress region may be of the order of 15,000 $Å^3$.

However for the high stress regions in the quenched morphologies of 6007 and 00240, the effective activation volume has been calculated more reliably. In these cases it is 2330 $Å^3$ in 6007 at 10 % strain, and 3450 $Å^3$ in 00240 at 10 % strain.

Figure 4·18

Second yield point in tension for the quenched morphology of 6007.

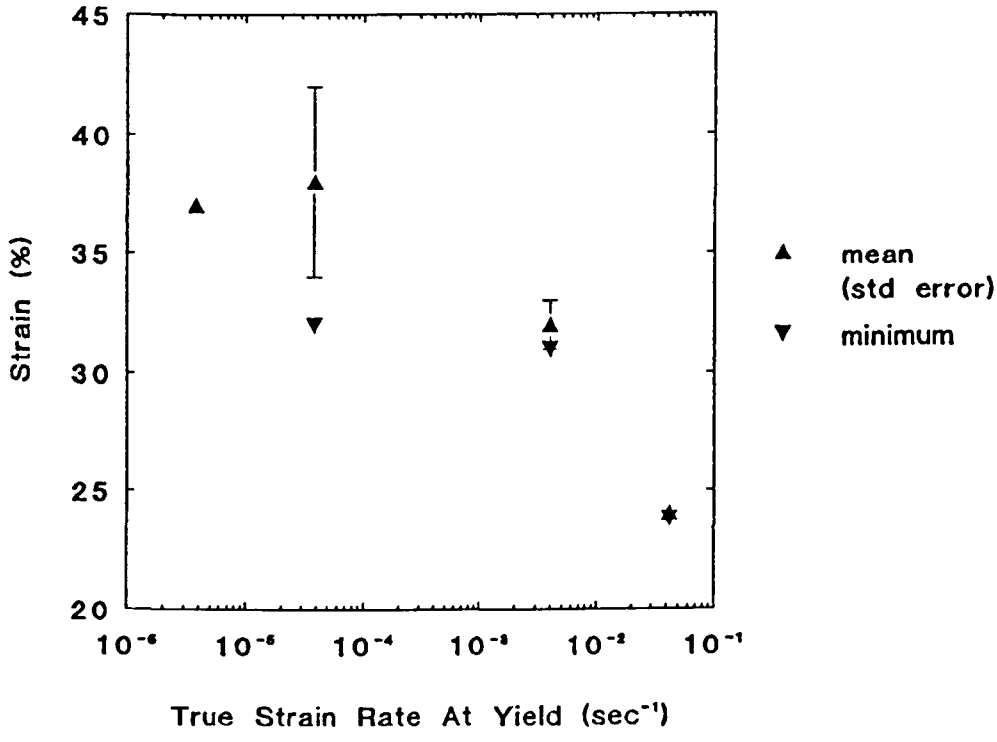

Figure 4-19

Strain recovered against time under load for the quenched morphology of isotropic 6007.

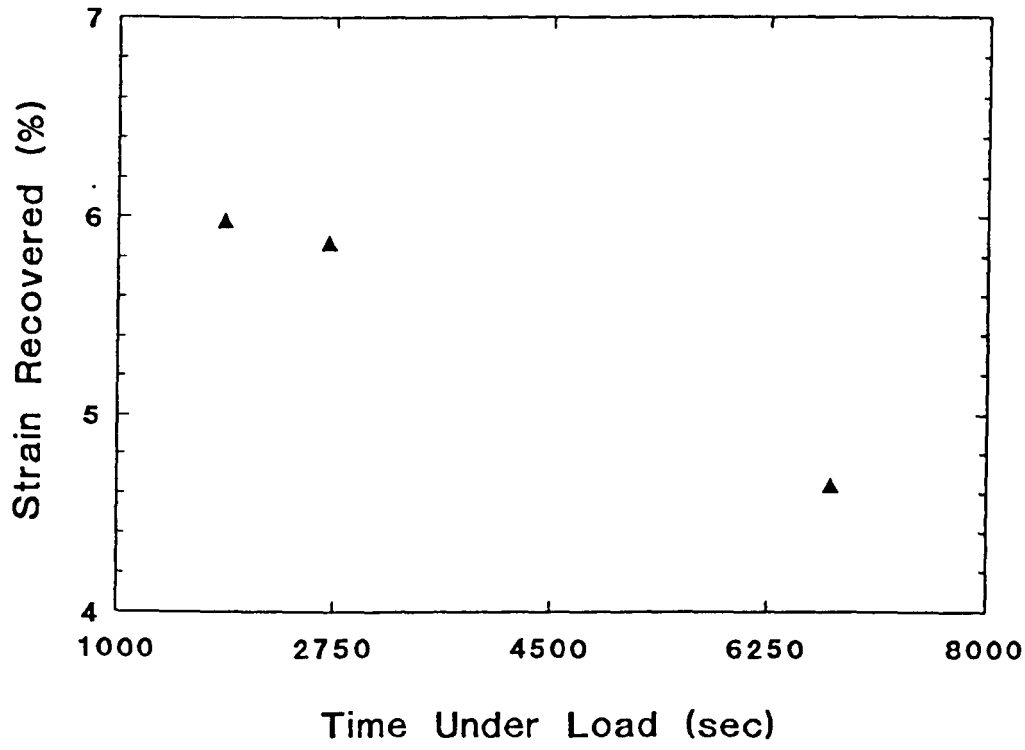

These activation volumes are comparable with those published by Truss[5] et al. of 538 Å$^3$ for Rigidex 50 and 1990 Å$^3$ for 00240 at yield, (the activation volumes for Rigidex 50 and 00240 have been converted by the author from the shear activation volumes reported by Truss using equation 4·6).

$$\text{Tensile Volume} = \frac{\text{Shear Volume}}{2} \qquad (4\cdot6)$$

These activation volumes are significantly larger than the activation volumes calculated for the oriented material, indicating that the mechanism controlling creep becomes more localised as the amount of orientation is increased.

### 4·4·6 Activation Energy

In addition to the experiments required to determine the activation volume, a series of elevated temperature tests were conducted on the quenched morphologies of 00240, 5502 and 6007. The activation energy was determined in the same manner as for the oriented material, by assuming that the data approximated to a single process in the region under study, and applying equation 1·5.

Both the high stress region and low stress region were investigated, but because of the lack of data in the low stress region the calculated activation volume is very uncertain, hence the activation energy for this region will also be uncertain, since the activation volume is required to calculate it.

The graphs from which the activation energies were derived are shown in figures 4·20 to 4·23.

The activation energies at 10 % strain are shown in Table 4·6 below.

| Grade and Process | Energy kJmol$^{-1}$ | Energy kcalmol$^{-1}$ |
|---|---|---|
| 6007 : 2 | 184·9 | 44·2 |
| 00240 : 2 | 189·9 | 45·4 |
| 5502 : 2 | 212·1 | 50·7 |
| 6007 : 1 | ≈271 | ≈65 |

**Table 4·6**

Table showing the activation energies at 10% strain for the quenched morphologies of 6007, 5502 and 00240.

Figure 4·20

Activation energy derivation for the 1st process in the quenched morphology of 6007, at draw ratio 1·1 and 11·55 MPa.

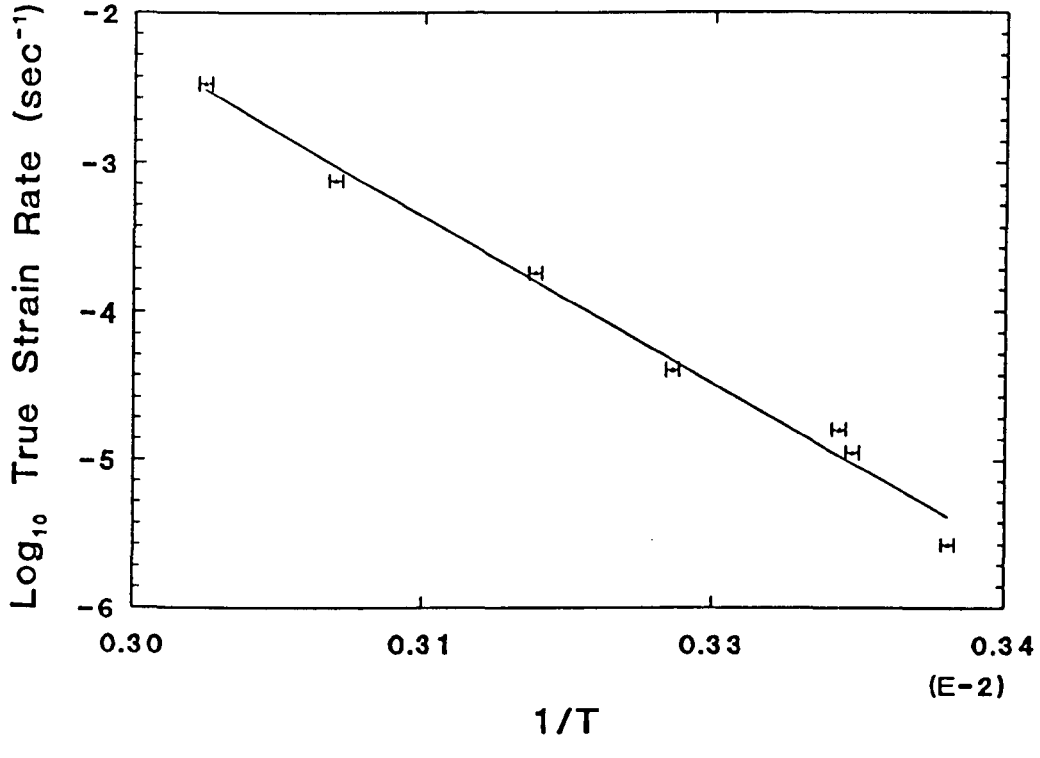

Figure 4·21

·Activation energy derivation for the 2nd process in the quenched morphology of 6007, at draw ratio 1·1 and 11·55 MPa.

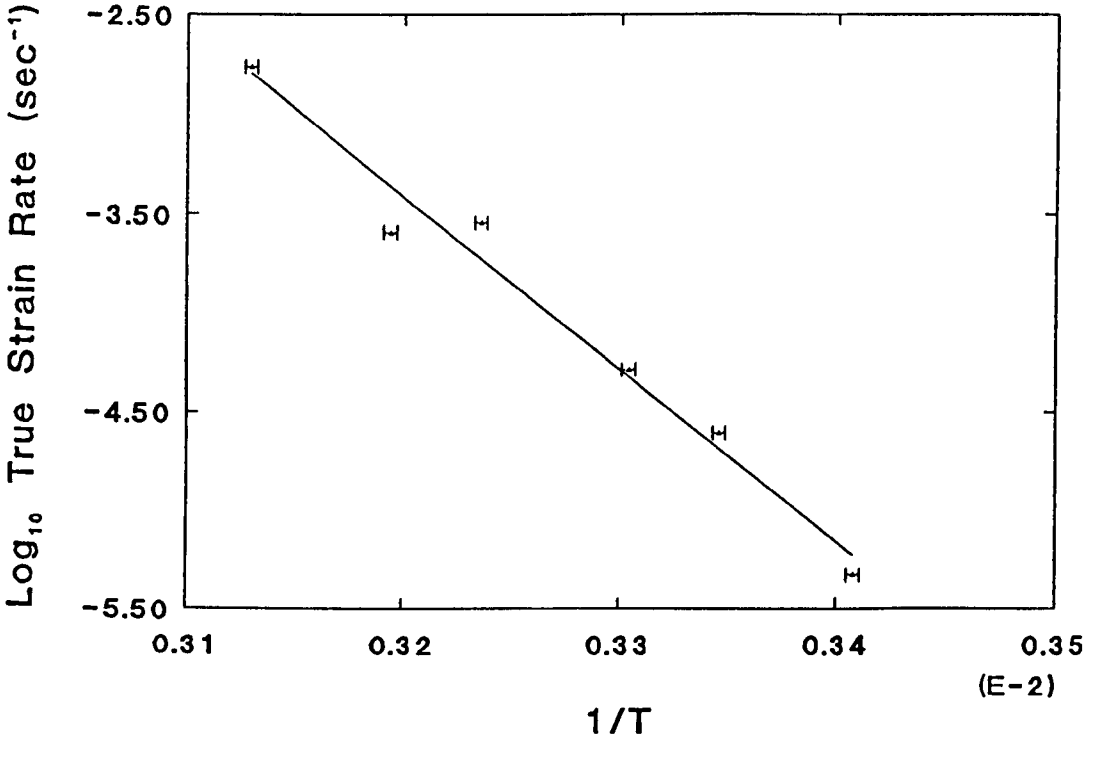

Figure 4·22

Activation energy derivation in the quenched morphology of 00240.

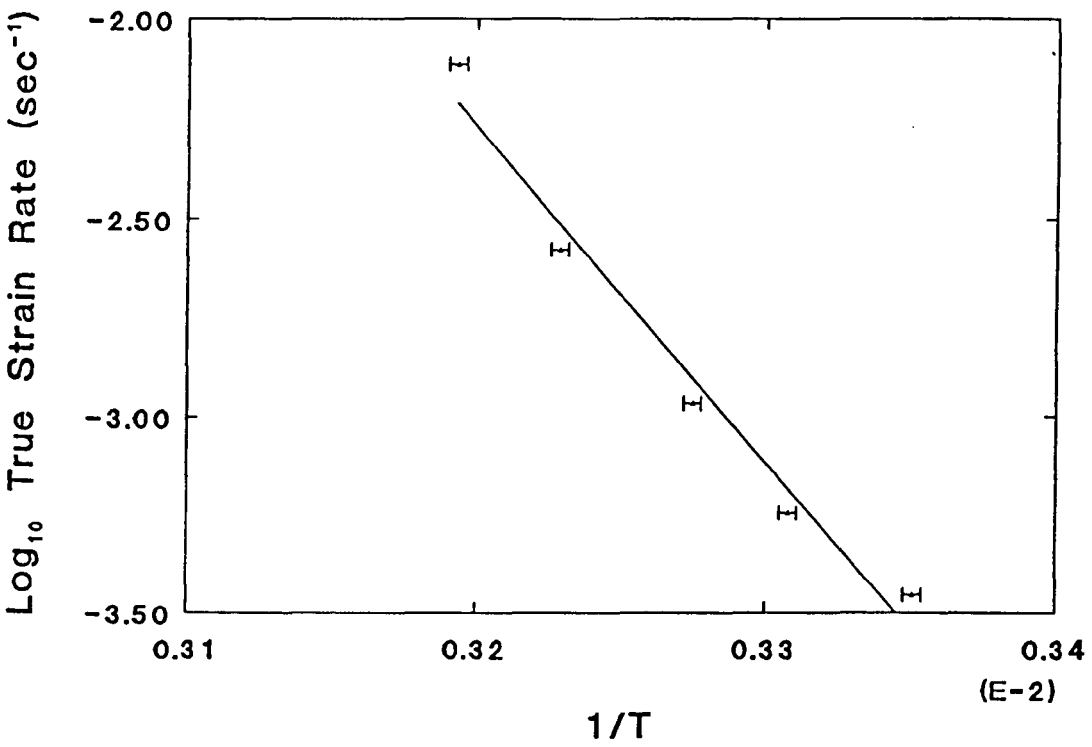

Figure 4·23

Activation energy derivation in the quenched morphology of 5502, at draw ratio 1·1. and 12·65 MPa.

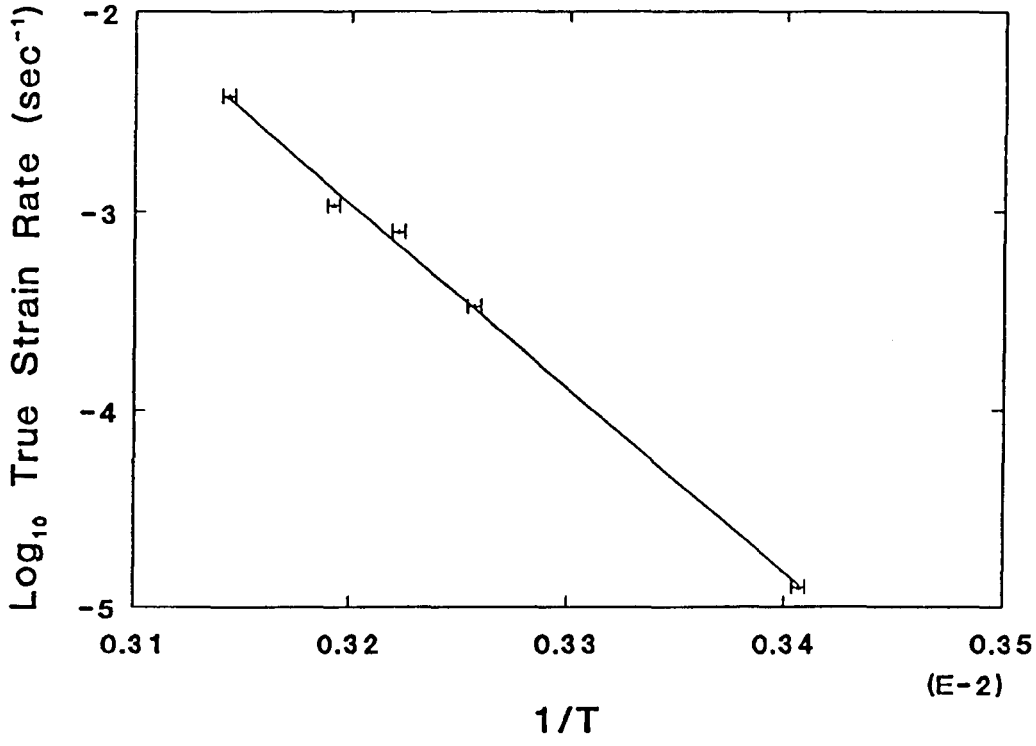

The activation energy of process 2, the high stress region, is in the region of the $\alpha_2$ activation energy,[6,7] indicating that creep under this regime may also be governed by c-shear. The activation energy for process 1, the low stress region, is much higher. It is in the region of the energy required to actually pull a polymer chain from a crystallite[5].

### 4·4·7 Fitting The Model

The fitting procedures used to fit the full expression, (equation 1·7), for the two process model to the data for the oriented material were employed to fit the isotropic creep data to the full model.

The resulting best fit is shown by the line in figure 4·24. It is apparent that although a fit can be obtained to the high stress region, it has not been possible to obtain a fit at all for the low stress region, and the inclusion of the low stress data into the fitting procedure generally decreases the accuracy of the fit in the high stress region. In fact when plotted over a larger range there is no sign of the calculated curve turning over in the same way that the actual data does.

It is not yet clear whether this is due to deficiencies in the fitting procedures used to fit the equation, (fitting was carried out on a PC), or a shortfall of the model itself. The data would seem to indicate that a two process model would fit, so the subject should be left open until more powerful and sophisticated fitting procedures are applied to the data.

## 4·5 Fotheringham And Cherry

The Fotheringham and Cherry [4] approach was used because of the success of Brooks in using it to model isotropic 00240. Because of the large amount of data the quenched morphology of 6007 was again used for fitting.

### 4·5·1 Effective And Recovery Stress Behaviour

The effective, recovery and applied stress all vary with strain rate and temperature at any given strain. The graphs of figures 4·25 to 4·27 show this. The dotted lines represent the plateau recovery stress value that was used in the calculation of the effective stress at high strain rates.

At low strain rates, (below $10^{-5}$ $sec^{-1}$), the effective stress is practically zero, and the applied stress is essentially the recovery stress. As the strain rate is increased the effective stress increases and the recovery stress reaches a plateau value. At high strain rates, ($10^{-2}$ $sec^{-1}$ and above), the recovery stress begins to fall and the effective stress becomes the dominant component of the applied stress.

Figure 4·24

Eyring fit to creep data for the quenched morphology of isotropic 6007 at draw ratio 1·1, room temperature.

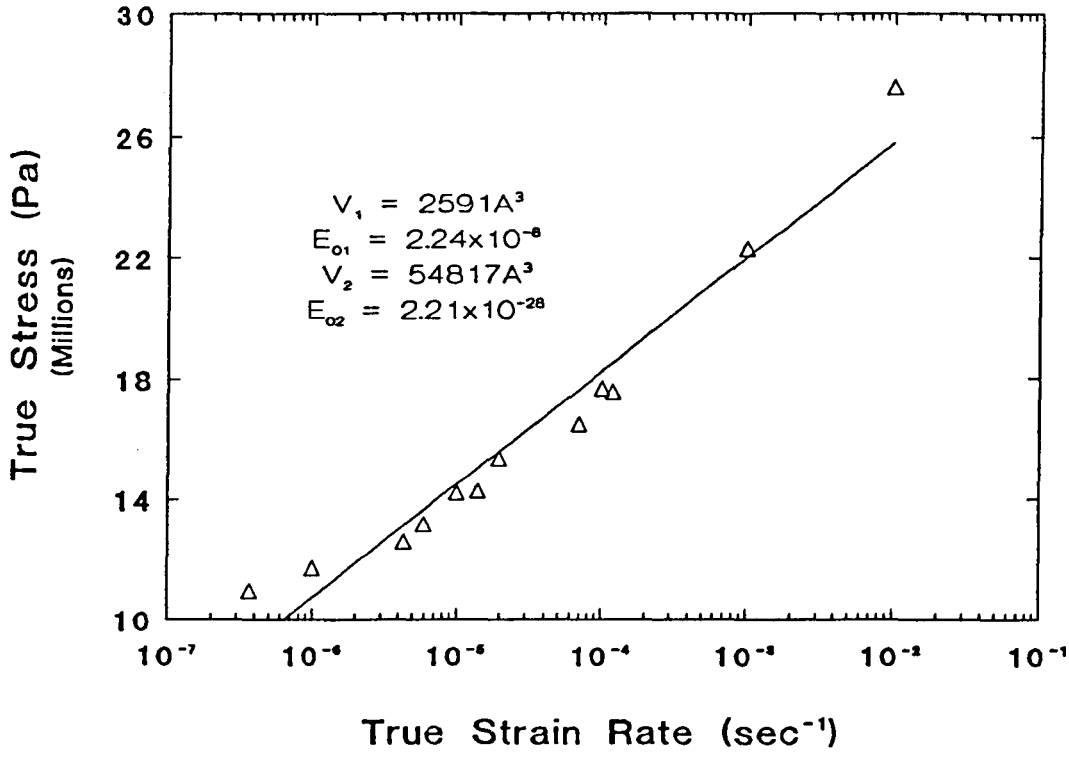

Figure 4·25

Recovery stress data for the quenched morphology of isotropic 6007 at draw ratio 1·1, 20°C.

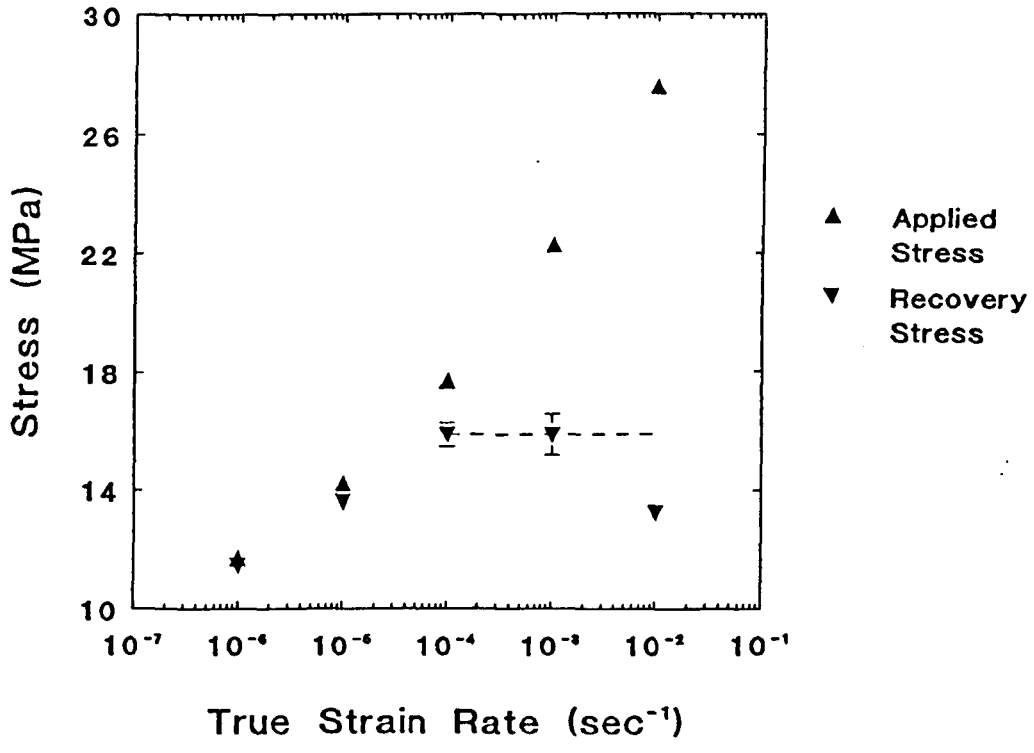

Figure 4·26

Recovery stress data for the quenched morphology of isotropic 6007 at draw ratio 1·1, 50°C.

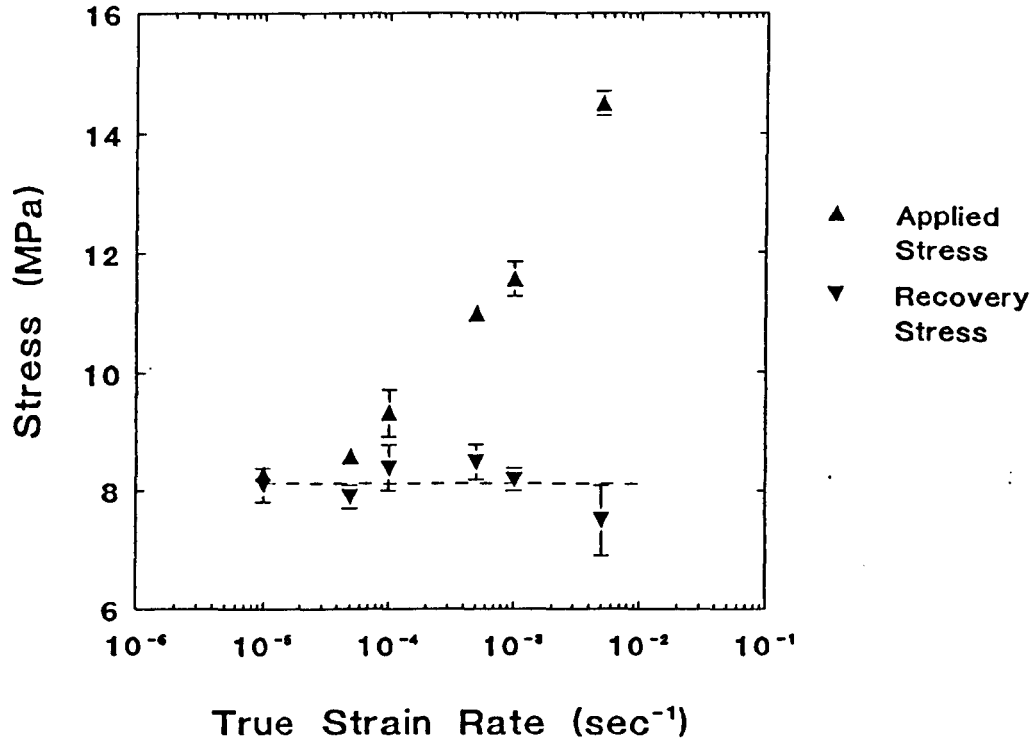

Figure 4·27

Recovery stress data for the quenched morphology of isotropic 6007 at draw ratio 1·1, 70°C.

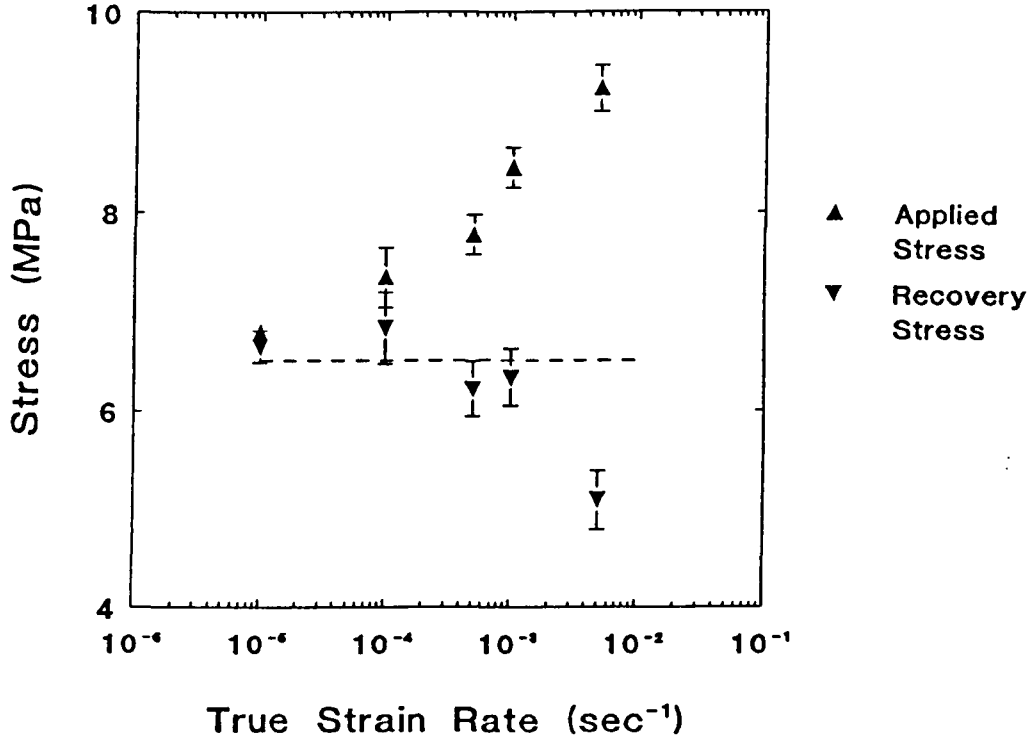

This fall in the recovery stress is uncertain as the machine overshoots the required stop position and then corrects itself at these high strain rates. Consequently large errors are associated with these recovery values, and hence the plateau recovery stress value was used to determine the effective stress in the high strain rate region.

This behaviour of the recovery stress was seen by Fotheringham and Cherry[4] in their work on linear polyethylene.

At high strain rates the polymer network present in the material begins to break down and hence the recovery stress would be expected to fall.

The effective stress rises as the contribution to the flow stress of dashpot 2 becomes more significant. At low strain rates the dashpot flows, but the contribution will be negligible. It is likely from viewing the applied stress data, figure 4·28 that this dashpot actually starts to contribute significantly to flow around a strain rate of $10^{-6}$ $sec^{-1}$, but the resolution of the apparatus is such that the very low effective stress that would be present in this region would be masked by noise from the machine itself.

In order to be certain that the effective stress seen at very low strain rates was real and not an artefact of the experimental method, experiments were performed on an Instron tensile testing machine. A sample was extended at a nominal strain rate of $1\times10^{-6}$ $sec^{-1}$ to 10% extension, when the crosshead was brought to rest. The consequent drop in stress indicated that the likely drop in the applied stress to the recovery stress is of the order of 1%, and so the drop in signal would be swamped out by the noise caused by the crosshead coming to rest after reversing and consequent vibrations through the frame of the machine.

A series of ultra long duration creep tests at low stress, (<8 MPa), were run by placing creep samples of the quenched morphology of 6007 in a frame and dead loading them in the same manner as for the normal creep runs. However a cathetometer was used to follow the travel of both the lower grip and the upper grip, (the increase in strain being the change in separation of the two grips), rather than a computer controlled data acquisition system. There was an initial slow increase in the strain of the sample, until the sample approached the first yield point. Around the strain of the first yield point the strain remained constant, (in that no change in the separation of the grips was measurable). This constant strain was held for several weeks before the sample failed. The site of failure was a clean break running perpendicular to the straight sides of the specimen with little to no sign of plastic deformation at the break.

Figure 4·28

True strain rate versus true stress data for the quenched morphology of 6007 at draw ratio 1·1.

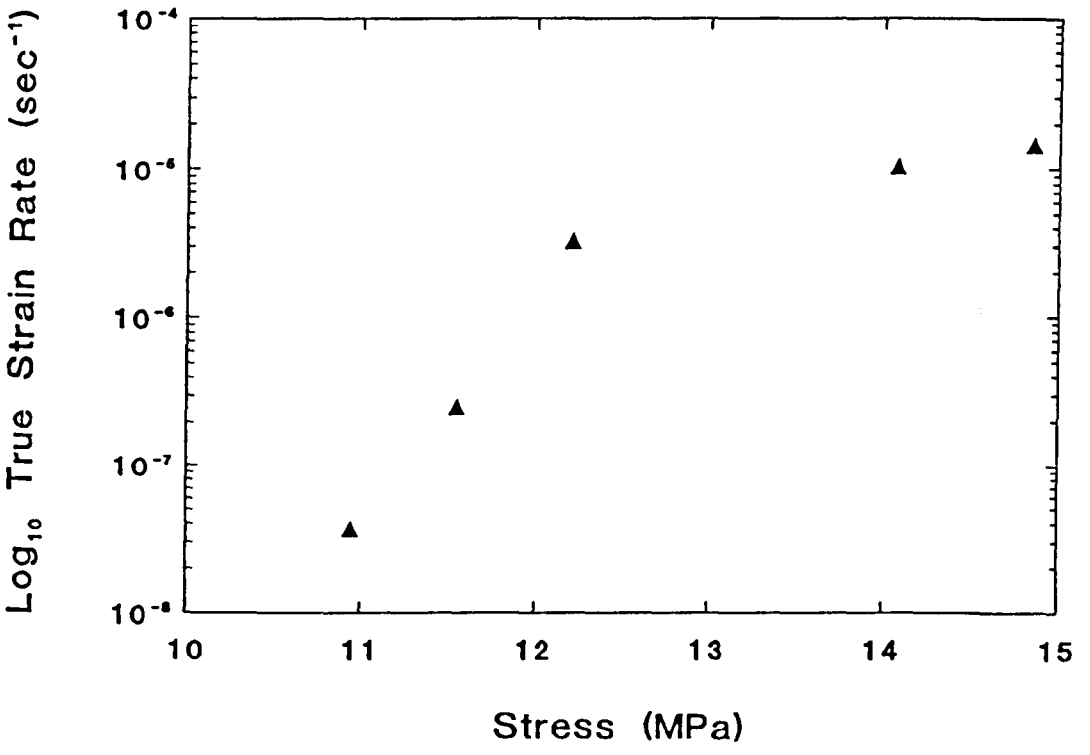

Figure 4·29 also shows the ratio of $\sigma_r$ to $\sigma_a$ as a function of strain rate and temperature. As can be seen the ratio is very sensitive to strain rate, but relatively insensitive to temperature. This is a puzzling feature since activated processes are normally dependent on both temperature and strain rate to a more or less equal extent. Indeed figure 4·20 shows that for only a 20°C change in temperature, there is a 2 order of magnitude change in the strain rate at a constant stress. This is far greater than is evident in figure 4·29, and this low dependence on temperature has yet to be explained.

### 4·5·2 Fitting The Model

A fitting routine supplied by Brooks[8] was used to fit the data to equation 1·18. The effective stress curves are shown in figure 4·30 and the master curve to which the equation was fitted and the fitted curve itself are shown in figure 4·31.

### 4·5·3 Comparison Of Derived Values

The derived values of the parameters $V^*$, n, nQ and $K_T$ are presented for this work on the quenched morphology of 6007, the work of Brooks et al.[1] on the quenched morphology of 00240 and the work of Fotheringham and Cherry[4] on linear polyethylene are presented in Table 4·7.

The values of $V^*$, n and $K_T$ were taken from the fitting routine, since these are the variables altered in order to produce a fit. The value of nQ was derived by plotting the shift factor for the effective stress curves as described in section 1·3·6, the plot is shown in figure 4·32.

| | 6007 | 00240 | LPE |
|---|---|---|---|
| $V^*$ (Å$^3$) | 151 | 480 | 570 |
| nQ (kJmol$^{-1}$) | 38·5 | 51·5 | |
| n | 2·34 | 3·24 | 3·1 |
| $K_T$ | 0·2 | 0·2 | 0·127 |

**Table 4·7**

Table comparing the parameters derived for three different types of polyethylene by the three different groups to have used the co-operative jump approach.

It can be seen that the values agree reasonably well across these three materials.

Perhaps more important is the actual value of Q. When this is calculated it is 16·4 kJmol$^{-1}$ for 6007 and 15·9 kJmol$^{-1}$ for 00240. This indicates the same mechanism is controlling creep in both materials.

Figure 4-29

Recovery stress as a percentage of the applied stress for the quenched morphology of isotropic 6007.

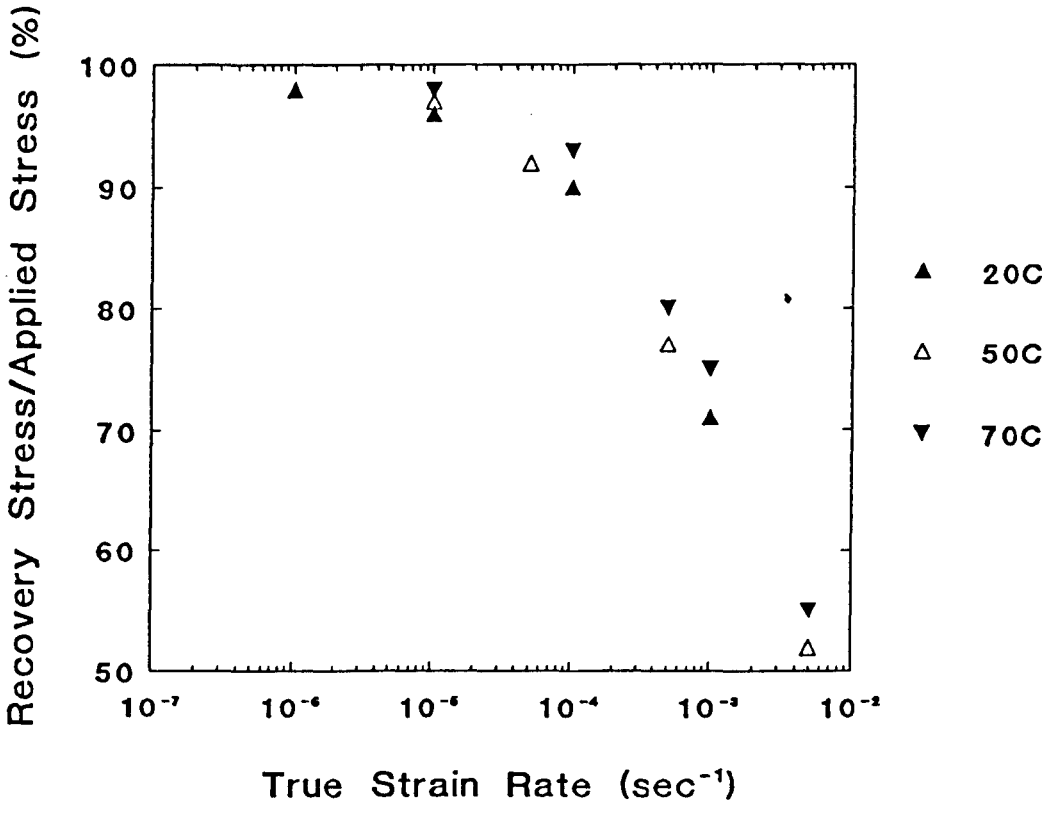

Figure 4·30

Effective stress data for the quenched morphology of isotropic 6007.

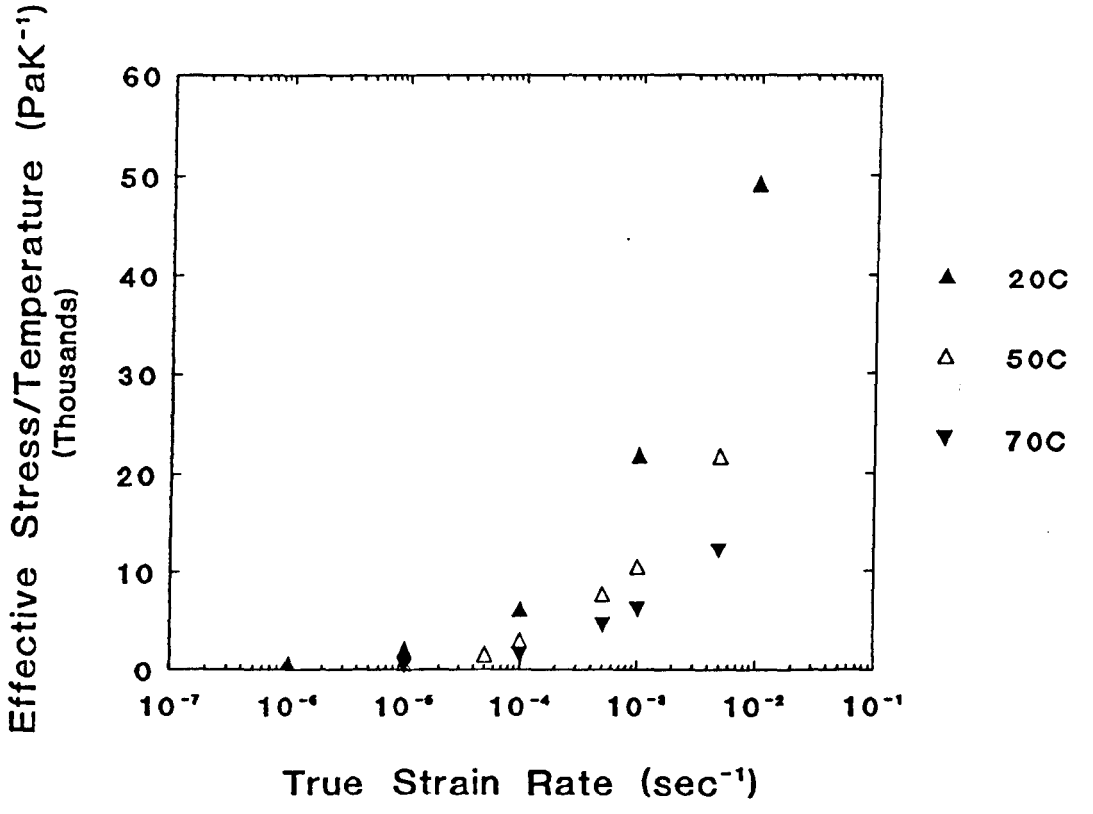

Figure 4-31

Fotheringham Cherry fit for the quenched morphology of isotropic 6007.

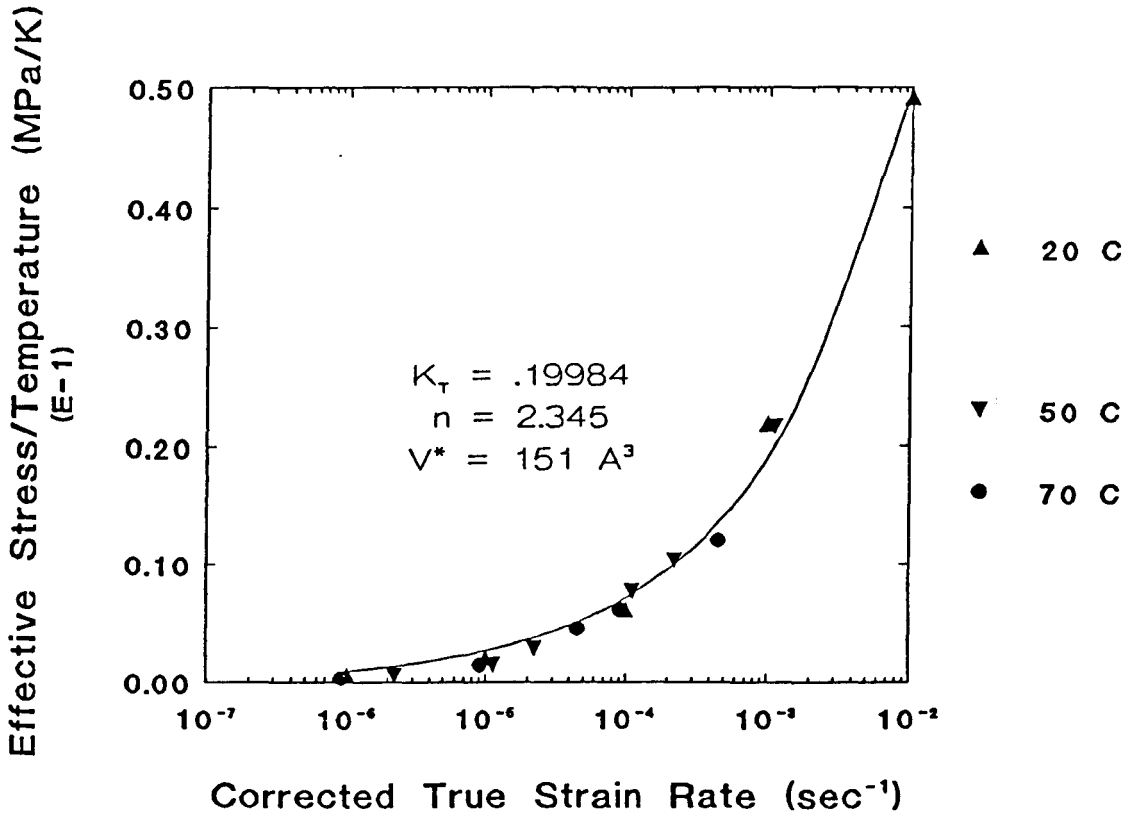

Figure 4·32

Derivation of nQ for the quenched morphology of 6007 at draw ratio 1·1.

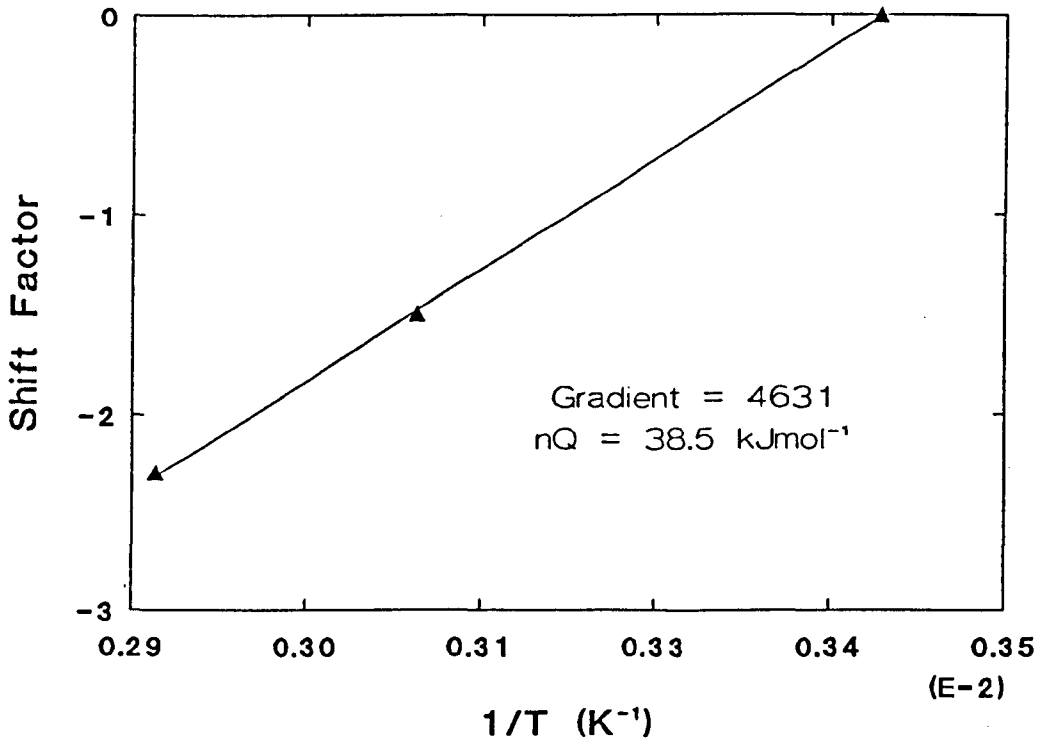

These are, however, very low activation energies. Flory[9] quotes activation energies of between 12 $kJmol^{-1}$ and 18 $kJmol^{-1}$ for the rotation of a polymer chain in related systems, (he does not quote a value for polyethylene). This would indicate a movement of the chains through a crystal by a rotational translation.

## 4·6 Conclusions

The crystallinity of the material is an important factor determining the mechanical properties of polyethylene.

There is a drastic change in morphology in the slow cooled material, although it is thought that the apparent increase in creep resistance between samples when loaded at equivalent nominal stresses is due to the increase in yield stress in the slow cooled samples. Thus in applications where a resistance to isotropic creep is required a simple method of improving response would be to alter the processing route to provide a greater yield stress, but care would need to be taken if the material was required to still yield and flow, as the yield stress could be made to exceed the brittle failure stress.

Evidence has been found in the creep and recovery experiments which supports the work of Brooks on the existence of two yield points in polyethylene.

The two Eyring process approach does not appear to be a complete representation of the behaviour of the material in this state, but the activation parameters derived compare favourably with those reported by previous workers.

The Fotheringham and Cherry approach appears to offer a more complete representation, in that it fits all the data gathered to date. However it does give extremely low values of activation energy, but the activation parameters determined in this work compare well with those derived both by Brooks and by Fotheringham and Cherry, using similar methods of analysis.

The difference in strain at which the polymer yielded in creep experiments and experiments performed on an Instron tensile testing machine may be due to a stress history dependence of dashpot 1.

## 4·7 References


1 Brooks, N.W., Duckett, R.A. and Ward, I.M., Polymer, **33**, (1992), 1872

2. Rasburn, J., Klein, P.G. and Ward, I.M., J. Polymer Sci. B., **32**, (1994), 1329

3. Wilding, M.A. and Ward, I.M., Polymer, **22**, (1981), 870

4. Fotheringham, D.G and Cherry, B.W., J. Mat. Sci., **13**, (1978), 951

5. Truss, R.W., Clarke, P.L., Duckett, R.A. and Ward, I.M., J. Polymer Sci. B., **22**, (1984), 191

6. Kajiyama, T., Okada, T., Sakoda, A. and Takayanagi, M., J. Macromol. Sci.-Phys., **B3**, (1973), 583

7. Alberola, N., Cavaille, J. Y. and Perez, J., J. Polymer Sci. B, **28**, (1990), 569

8. Brooks, N.W., Phd Thesis, University of Leeds, 1993

9. Flory, P.J., Statistical Mechanics of Chain Molecules, Interscience, New York, 1969

# Chapter 5

# Conclusions And The Future

## 5·1 Conclusions Of This Work

This work has reached a number of conclusions about the mechanical properties of the polyethylenes studied, in both the oriented and isotropic states.

## 5·2 The Oriented State

### 5·2·1 General Creep Performance

The work that has been presented here has provided evidence for the existence of unique relationships between true stress, total plastic strain and true strain rate for each grade of material studied, similar to those of Coates and Ward[1], providing that the initial morphology of the material is equivalent. It has concluded that in the oriented state the materials studied are more resistant to creep than in the isotropic state. This is evident from the fact that in the isotropic state a stress in the region of 10 MPa will produce a measurable amount of deformation within a relatively short time scale, (under 1 week), whilst in the oriented state a stress of 80 to 100 MPa is required to produce a measurable amount of deformation in the same time. This has been attributed primarily to the increased orientation of the polymer chains in the oriented state.

The copolymer, (00240), has better creep resistance than the linear homopolymer, (6007), which has been attributed to the increased number of pinning sites in the copolymer, due to the higher concentration of short chain branches.

The slow cooled morphology of the materials show the same ranking in creep performance as the quenched morphologies, and in the case of 00240 and 6007 the creep resistance of the specific grade is reduced. It is thought that this reduction in performance is due to the greater number of tie molecules in the quenched morphology. These tie molecules are long polymer chains which connect two or more crystalline regions, and are more likely to be present in the quenched material, where the random morphology of the molten state is frozen into the material, than the slow cooled material, where the greater amount of time during cooling means that more perfect crystal regions incorporating more of the high molecular weight, (and therefore long), molecules can be formed.

The equivalence in performance of 5502 between the quenched and slow cooled morphologies may be due to a competition between the reduction in the number of tie molecules and the increase in the overall crystallinity on slow cooling. This is more likely to balance in the 5502 which is intermediate in crystallinity between the linear 6007, (which is highly crystalline), and the highly branched 00240, (where the crystallinity is limited by the side group content).

### 5·2·2 Region 1 Of The Sherby Dorn Plot

This work has concluded that, in the oriented state, region 1 of the Sherby Dorn plot is caused by the material having a memory of the greatest extension applied to it; it is a region of transient creep until the strain has reached the maximum strain applied during the drawing process. The data gathered in region 1 is of no use in modelling the plastic deformation behaviour of the material, since the shape of the graph in region 1 is likely to be dependent upon how the material was unloaded and the thermal history of the sample after drawing. At the end of this region of deformation the creep behaviour is a function of the total strain for a given applied stress.

### 5·2·3 Modelling

A model consisting of two activated Eyring processes in parallel[2] has been shown to describe the behaviour of the material with good accuracy. The two processes in this model have differing activation parameters. One process has a relatively small activation volume, and whilst it carries little of the applied stress at low creep rates, it dominates the overall behaviour at high creep rates. The second process has a larger activation volume, and effectively controls the behaviour of the material at low creep rates. This confirms the results of previous workers in the field who also obtained good results from this model.

It was not possible to use the Fotheringham Cherry co-operative jump model[3], (which consists of a single process, but with multiple entities participating in the process during each strain changing event), to describe accurately the creep behaviour of the oriented material.

### 5·2·4 Mechanisms Controlling Creep

The modelling that has been performed on the materials indicates that the activation energy of the rate controlling process in the oriented material lies between 22 and 34 $kcalmol^{-1}$, (80 to 140 $kJmol^{-1}$). Thus it appears that the rate controlling mechanism is related to the $\alpha$ relaxation process, which has an activation energy[4,5] between 28 and 46 $kcalmol^{-1}$, (120 to 200 $kJmol^{-1}$). The $\alpha$ relaxation process is generally associated with a c-shear mechanism in the polymer.

Although the values for the activation energy for the large activation volume processes in the different materials had larger uncertainties, they are also of similar magnitude. Thus it appears possible that the same molecular process controls both this and the small activation volume process, and that this process is also a c-shear type mechanism.

## 5·3 The Isotropic State

### 5·3·1 General Creep Performance

The linear homopolymer, (6007), has the best creep resistance in the isotropic state of the 3 grades, the copolymer, (00240), has the worst. This has been attributed to the greater crystallinity of the homopolymer since it is known that an increase in crystallinity increases the yield stress. The slow cooled morphologies show better creep resistance than the quenched morphologies, (at the same levels of true stress and deformation), and this can also be attributed to the increased crystallinity, since the creep performance of each grade is apparently equivalent if the same fraction of the yield stress is applied.

### 5·3·2 Two Yield Points

For the first time creep experiments have provided evidence for the existence of double yield points in isotropic polyethylene, similar to those found by Brooks et al.[6]. The first yield point occurs at relatively constant deformation levels, (between 5 and 8%), for all three grades under the conditions studied here. The second yield point occurs at varying deformation levels, between 20% and 40%, and differs between grades as well as appearing to be strain rate dependent.

No morphological or molecular explanation of these yield points has been attempted by this work, although they are thought to be equivalent to the yield points discussed by Brooks et al..

### 5·3·3 Modelling

Both the activated Eyring process model[2] and for the first time the Fotheringham and Cherry model[3] have been used to describe the behaviour of the isotropic state of 6007.

The full formulation of the Fotheringham and Cherry model was applied successfully to the quenched morphology of 6007. Due to limitations in the computer systems used to perform the fitting routines, and a lack of data in the low stress region it was not possible to test satisfactorily whether the data could also be described in terms of the two Eyring process model and so a simplified version of the Eyring activated process model was used.

### 5·3·4 Mechanisms Controlling Creep

The models have provided 2 different activation energies for the creep of isotropic polyethylene.

The activated Eyring process model has provided an effective activation energy of around 45 kcalmol$^{-1}$ for the region where both processes are activated. This is in the upper band of values quoted for the $\alpha$ relaxation process[4,5], and so it would appear that, (according to this model), a c-shear mechanism also controls creep in the isotropic state.

The Fotheringham and Cherry model has provided an activation energy of around 4·1 kcalmol$^{-1}$, (16·4 kJmol$^{-1}$). This is very low, and is in the region of the activation energy for a rotational translation of a polymer chain[7]. The number of events occurring co-operatively according to this model is less than the number required to bring the activation energy for the entire transition, (the activation energy per transition event multiplied by the number of transition events which occur simultaneously), up to that of the activated Eyring process model. The significance of this has not been addressed by this work.

**5·4 The Future**

This work has raised several interesting points which are worthy of further investigation.

The equivalence in performance of the slow cooled and quenched morphologies of 5502 has been touched upon. It would benefit greatly from further study, perhaps including some x-ray work in order to characterise the two morphologies in terms of changes in crystallinity on drawing and the amount of tie chain molecules present.

A unique relationship between true stress, total plastic strain and true strain rate has been shown to exist for strains above the natural draw ratio. It would be instructive to perform further experiments to determine whether a similar relationship also exists at lower strains starting from the fully isotropic region, (before a neck is formed and orientation begins to take place), and within the neck itself. It is thought that the experiments required to determine the existence or otherwise of this relationship in the isotropic region could be performed with relative ease on an Instron tensile testing type machine modified to run at constant true strain rate, with a handful of creep tests designed to test the uniqueness of the results. The experiments required to determine the existence or otherwise of the relationship in the neck would obviously require some form of photographic technique to measure the distribution of strains in the inhomogeneous deformation.

It may be worthwhile to perform the long duration creep tests necessary to acquire low stress data in the isotropic state in order to have more data to distinguish between the activated Eyring process and Fotheringham and Cherry models.

A complete investigation of the isotropic material with the activated Eyring process model would allow a more thorough discussion of the results. At the moment it appears that the same process, the c-shear mechanism, controls creep in both the isotropic and oriented states, but there is a large change in the localisation of the event. This certainly requires further investigation and discussion.

Also, with a more extensive investigation of the application of the activated Eyring process model to creep of polyethylene in the isotropic state, a better understanding of the reason why the values derived from it and the Fotheringham and Cherry model are so radically different may be established.

In short the ability of both models to adequately describe the creep behaviour of isotropic polyethylene must be tested. If one model proves to be more reliable than the other, can the activation parameters be interpreted and physical events assigned to them? Or if both models are reliable, (given sufficient data), are the activation parameters comparable, and if not why not?

Finally an investigation into the apparent critical stress required to produce plastic deformation in the isotropic state would be informative, both from a pure curiosity viewpoint, and also because of its relevance to engineers, who may wish to either avoid the failure associated with it, or to make active use of it.

## 5·5 References


1. Coates, P.D., and Ward, I.M., Journal of Materials Science, **13**, (1978), 629
2. Wilding, M.A. and Ward, I.M., J. Polym. Sci., Polymer Physics Edition, **22**, (1984), 561
3. Fotheringham, D.G. and Cherry, R.W., J. Mat. Sci., **13**, (1978), 951
4. Kajiyama, T., Okada, T., Sakoda, A. and Takayanagi, M., J. Macromol. Sci.-Phys., **B3**, (1973), 583
5. Alberola, N. Cavaille, J. Y. and Perez, J., J. Polymer Sci. B, **28**, (1990), 569
6. Brooks, N.W., Duckett, R.A. and Ward, I.M., Polymer, **33**, (1992), 1872
7. Flory, P.J., Statistical Mechanics of Chain Molecules, Interscience, New York, 1969

# Appendix 1

## Applications To Slow Crack Growth, A Computer Model

## A1·1 Introduction

It has been known for some time that the presence of a flaw or crack in a polymeric material leads to a stress concentration, thus forming a yield zone in order to prevent the formation of a stress singularity.

Within this yield zone small voided regions are formed. As the yield zone grows these voided regions coalesce to produce the fibrillar structure commonly referred to as a craze. Crazes are seen in most slow crack growth situations in polyethylene.

Work by Bhattacharya and Brown[1] has shown that there are three processes involved in the growth of a craze. These are shown on figure A1·1.

These three processes are

1. New material is drawn into an established fibril at the interface of the fibril and the bulk material. This would extend the fibril without the need for the existing drawn material to deform.
2. The extension of the established fibrils. This would extend the fibril without requiring new material to be drawn into it.
3. The propagation of the yield zone into the bulk material, and the formation of new fibrillar material.

It has also been shown, by the same workers[1] that craze growth takes place linearly until the time at which the fibrils at the base of the craze fail. At this time crack growth, (the growth of the space behind the craze), becomes much more rapid, and failure of the material is imminent. This would imply that either process 1 or 2 controls the lifetime of the crack. In order to prepare materials that are more resistant to slow crack growth it is necessary to determine exactly which of these processes is dominant.

It has also been shown, by Cawood et al.[2], that there is a good correlation between the creep performance of a material and its stress crack performance. Given the apparent dependence of the craze growth rate on the extension of a fibril this is not a surprising result.

## A1·2 Modelling The Extension Of A Fibril

A computer model for the extension of established fibrils has been produced within this department by Dr. P. A. O'Connell using the creep data gathered for the quenched morphology of 6007 and the slow cooled morphology of 5502, in this investigation, and a joint paper[3] has been accepted for publication.

Figure A1·1

Schematic representation of the mechanisms involved in slow crack growth in polyethylene.

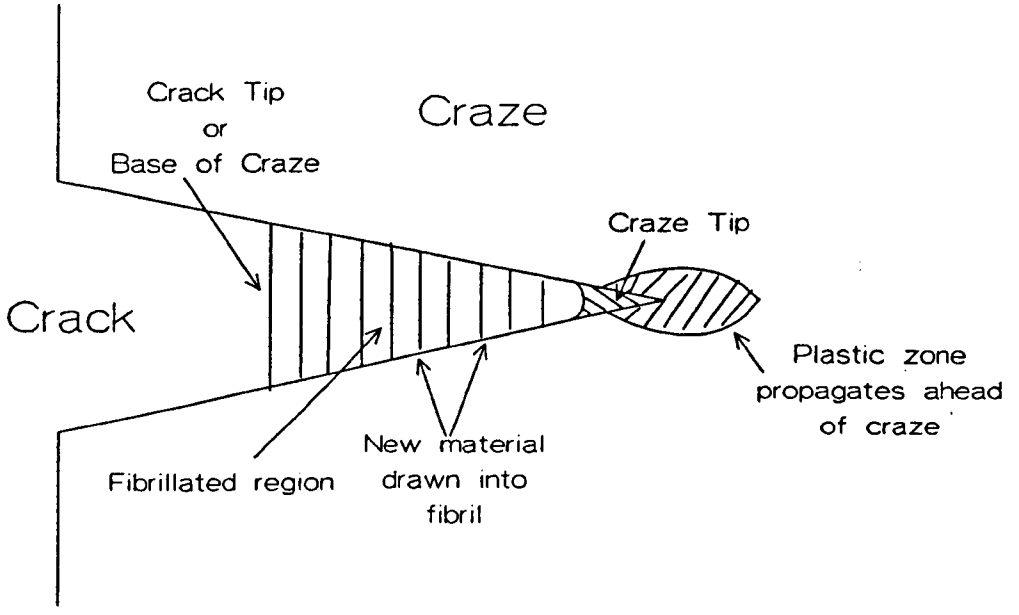

The unique nature of the relationship between true stress, strain and true strain rate has meant that it was possible to represent the relationship as a surface in true stress, strain, true strain rate space, as shown in figure A1·2. Any test then follows a path over this surface. Figure A1·2 has several contour lines drawn upon it, and these all represent paths across the surface with one constant condition, (stress, strain or strain rate). A creep test would have a slightly more complex path since there are no constant variables. This surface can be represented mathematically by a series of equations and hence it was possible to produce a routine which interpolated from the gathered data points to predict, in this case, the true strain rate at any given stress and strain.

In order to turn this into a model for the extension of a fibril a set of initial true stress and draw ratio, ($\sigma_1$, $\lambda_1$), conditions were taken and fed into the above routine. This provided a true strain rate. This true strain rate was then used to calculate the change in strain and hence the extension, ($\Delta x$), of the fibril during a short time period, see figure A1·3. Because the assumption that the volume of the specimen remained constant during creep was used in the creep work and proved to be valid, it was also used in this model.

Hence the increase in extension, $\Delta x$, caused a reduction in the cross sectional area. Because it was assumed that the load remained constant, (as in the creep tests, or in terms of slow crack growth this is the same as the stress at the interface of the bulk material and the fibril remaining constant), there was an increase in the true stress.

The new values, ($\sigma_2$, $\lambda_2$), were calculated and were fed back into the routine, (so that $\sigma_2$ became $\sigma_1$, and $\lambda_2$ became $\lambda_1$), and the whole process was repeated several hundred times.

In order to know when to stop, i.e. when the fibril fails, a failure criterion was required.

For the purposes of the program a failure strain of draw ratio 15 was used. This was because no research had been conducted on the failure point of the creep tests at that point, and only a very small fraction of the tests had extended significantly beyond this draw ratio.

However more recent work has shown that, in the case of the bulk material tapes used to simulate the fibrils, a failure stress is a more general failure criterion. Evidence to support this has been provided from two sources.

Firstly a series of tests were conducted on an Instron tensile testing machine where the sample was loaded and extended at constant crosshead velocity until failure occurred and the stress and strain at rupture were determined. These results are plotted in figures A1·4 to A1·9.

Figure A1-2

Surface in true strain rate, strain, true stress space for the quenched morphology of oriented 6007.

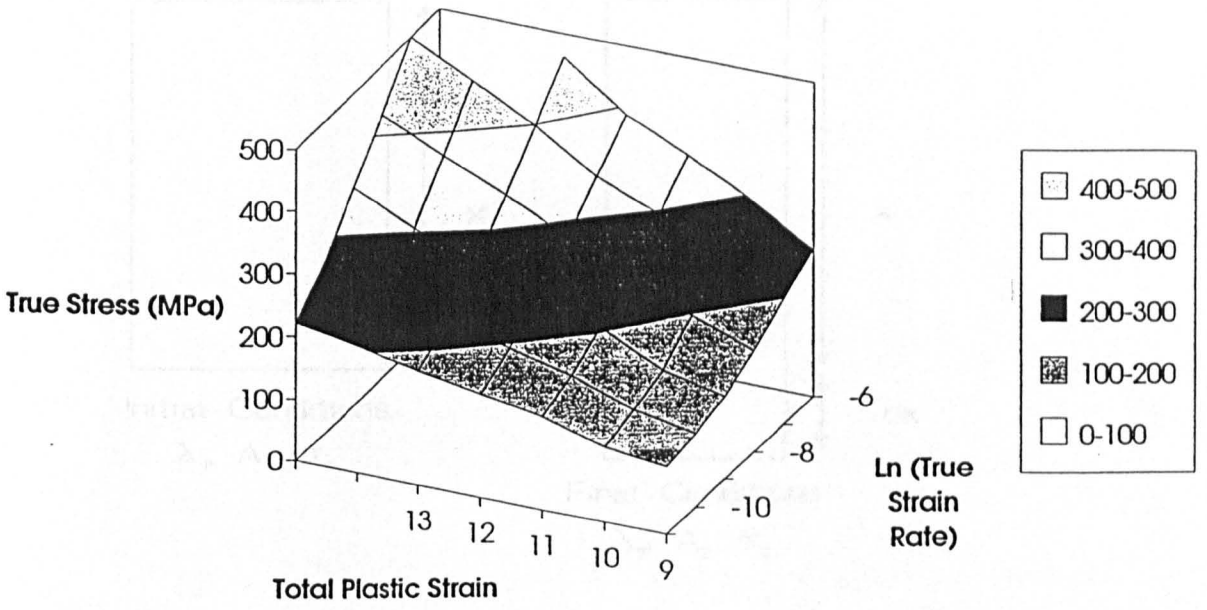

Figure A1·3

Schematic representation of the change in dimensions of a specimen, (or fibril), under creep.

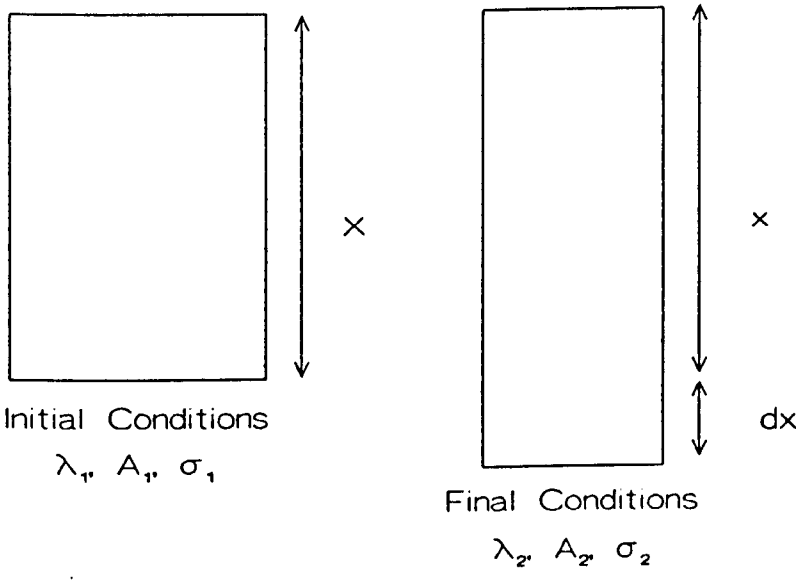

Figure A1-4

Failure strain versus crosshead speed for quenched 6007.

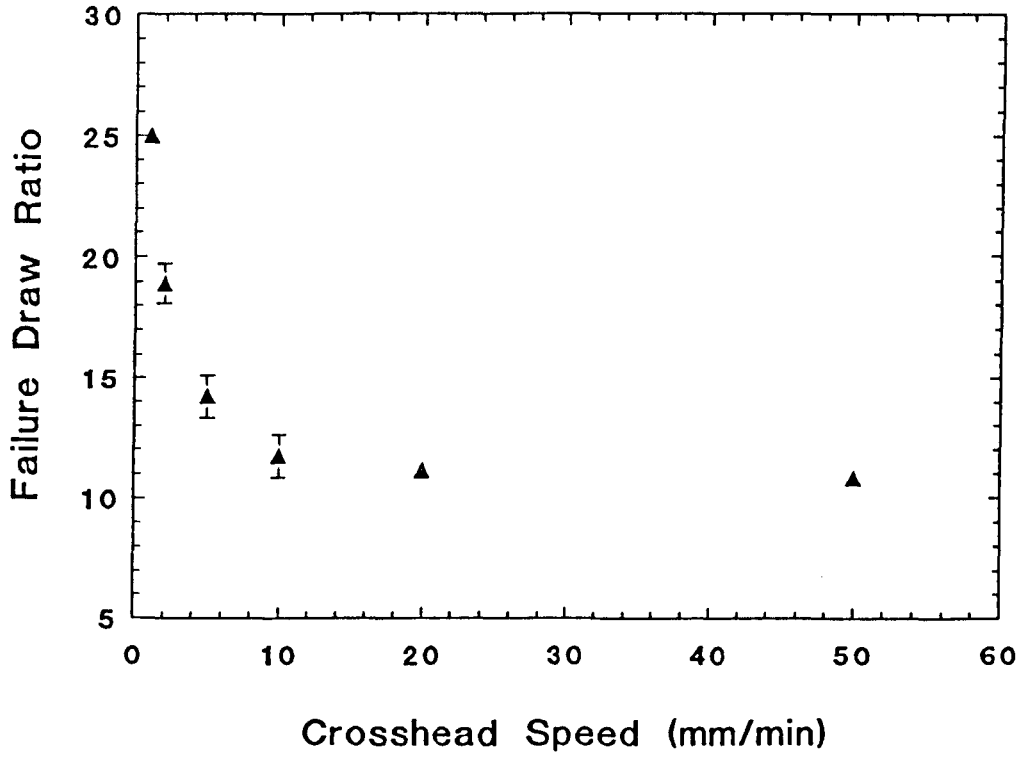

Figure A1·5

Failure stress versus crosshead speed for quenched 6007.

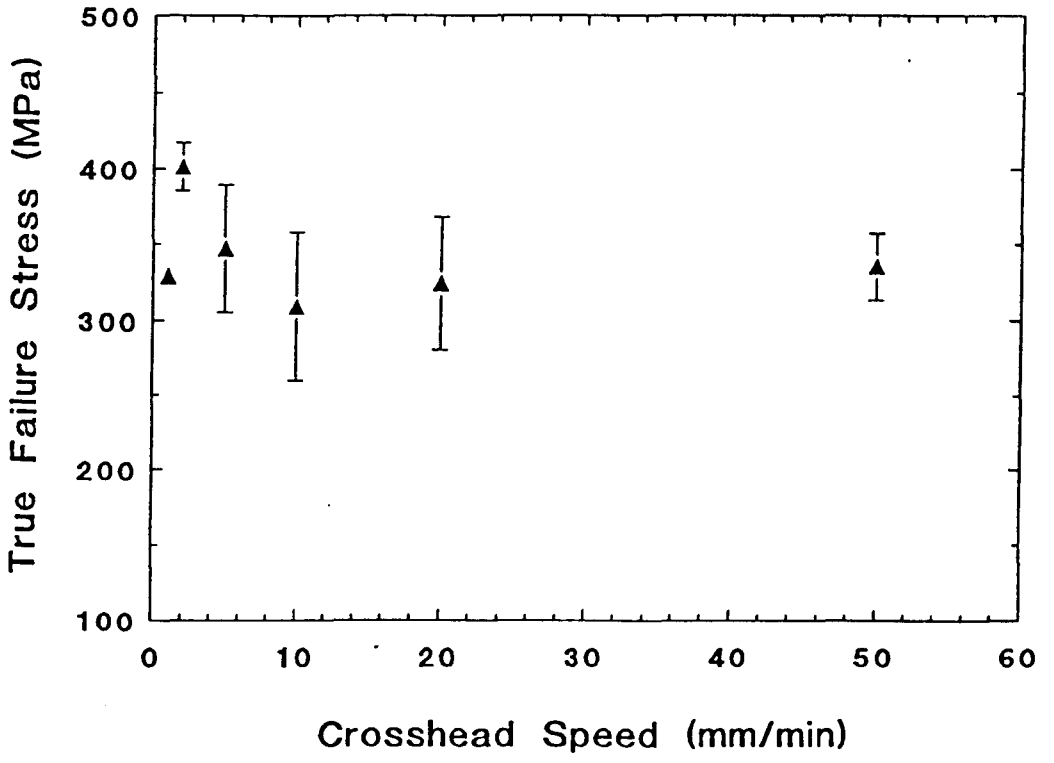

Figure A1·6

Failure strain versus crosshead speed for quenched 00240.

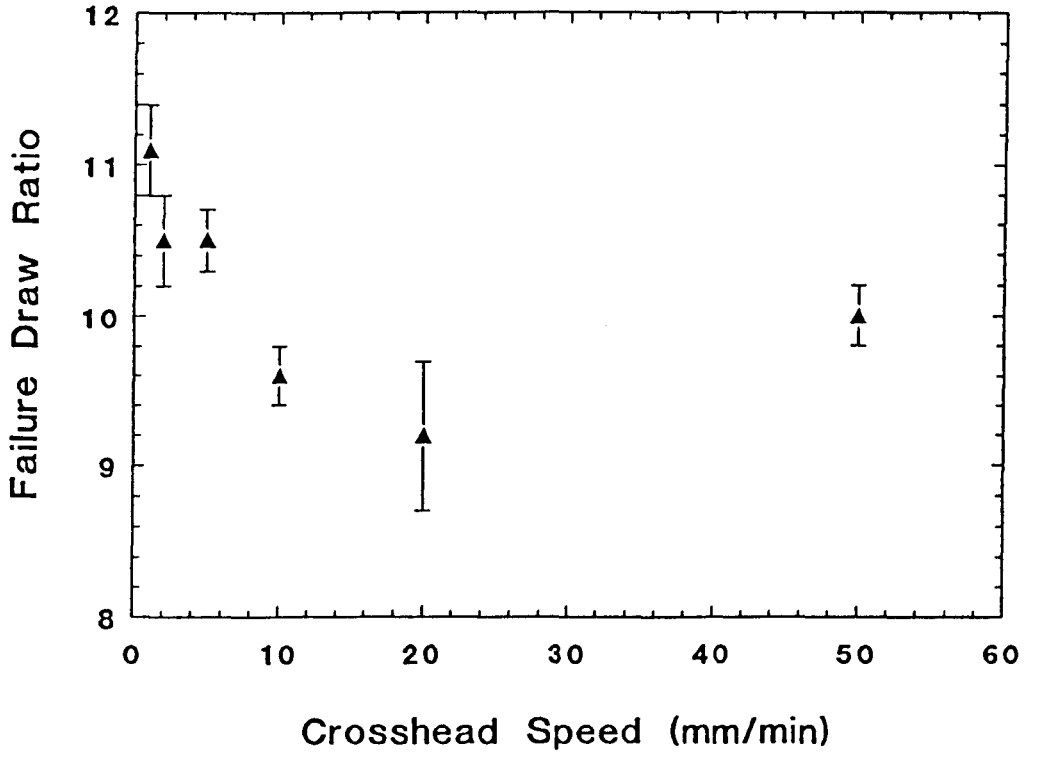

Figure A1·7

Failure stress versus crosshead speed for quenched 00240.

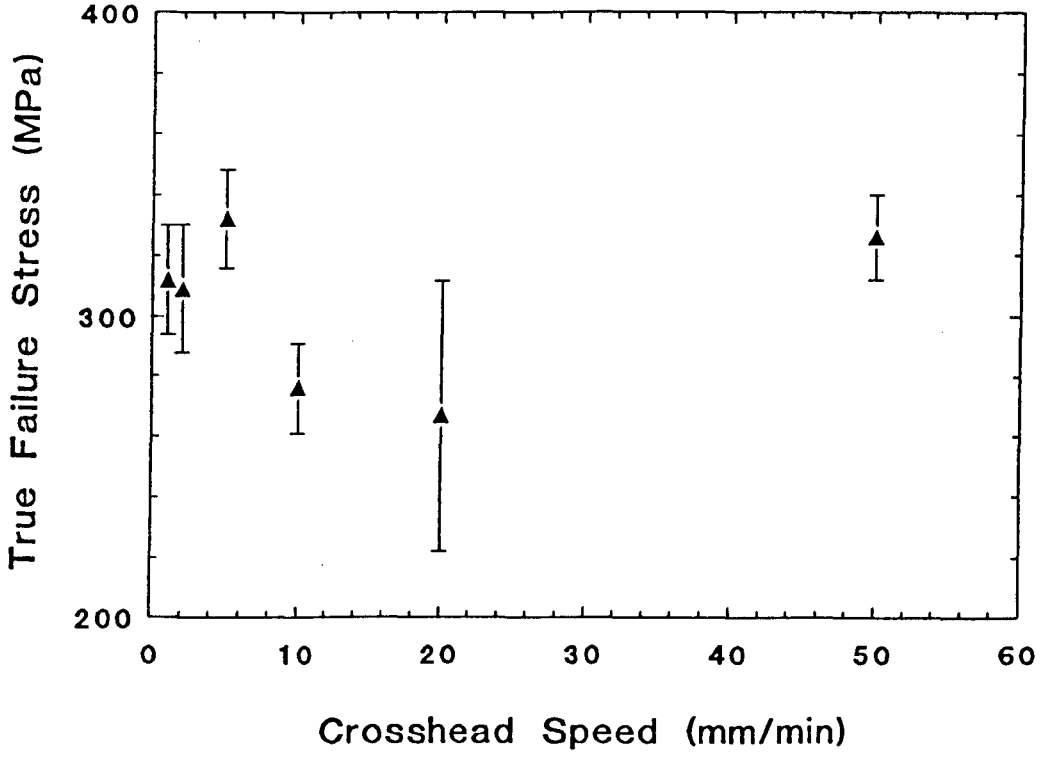

Figure A1·8

Failure strain versus crosshead speed for slow cooled 00240.

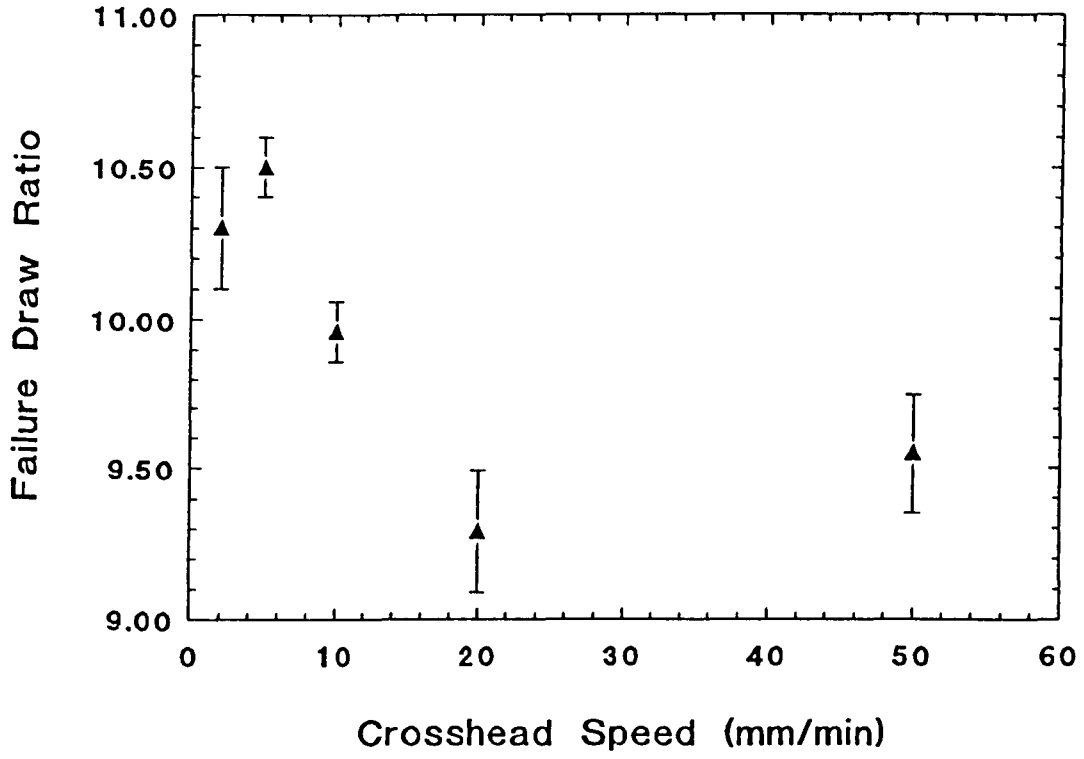

Figure A1·9

Failure stress versus crosshead speed for slow cooled 00240.

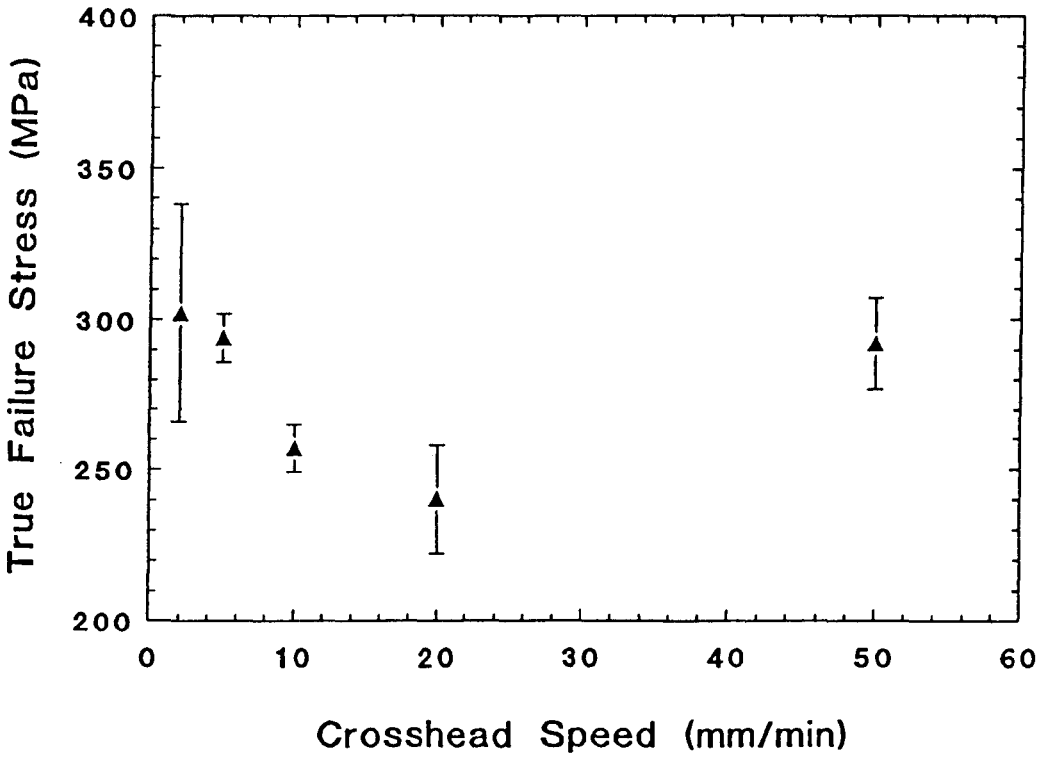

Although the same trend can be seen for all the three morphologies studied, the most pronounced is for the quenched morphology of 6007. In this case it is obvious that the failure strain is not constant, and increases as the strain rate is reduced. The failure stress, however, remains relatively constant throughout the strain rate regime.

Secondly, further creep tests have been performed, together with reanalysis of earlier tests. These have shown that failure of the samples occurred at differing strains, but within a narrow range of stresses, (figure A1·10, initial stress on top, failure stress underneath).

There does, however, appear to be a difference in the failure stress between the creep experiments and the Instron experiments when the data is viewed as a whole. It must be pointed out though that if the entire amount of creep data is considered then there are two different average failure stresses present, one around 240 MPa, (as shown in figure A1·10), and one around 300 MPa, closer to the value obtained in the Instron tests. It is not known why this should be the case.

It should also be noted that very occasionally creep tests extended to much higher, (≈400 MPa), before failure.

In the case of the creep experiments failure is characterised by a fibrillar structure being visible at the point of rupture. This indicates a breakdown in the internal morphology of the material, not a geometric thinning effect.

Hence in order to make the model completely general the failure stress criterion must be used. However in the specific context in which this program was applied, (being used to model the growth of fibrils within a craze), failure at draw ratio 15 is reasonable as this is close to the average draw ratio at failure which would be encountered in the strain rate regime of the experimental crack growth work to be described later.

This failure discussion is valid for the bulk material tapes which were being used to simulate the fibrils in a craze. Within the craze itself the situation is likely to be complicated by the increased time under load of the fibrils.

As an example the 00240 material can withstand cracks for long periods of time. Hence there will be significant effects due to ageing, and also to the environment in which the craze evolves.

It must also be emphasised that reasonable predictions could only be made by this program within the envelope covered by the experimental creep data. Once a variable progressed outside this envelope the predictions started to become unreasonable, and if the variable was far enough outside the range, physically impossible.

Figure A1·10

Sherby Dorn plots failure stress for the quenched morphology of oriented 6007.

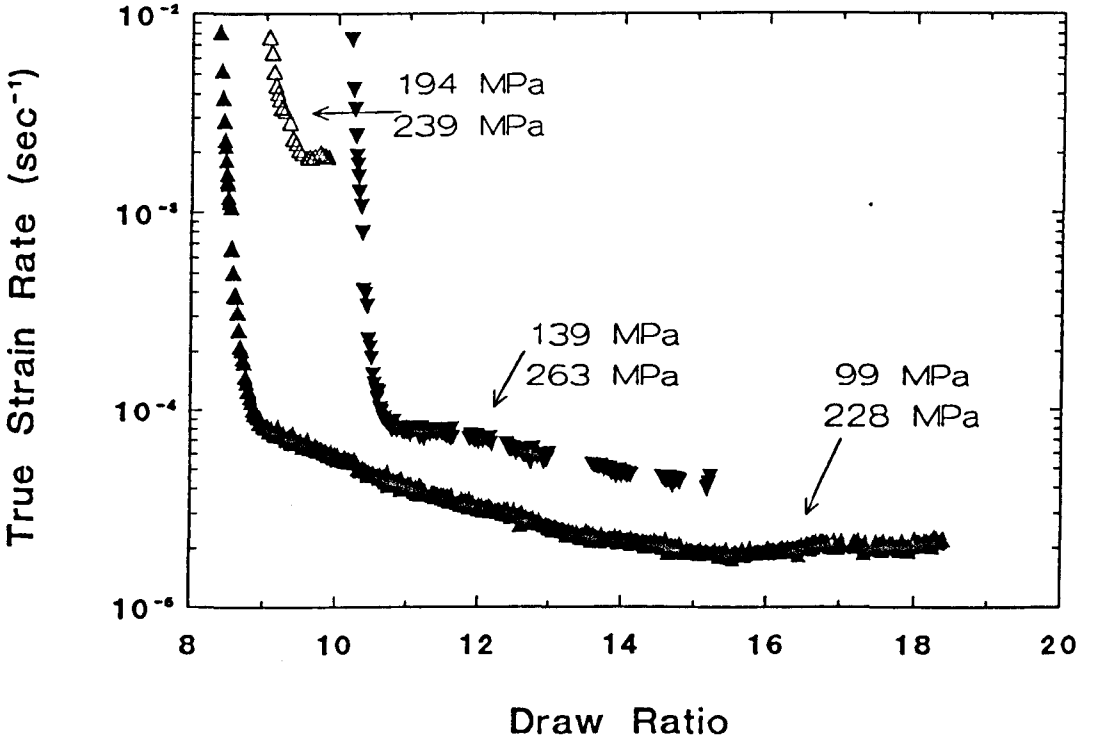

### A1·3 Application To Slow Crack Growth

The program was capable of modelling the extension of a single fibril, (assuming that a single fibril could be represented experimentally by the bulk material tapes used in the creep tests), effectively up to the point of failure. However to model crack growth is more complicated.

In order to model the growth of the fibril at the base of the craze we need to know the stress acting upon it. This is based upon the stress acting on the interface of the bulk material and the fibril, but since the material has been oriented the true stress will rise, due to the reduction in cross sectional area, hence the stress acting on the fibril at any point is the interface stress multiplied by the draw ratio of the fibril at that point. There is currently no experimental method which allows us to determine this interface stress directly.

The interface stress is of critical importance when making predictions of the lifetimes of cracks.

In order to determine this interface stress it is necessary to run the fibril extension model at several different levels of stress, assuming that the fibril in the craze starts at the natural draw ratio of the material. There is no evidence available to support this assumption, but since it is not possible to extend the true stress, true strain rate strain relationships into the region between the second yield point and the natural draw ratio, it seemed logical to assume that the material was oriented this far as it was drawn in, especially since it was necessary to make some assumption of the starting conditions of the fibril.

This provides a range of failure times for the fibril.

This data is then compared with data from standard Single Edge Notched, (SEN), experiments on the same material, (performed by Mr A. D. Channell of BP Chemicals, Grangemouth, and described in greater detail in the paper[3]).

These SEN tests were performed using standard SEN testing geometry, (figure A1·11). The geometry was constant for all tests, the only variable being the applied bulk stress. A sliding cathetometer was used to take measurements of the Crack Opening Displacement, (COD), the distance between the bulk material at the base of the crack and the length of the longest fibrils. In order to minimise edge effects the COD measurements were taken from the centre of the sample. Bulk stresses of 2, 3, 4 and 4·5 MPa were applied.

A schematic COD versus time plot is shown in figure A1·12.

Figure A1·11

Schematic diagram of a SEN specimen.

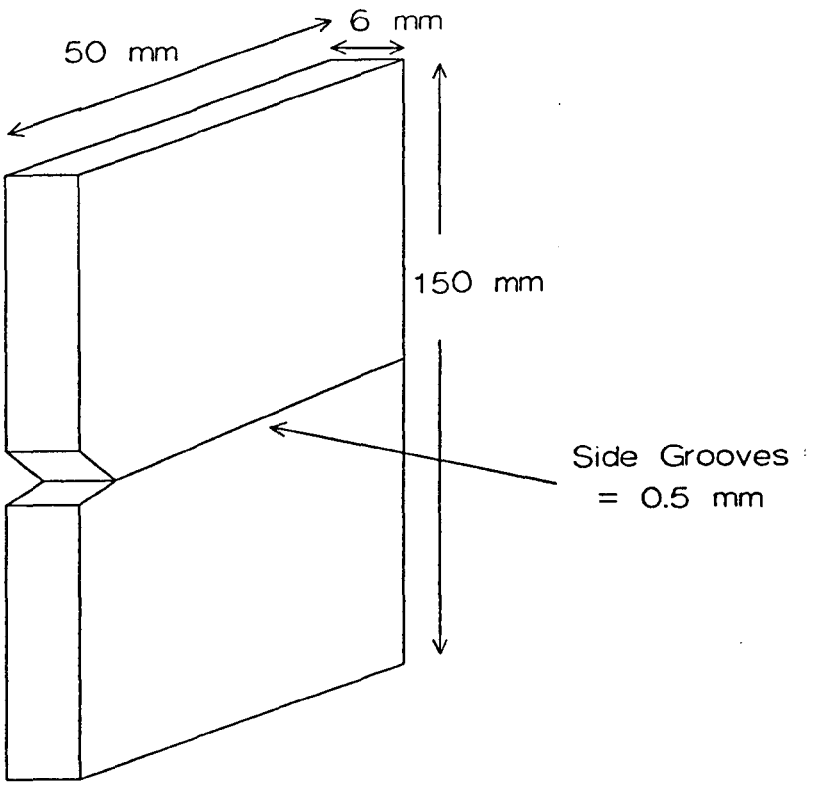

Figure A1·12

Schematic representation of a COD versus time plot.

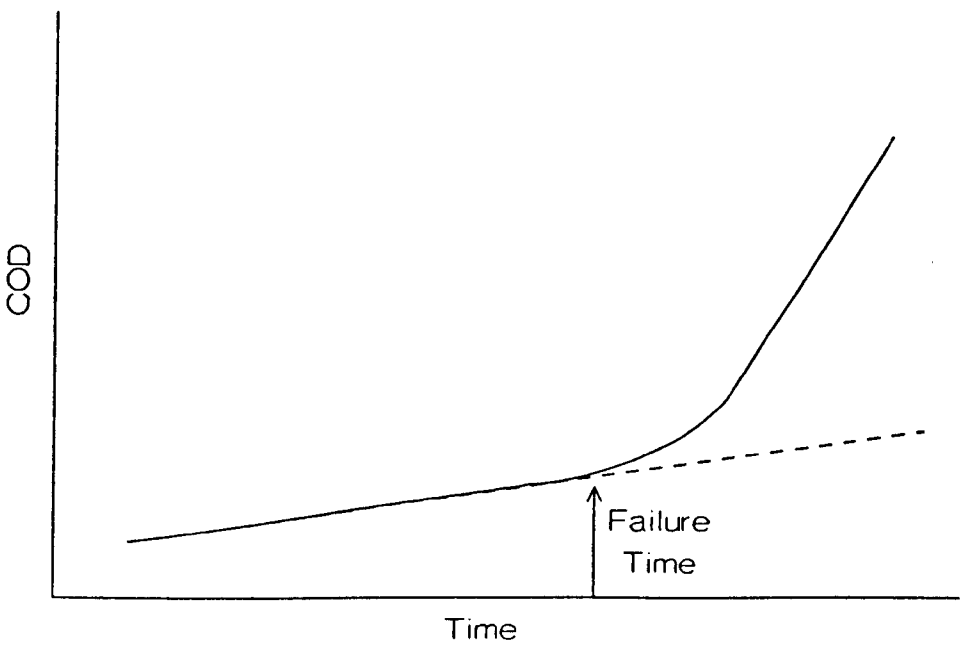

The SEN tests produced two sets of data. One is the COD rate, the rate at which the crack grows, and the failure time. The failure time is the point at which the COD rate becomes non linear, and it is at this point that fibril failure is seen to occur, (figure A1·12).

It is a simple matter to then take the SEN failure time and by examining a graph of fibril failure time versus applied stress, determined by running the computer model at various applied stresses, to calculate the effective stress at the interface between the bulk material and the fibril.

The bulk and interface stresses for the quenched morphology of 6007 and slow cooled morphology of 5502 are shown in Table A1·1.

| Bulk Stress (MPa) | Interface Stress (MPa) | Interface Stress (MPa) |
|---|---|---|
| | 5502 | 6007 |
| 2 | --- | 5·15 |
| 3 | 7·98 | 7·30 |
| 4 | 14·83 | 15·47 |
| 5 | 19·26 | 18·38 |

**Table A1·1**

Table showing bulk and interface stresses for the quenched morphology of 6007 and slow cooled morphology of 5502.

It can be seen that the interface stresses are approximately the same for the two morphologies, implying that the concentration factor is relatively independent of the grade and morphology.

It should be pointed out that in this process only the central element of the fibril is considered, since this is the point at which fibril failure occurs, because this is the point of maximum deformation, (simply due to the greater amount of time which this section has to deform).

By using the effective stress derived in this manner, and the failure criterion discussed above, it is possible to work back and predict the lifetime of a SEN test, and hence to predict the lifetime of a sample undergoing slow crack growth.

Although the stress acting at this interface has now been obtained, and it is possible to predict the lifetime of a crack, it is still not possible to model the growth of a crack. Running the model using just the fibril extension does not match the COD rate of the SEN tests.

It is necessary to add in the effect of new material being drawn into the fibril from the bulk material at the interface of the bulk material and fibril.

To accomplish this a fibril at its natural draw ratio with an initial length equal to the initial length of the damage zone present in the SEN sample prior to loading was assumed and the extension model using the routine described previously. However at the next iteration of the program a small amount of new material was assumed to be drawn into the fibril, figure A1·13. This material was assumed to increase the total length of the fibril, (and hence increase the COD), and was also assumed to draw to the natural draw ratio. During the next iteration this new section was extended after the original section and the two new lengths combined. A further section of virgin fibril was then created and the process repeated until the original centre section of the fibril reached the failure criterion. Thus an entire fibril which constantly acquired new material was grown, figure A1·14. This does produce a somewhat artificial shape for the fibril, but as the period of deformation time for each iteration is decreased the shape of the fibril tends towards a much smoother, more acceptable outline, (figure A1·15), which is more like the fibrils viewed in experimental work.

The time intervals used varied between 10 seconds and 10 minutes depending upon the applied stress.

By including the drawing in of material into the model, and by varying the rate at which new material was acquired by the fibril, the program could be used to model the experimentally observed COD data up to the point of failure.

The total growth rate of the fibril was then matched to the experimentally derived COD rate by varying the amount of new material drawn into the fibril from the bulk at each step.

The size of the initial damage zone was approximately constant in these tests, ranging between ~55 μm and ~69μm, but the rate of drawing of the new material increased as the bulk stress was increased.

Figure A1·13

Schematic representation of two iterations of the program.

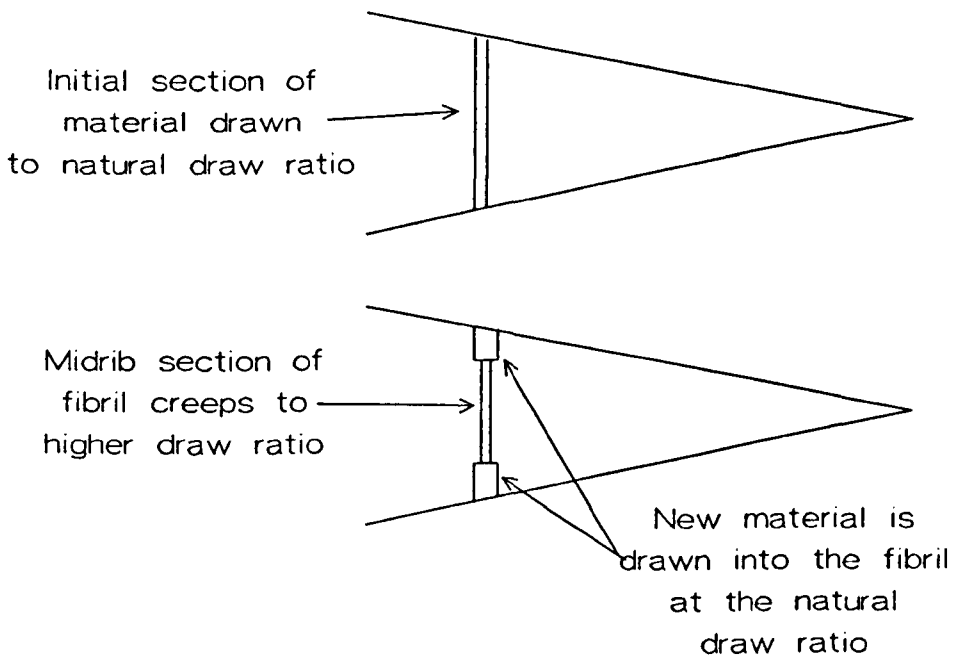

Figure A1·14

Schematic representation of the results of several iterations of the program.

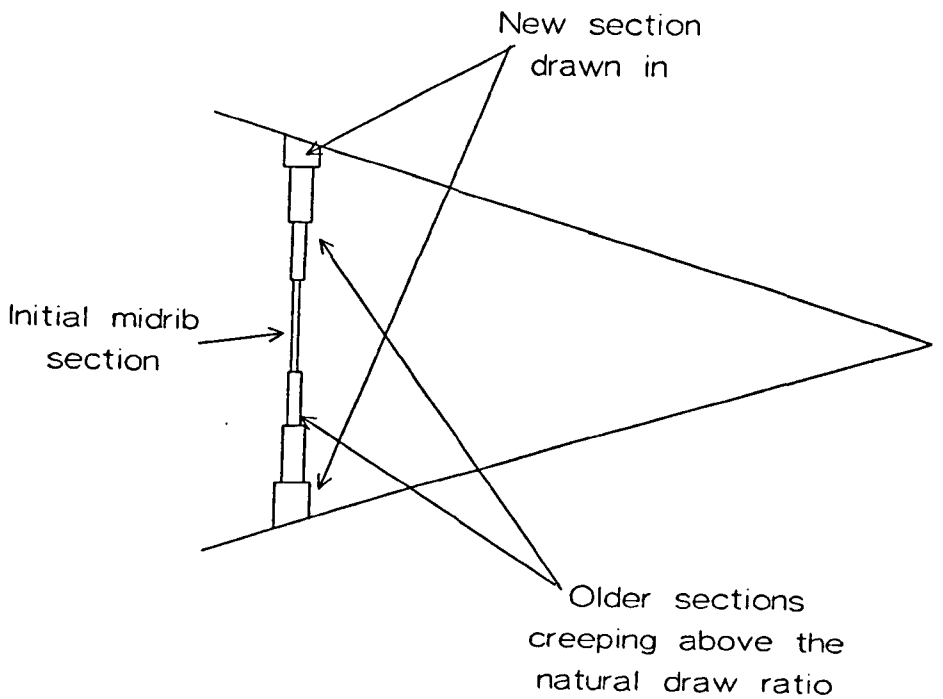

Figure A1·15

Representation of the shape of the modelled fibril as the time interval of the iteration tends to zero.

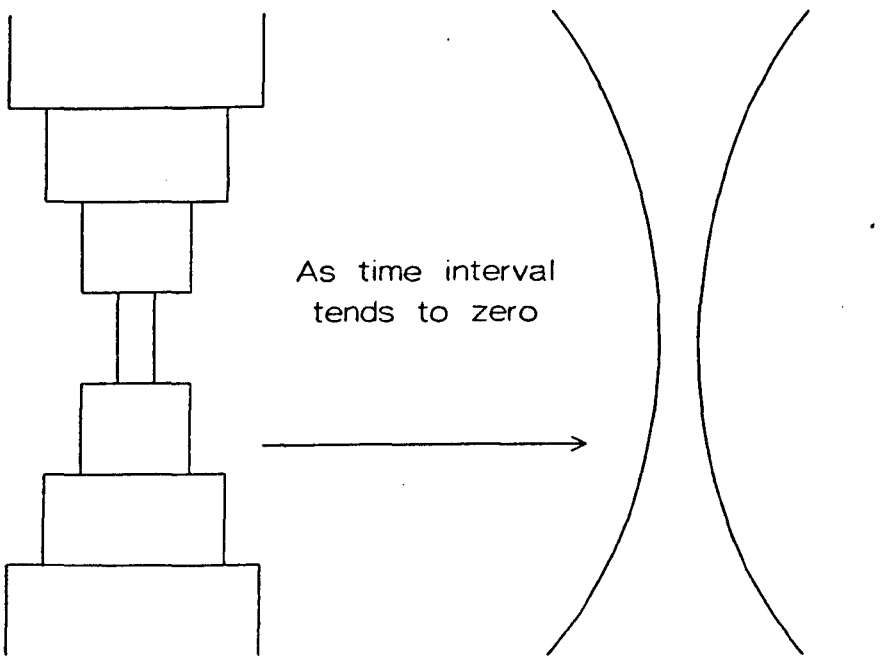

**A1·4 Further Discussion**

It is apparent when viewing the Sherby Dorn plots produced from creep experiments, that the true strain rate decreased as the strain increased, even though the true stress was also increased. This indicates that strain hardening occurs.

A material with a good strain hardening characteristic would reduce in true strain rate much more rapidly than a "weaker" material, and hence extend the time to failure in slow crack growth situation.

The measure of strain hardening used by Cawood et al.[2] was the gradient of the second region of the Sherby Dorn plot, i.e.

$$\frac{d \ln \dot{\varepsilon}}{d\sigma} \qquad \text{(A1·1)}$$

The computer model gives gradients of

-0·0073 $MPa^{-1}$ for the quenched morphology of 6007 and

-0·0127 $MPa^{-1}$ for the slow cooled morphology of 5502.

The greater strain hardening of the 5002 is reflected in the failure times of the SEN tests, from 338 minutes for the quenched morphology of 6007 to 1,200 minutes for the slow cooled morphology of 5502, both at a bulk stress of 4 MPa.

Care is needed with the idea that slow crack growth can be predicted simply by the gradient of the second region of the Sherby Dorn plot, since it contains no information on the natural draw ratio or the failure criteria. However the excellent results produced by Cawood[2] may indicate that all variables involved in slow crack growth are uniquely determined by the morphology and true stress, strain and true strain rate relationship.

Previously in slow crack growth work the interface stress was assumed to be the yield stress. The range of stresses produced by this work is an indication of the rate dependence of the yield stress.

Lastly in order to show the derived interface stresses are reasonable a log-log plot of COD versus interface stress was produced, figure A1·16.

Figure A1·16

Log log plot of COD rate versus interface stress.

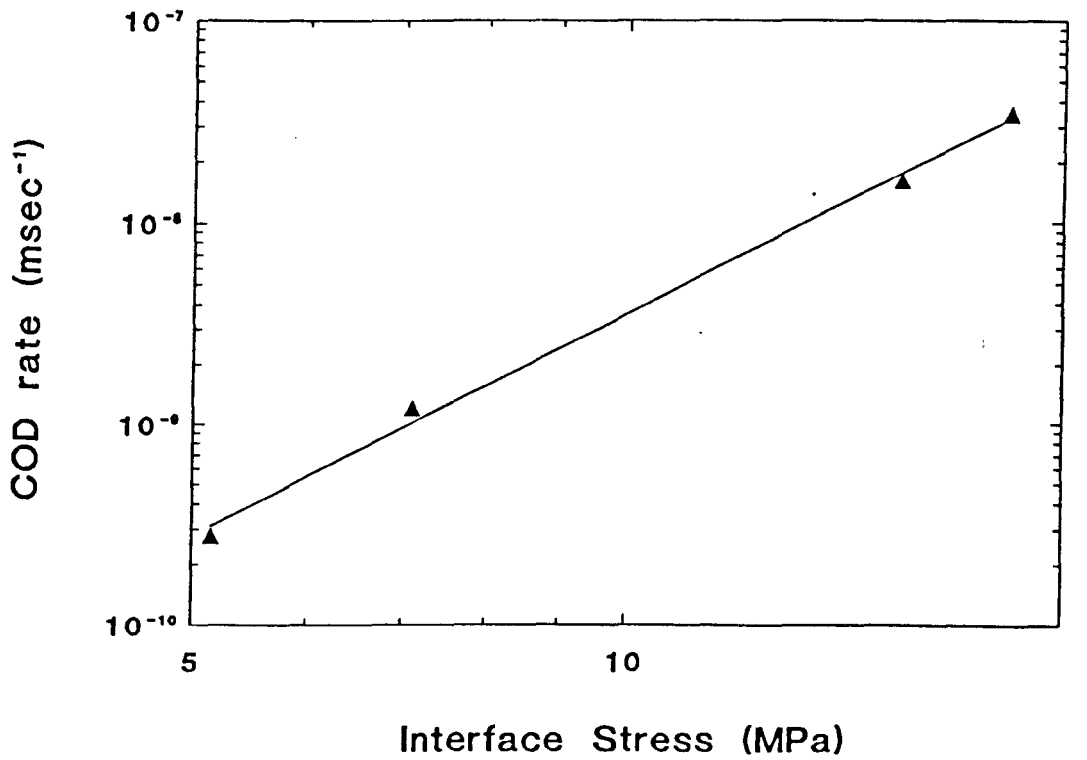

As can be seen this log-log plot is linear with a COD rate of

$$\text{COD rate} = 4{\cdot}14\times10^{-8}\sigma^{3{\cdot}7}\ \text{msec}^{-1} \qquad \text{(A1·2)}$$

This compares well with crack velocity results of

$$V = A\sigma^{4} \qquad \text{(A1·3)}$$

by Chan[5], and

$$V = A\sigma^{4{\cdot}2} \qquad \text{(A1·4)}$$

by Brown and Bhattacharya[6].

**A1·5 Conclusions**

It has proved possible to take the two elements occurring in the growth of a fibril at the base of a craze and to incorporate them into a model which can then match the growth of a craze to experimentally derived COD rates.

In order to predict failure times it is necessary only to have a knowledge of the creep behaviour, (including a failure criterion), of the material and the stress acting on the interface between the bulk material and the fibril. It is not necessary to consider the drawing in of new material into the fibril.

Thus, provided that a suitable set of test conditions can be derived, it should prove possible to make initial judgements of a material's stress crack resistance with a few, (or even a single), simple creep tests.

The interface stresses derived using the process described previously differ from the views of Brown[4] in that they are substantially below those stresses reported in his work. This disagreement must await a reliable experimental technique in order to be resolved.

In order to model fully the crack growth of a material the amount of material drawn into the fibril from the bulk material must be taken into account.

**A1·6 References**

1. Bhattacharya, S.K. and Brown, N., J. Mat. Sci., **19**, (1984), 2519
2. Cawood, M.J., Channell, A.D. and Cappacio, G., Polymer, **34**, (1993), 423
3. O'Connell, P., Bonner, M.J., Duckett, R.A. and Ward, I.M., Polymer, **36**, (1995), 2355
4. Brown, N., Wang, X. and Fager, L., Polymer, **30**, (1989), 453
5. Chan, M.K.V. and Williams, J.G., Polymer, **24**, (1983), 234
6. Brown, N. and Bhattacharya, S.K., J. Mat. Sci., **20**, (1985), 4553